

EMPTY OPEN NEST DETECTOR REDESIGN

A Major Qualifying Project Report

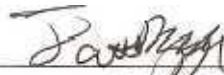
Submitted to the Faculty of

WORCESTER POLYTECHNIC INSTITUTE

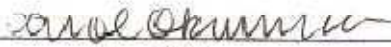
In partial fulfillment of the requirements for the

Degree of Bachelor Science

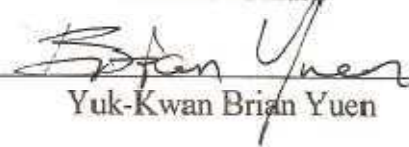
By



Davis Nguyen



Carol Okumura



Yuk-Kwan Brian Yuen

Date: December 18th, 2009

This project report is submitted in partial fulfillment of the degree requirements of Worcester Polytechnic Institute. The views and opinions expressed herein are those of the authors and do not necessarily reflect the positions or opinions of the sponsoring company or Worcester Polytechnic Institute.

This report is the product of an educational program, and is intended to serve as partial documentation for the evaluation of academic achievement. The reader should not construe the report as a working document.

Acknowledgements

Robert L. Norton	Project advisor / Engineer / Software developer
Corey Maynard	Project liaison / Engineer (Mechanical)
Kenneth Belliveau	Project liaison / Engineer (Mechanical)
Charles Gilles	Project liaison / Engineer (Mechanical)
Dave Clancy	Engineer (Mechanical)
Art Borgeson	Engineer (Electrical)
Eileen Souliotis	Engineer (Electrical)
George Kirby	Engineer (Electrical)
Ernie Chandler	Photographer, Videographer
Toan Nguyen	Shop manager
Adam Lane	Production manager
Mike McGourthy	Mechanic
Larry Clinton	Mechanic
John Chan	Mechanic
Tom Cotta	Mechanic
Paul Lopes	Mechanic
Gerry Bushway	Mechanic
Stephen Cavalier	Mechanic
Michael Healy	Keyence sensor sales person
Barbara Furhman	Department secretary (WPI, ME Dept)

Abstract

The sponsor company encountered problems with a station on an assembly machine designed to detect an empty and open condition on a nest. Current detector was found to be problematic, causing many false positives and unnecessary machine stops. These problems are caused by small tool stroke and failed insulations on electrical contacts. The solution includes a mechanical linkage to increase tool stroke and a non-contact through beam sensor. Prototype of the design proves to be successful during full-speed testing.

Table of Contents

Acknowledgements.....	2
Abstract.....	3
List of Figures.....	6
List of Tables.....	7
Introduction.....	8
Background.....	9
The Empty Open Nest Detector.....	10
Problems with Current Design.....	12
Goal Statement.....	14
Design Specifications.....	14
Computation Modeling.....	15
Measured Data.....	19
Theoretical and Measured Data Comparison.....	21
Design Ideas.....	23
Single Lever Solutions.....	23
Single Lever with Through Beam.....	23
Single Lever with Displacement Sensor.....	24
Slider Solution.....	26
Four-bar Linkage Solution.....	26
Four-bar Linkage Design.....	27
Initial Four-bar Mechanism.....	27
Optimized Four-bar Mechanism.....	30
Frame.....	31
Sensor Holder.....	32
The Crank.....	32
The Coupler.....	34
The Rocker.....	35

Spring-Loading the Rocker	35
Detection	37
Error Analysis	38
Testing Prototype	39
Revised Prototype	40
The Frame	40
The Crank.....	41
Spring Selection.....	42
Testing.....	43
Final Design	44
Crank.....	47
Coupler & Pin Fitment.....	48
Rocker	48
Sensor Holder.....	49
Frame	50
Conclusion & Recommendation	51
Material Considerations	51
Modification to Slider’s Height	51
Modification to Slider’s Nose	51
Modification to Casting	51
Bibliography	52
Appendix.....	53
Appendix A - Empty Open Nest Detector Station Mass Model	53
Equivalent Mass and Spring Calculations.....	53
MatLab File : twodof.m	56
MatLab File : twodofemode1	59
MatLab File : twodofemode2.....	59
Appendix B – MathCAD, Linkage Position Analysis	60
Appendix C – MathCAD, Optimizing Geometry of Links.....	61
Appendix D – Four-bar Linkage Mass Model	63
Appendix E – Linkage Pre-load.....	64
Appendix F – FEA Results	65
Lower Lever Arm	65

Upper Lever Arm.....	66
Appendix G – Stress Applied on Pins.....	67
Rocker-to-ground (Pin 1-4).....	68
Coupler-to-Crank, Coupler-to-Rocker, Ground-to-Crank (pin12, 23, 34).....	70
Appendix H – Setup Procedure.....	73
Appendix J – Drawings of Final Parts	74

List of Figures

Figure 1 - The Empty Open Nest Detector Station.....	9
Figure 2 - Empty Open Nest Detector	10
Figure 3 - Empty Open Nest Detector Cycle.....	11
Figure 4 - False positive causes on the Open Nest Detector.....	13
Figure 5 - One DOF, one mass model [1].....	15
Figure 6 - One DOF, two mass model [1].....	15
Figure 7 - Two DOF, three mass model [1].....	15
Figure 8 - Moving components of the Empty Open Nest Detector station.....	16
Figure 9 - Deflection of lower lever arm with applied force as calculated by FEM.....	17
Figure 10 - Computations results of three mass, three DOF model.....	17
Figure 11 - Accelerometer locations during testing.....	19
Figure 12 - Test data overlaid with theoretical accelerations.....	20
Figure 13 - Mass one acceleration comparison.....	21
Figure 14 - Mass two acceleration comparisons.....	22
Figure 15 - 15 Inch Lever Design	23
Figure 16 – Single-Lever Mechanism with Proximity Sensor.....	24
Figure 17 - Slider Design.....	26
Figure 18 - Initial Four-bar Mechanism Design	27
Figure 19 – Four-bar Mechanism Front View	28
Figure 20 - Optimizing Crank Geometry	29
Figure 21 - Final Four-bar Mechanism Front View.....	30
Figure 22 - Frame for four-bar solution	31
Figure 23 - Beam holder for four-bar solution.....	32
Figure 24 - Determining Crank Pin Positions.....	33
Figure 25 - Determining Crank Pin Positions.....	33
Figure 26 - Final Crank Dimensions.....	34
Figure 27 – Coupler Geometry and Dimension.....	34
Figure 28 - Final Rocker Dimensions.....	35

Figure 29 - Modifying the station cam to simulate detector motion.....	36
Figure 30 - Spring-loaded four-bar linkage system	36
Figure 31 -Four-Bar Linkage Fail-Safe Conditions	37
Figure 32 - Spring inside detector body.....	39
Figure 33 - Spring forces schematic on detector.....	40
Figure 34 - Frame Design II.....	41
Figure 35 - Crank Design II	42
Figure 36 – Springs between Slider and Over-travel Mechanism	43
Figure 37 - Overall view of final design	44
Figure 38 - Left view of final design	45
Figure 39 - Right view of final design	46
Figure 40 - Crank for final design.....	47
Figure 41 - Coupler for final design.....	48
Figure 42 - Rocker for final design.....	48
Figure 43 - Sensor holder for final design	49
Figure 44 - Frame for final design	50
Figure 45 - Pin forces as calculated by Four-bar	67

List of Tables

Table 1 - Machine Stops Caused by the Open Nest Detector in a Two-month Period.....	12
Table 2 - Error Analysis.....	38

Introduction

Automated assembly machines are currently used by the client company to assemble household products. These machines consist of multiple stations, each performing a specific task in the assembly process. Each product is held in an independent nest that moves transversely to each of these stations. The first station on these machines, the empty open nest detection station, ensures that the nest jaw is in the open position, and that the jaw and break pin surface is free from debris. Satisfaction of the three conditions ensures that each nest is ready for a new production cycle.

The stop frequency data gathered from each machine suggests that approximately 20% of the machine stops originated from the empty open nest detector. A majority of these stops are considered false positives, meaning that an error condition was detected even though the failure criteria were not actually met. The geometry and motion of the detector brought about these problems, which makes the station difficult to setup and prone to moisture.

Magnifying this motion on the slider would allow for a greater detection gap. A combination of different mechanisms and detection sensors were investigated for this purpose: a one-link mechanism with a through-beam sensor, a one-link mechanism with a proximity probe, and a four-link mechanism with a through-beam sensor.

The four-link mechanism that uses a through-beam sensor was chosen for prototyping, because it offers the most magnified motion when compared to the other two alternatives. Testing shows that the principle of the mechanism is sound, and the detector is able to accomplish the specified task. The design was improved over the course of testing, and slowly evolved into our final design which addresses each of the issues encountered during testing.

Background

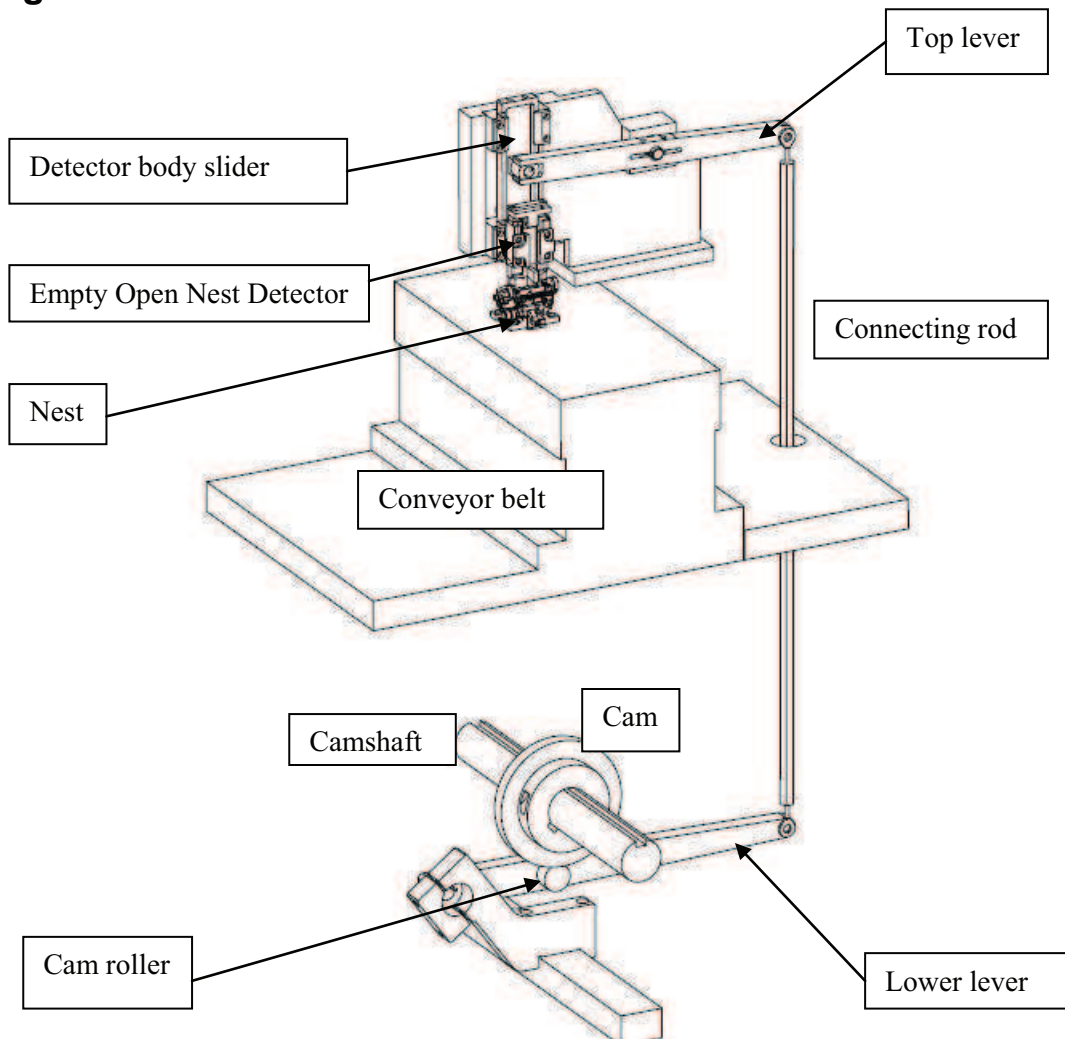


Figure 1 - The Empty Open Nest Detector Station

The empty open nest detector station's function is to check that the nest (1) has an opened jaw, (2) has a clean break pin surface, and (3) the jaw is clean. As shown in Figure 1, the station is a cam-follower system that drives the detector body slider. The lever arm is spring loaded by an air cylinder from the chassis of the machine, so that the roller and the cam are kept in constant contact. The mechanism is driven by a single dwell cam, during the dwell of which the detector contacts the nest. The rise and fall motion associated with this cam provides sufficient time for a nest to index forward. A connecting rod links the lower lever arm to the upper lever arm that is moving the slider.

The Empty Open Nest Detector

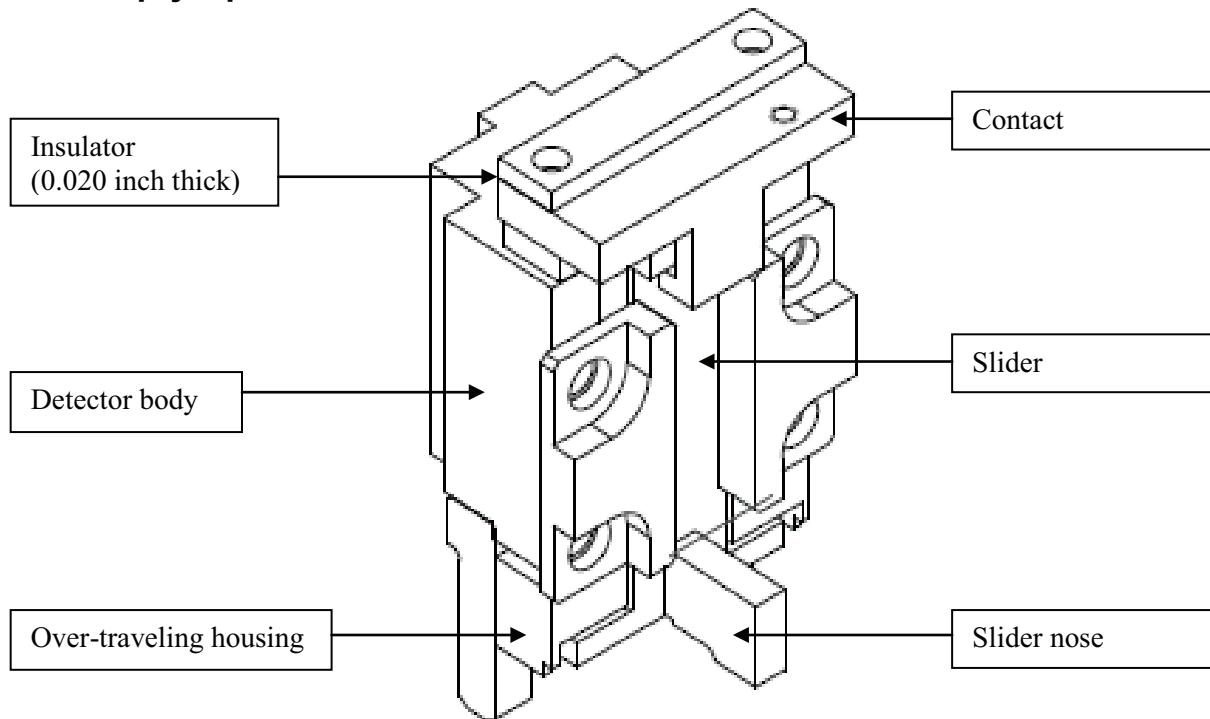


Figure 2 - Empty Open Nest Detector

The empty open nest detector comes in contact with every nest passing by. The device's main components include: the slider, contact, and the over-travel housing. Figure 2 shows the detector and the physical arrangements of its components. The slider is spring loaded downwards so that when hung freely, the slider will be pressed against the contact. When the detector is retracted upwards, this contact provides for the fail-safe detection. Similarly, the over-travel housing is spring loaded so that it will be coupled to the detector body until the cam-driven links have pushed the detector body beyond the position of contact. By adjusting the length of the connecting rod, the mechanic can setup the machine so that the detector always over-travels and contacts each nest regardless of their slight height differences.

The operation of the detector is best explained beginning from its upward most position, where the slider is resting on the contact. As the detector travels downwards, the nose piece on the slider, whose geometry is specially designed to check for both an open and empty nest, comes into contact with the nest's jaw and break-pin surface. As the cam continues to move the detector body down, the slider is pushed up, and at some point, the base of the over-travel housing contacts the break-pin surface as well. The amount that the slider travels with respect to the over-travel mechanism is most critical, since the contact is mounted on the over-travel housing. The gap between the slider and the contact corresponds to the 0.003inch

thickness of the product fragments that can be in the nest. This distance is adjusted during set up by the addition of a shim approximately 0.020in thick.

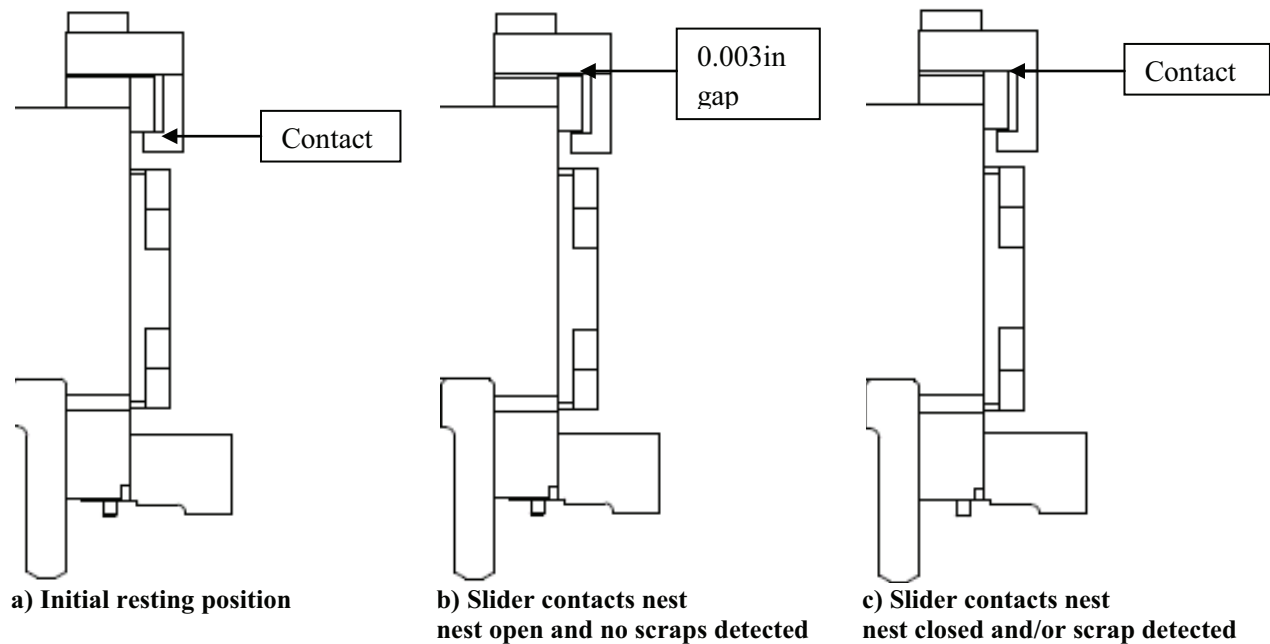


Figure 3 - Empty Open Nest Detector Cycle

The detecting cycle is depicted using the side view of the open nest detector in Figure 3. An electrical circuit is made whenever the slider touches the contact, as shown in Figure 3(a) and Figure 3(c). A completed circuit sends a positive signal to the controller, indicating a “fail” signal. Whereas a broken circuit as depicted in Figure 3(b) indicates a “pass.”

- a) Before the slider comes in contact with the nest, it is resting on the contact, making an electric circuit—as it can be seen from Figure 3(a). This is a fail-safe system assuring the mechanism is working properly before detection takes place.
- b) When the slider nose comes in contact with an open and empty nest, Figure 3(b), the slider travels upwards and its upper portion makes no circuit with the contact. The slider simply sits in between the upper and lower part of the contact without touching either part.
- c) Figure 3(c) shows the slider behavior when the nest is closed, or when scrap is found. The upper part of the slider will travel the 0.003inch upwards and come in contact with the upper portion of the contact and make a circuit, which produce a “fail” signal and stop the machine.

The computer checks for the “fail” signal at the beginning of the downward travel for the fail safe, and for the “pass/fail” signal at the end of the dwell. Therefore, for every nest, the ideal detection cycle is: circuit

(fail-safe), no circuit (pass), and then the cycle repeats. When nest is closed or scrap is found, the cycle results in: circuit (fail-safe) and circuit (fail), stopping the machine.

Problems with Current Design

Error reports were collected for this assembly machine for a two-month period. These reports list the number of machine stops along with their origins. The open nest detector is consistently ranked at the top five causes for machine stops. Table 1 lists the machines stopped most often by the empty open nest station, and shows open nest detector stops compared to total number of stop incidents.

Machine #	Empty Open Nest Stops #	Total Incidents #	Percentage Caused by Open Nest (%)
A	1590	7673	20.72
B	1152	5747	20.05
C	980	5323	18.41
D	1000	5957	16.79
E	1266	7807	16.22
F	860	5562	15.46

Table 1 - Machine Stops Caused by the Open Nest Detector in a Two-month Period

The open nest detector can account for about 20% of machine stops during production. To put this into perspective, this would translate to around 35 hours or 2100 minutes of machine production per month, assuming an eight-hour work day.

Based on information gathered from different machine operators, about half of the stops caused by the open nest detector are a *false positive*, meaning that the station is faulty in detection. Input from several mechanics and engineers suggested the following causes:

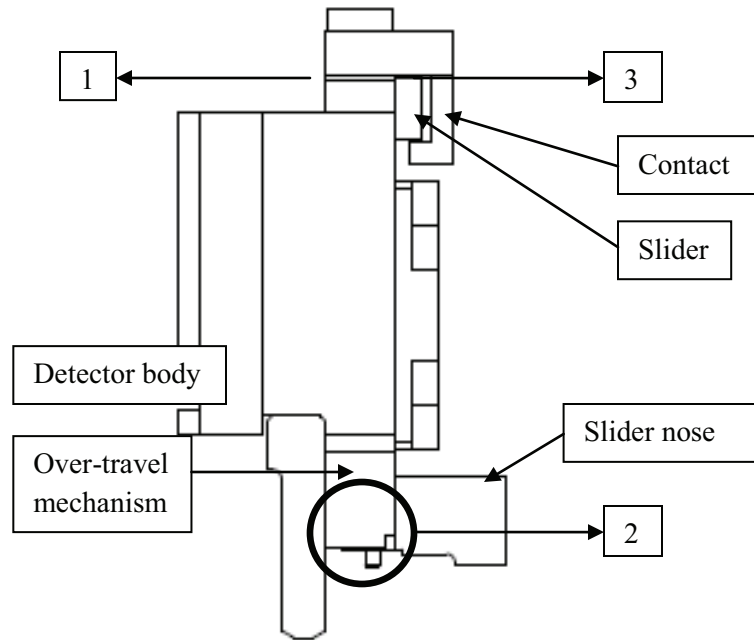


Figure 4 - False positive causes on the Open Nest Detector

- 1. Insulation fails due to moisture-** The insulation between the contact and the over-travel housing needs to be kept dry. If moisture is accumulated in the insulator, the over-travel mechanism will be electrically charged. The over-travel housing and contact will form a circuit with the slider, and report a false positive.
- 2. Wear at the impact surface of the over travel mechanism-** The over travel housing comes in contact with the nest every cycle, causing the contact area (circled) to wear out. This results in an extra travel for the slider, and a false detection of an error.
- 3. Rust between the contact and the slider-** Rust can develop between the contact and the slider, which prevents electrical contact and the “fail” signal to be emitted.
- 4. Electrical to mechanical timing mismatch-** The electrical timing in which the detection takes place may sometimes differ from the mechanical timing of the detector. In other words, there is a difference between the cam shaft and the PLC.

Many of the problems listed above occurred because of the small 0.003 inch gap adjusted for detection. Therefore, magnifying the 0.003 inch of upward motion caused by a fail criterion would solve some of these problems. Another major cause of the observed issues is the dependency on electrical contact between ferrous components.

Goal Statement

Design a robust and reliable mechanism for the empty open nest detector station to detect debris or closed nest scenarios, featuring a fail-safe check every cycle.

Design Specifications

- 1.) Detect the presence of debris on the break pin with 0.003 inch thickness or greater.
- 2.) Detect whether the nest jaw is open or closed.
- 3.) Convert debris presence into Boolean electrical signal.
- 4.) Retain fail-safe operation of the existing detector that must occur every cycle.
- 5.) Mechanism must allow access to yoke assembly three inches above detector.
- 6.) Detector can only extend three inches to the front, in the direction of indexing.

Computation Modeling

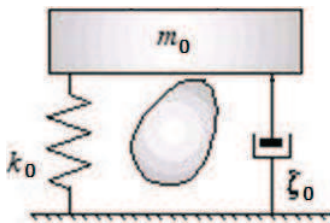


Figure 5 - One DOF, one mass model [1]

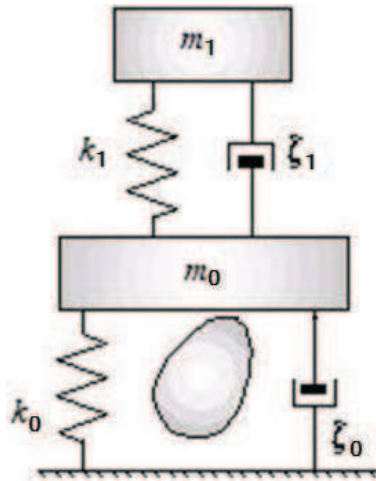


Figure 6 - One DOF, two mass model [1]

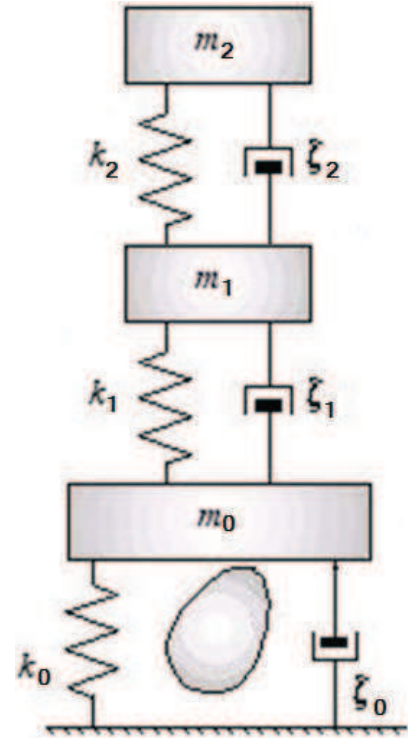


Figure 7 - Two DOF, three mass model [1]

The behavior of the open-empty nest detector station was modeled with multi-degree of freedom (DOF) models. Three models of increasing complexity were created: one DOF (one mass), one DOF (two masses), and two DOF (three masses). These models are schematically presented in Figure 5, Figure 6 and Figure 7. Outputs of the computations are compared to measurements from accelerometers attached to appropriate locations. If the computation and experimental data are aligned, then the behaviors of the new designs can be approximated with similar models.

These computational models require that each moving component be defined in terms of its own equivalent mass and spring constant. A model of all the moving components for the open empty nest detector station is shown in Figure 8. Equivalent masses are created for rotating links that are pivoted at some fixed radius. Given the rotational inertia of a part about its rotating axis, a point mass can be placed at the pivoted radius to create the same inertia. This is accomplished by using the definition of the rotational inertia of a point mass:

$$Inertia_{rotational} = mass \times radius^2$$

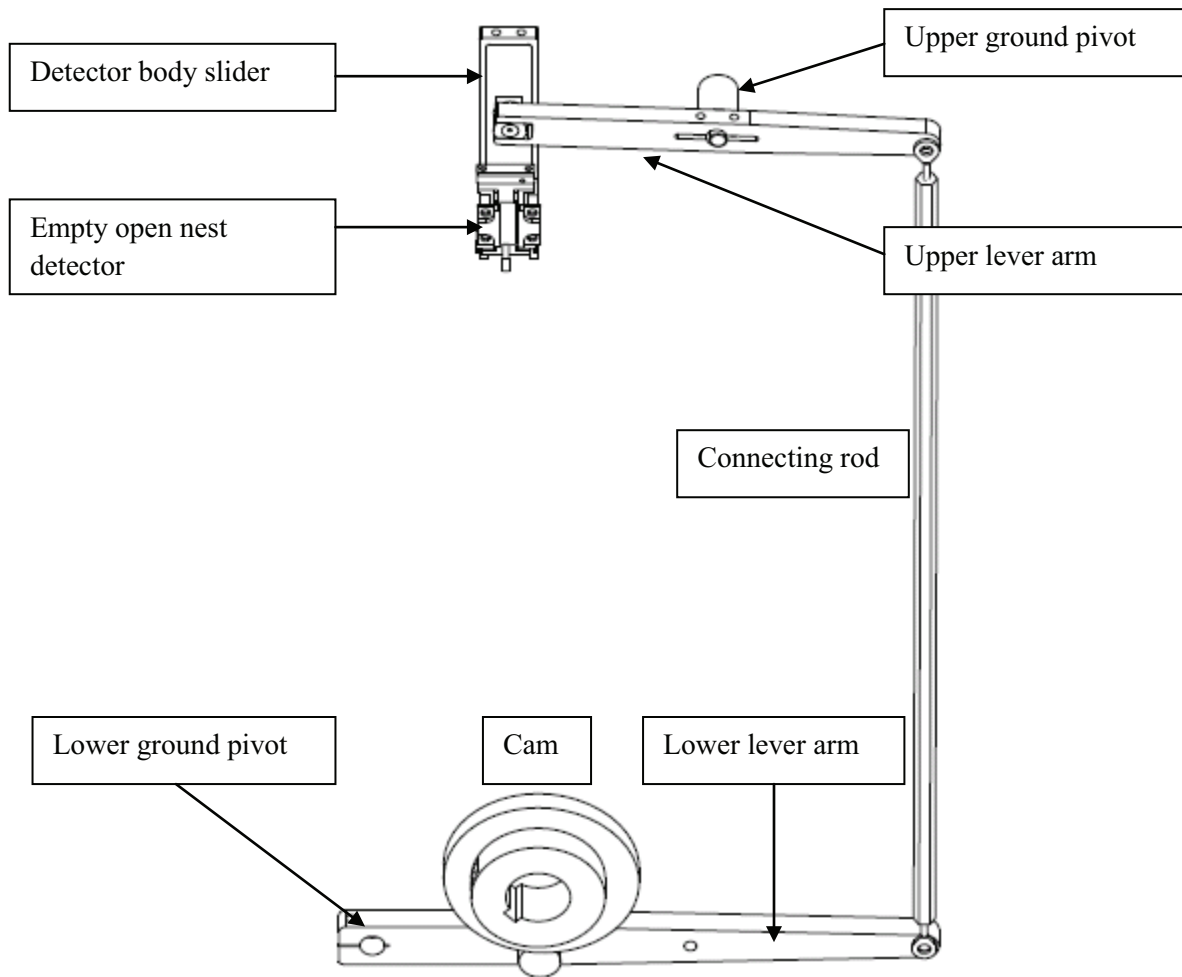


Figure 8 - Moving components of the Empty Open Nest Detector station

Spring constant of a load bearing component can be calculated by its geometry, material, and mounting method. The deflection of the component for a given load can be calculated either analytically or via finite element methods (FEM). The result of a FEM analysis is shown in Figure 9, which shows the deflection of the lower lever arm with a 100 pounds force applied to its tip. These values will then be lumped into strategic points that bear physical significance.

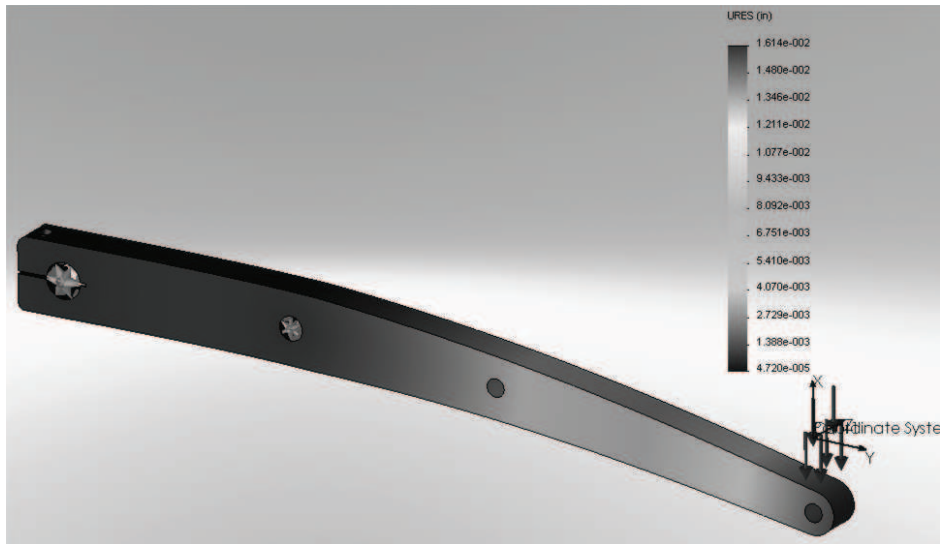


Figure 9 - Deflection of lower lever arm with applied force as calculated by FEM

A one mass model, schematically shown in Figure 5, is used to define the spring constant required to hold the follower train against the cam[1]. The equivalent mass of the follower train is concentrated at the cam roller, and is designated as m_0 . This model serves little purpose to this study, because the spring needed for cam contact has already been designed and function as expected.

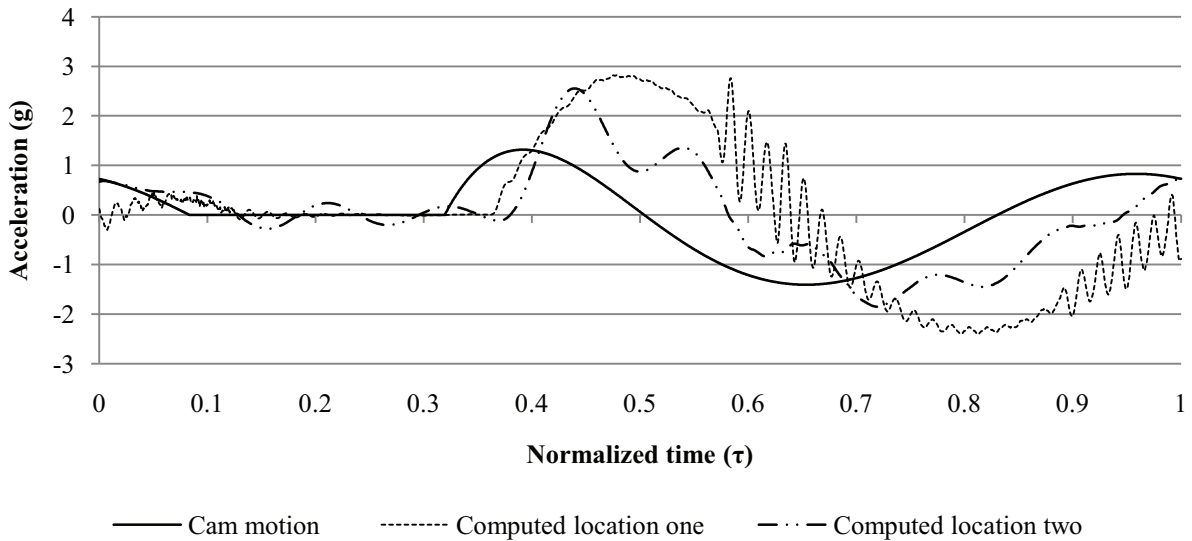


Figure 10 - Computations results of three mass, three DOF model

A two mass model (Figure 6) is created to predict the motion of the detector body with the elasticity of the linkages taken into account. The mass of the detector body and over-travel mechanism were separated from the remainder of the follower train. These masses are designated as m_1 , as shown in Figure 6, while the two lever arms and connecting rod is lumped into m_0 . However, the equivalent springs of the connecting components are very stiff, and the resulting computation was unrealistic.

A more detailed analysis was created with a two-DOF model that takes into consideration the over-travel spring which couples the over-travel housing to the detector body. This over-travel spring is significant softer than the elasticity of the solid connecting rods and levers, and generates a low numerical value for k_2 . The placement of the springs k_1 and k_2 is shown in Figure 7. The numeric values of these springs created the expected high frequency noise in the computed values. As indicated by Figure 7, the masses of the follower train are divided into three masses. The mass m_2 consist of the components hanging on the over-travel mechanism, including the slider, contact and the over-travel mechanism itself. The mass m_1 consist of the detector body, while the remainders of the parts are lumped into m_0 .

Figure 10 shows the result of this computation showing the behavior of the three masses over one cycle of machine time (τ). There exists a slight phase lag at the initial lift motion after 0.40τ between the motions of the three components, which is caused by the spring's ability to resist motion. The over-travel mechanism denoted as m_2 demonstrate low frequency oscillations where as the detector body, m_1 , show more high frequency noise.

Measured Data

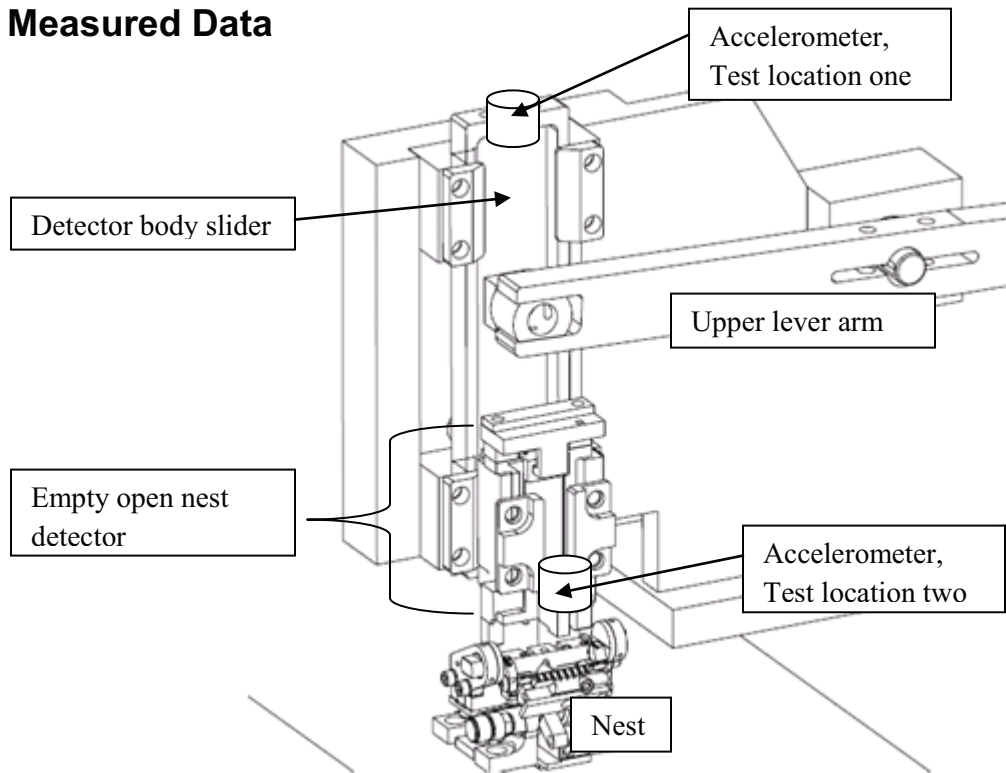


Figure 11 - Accelerometer locations during testing

For the purpose of this project, two strategic points on the station are selected and their locations are shown in Figure 11. Location one, at the top of the detector, is on the component closest to the contact point while not hung on a spring. Location two represents the closest point possible to the contact location. The two locations properly reflect the mass placement of the computation model presented.

Test data are graphed in Figure 12, where the two data sets are layers on top of the theoretical motion. As predicted by the computation model, some phase lag is present between 0.30τ and 0.40τ after the dwell motion.

The identical motion of the two test locations in the range between 0.45τ and 0.94τ (Figure 12) was not predicted by the computed data. This matching motion is caused by the coupling of the over-travel mechanism as the detector lifts from the break pin. In the case of the simulated model, the masses are considered to be hung from each connecting mass via a spring.

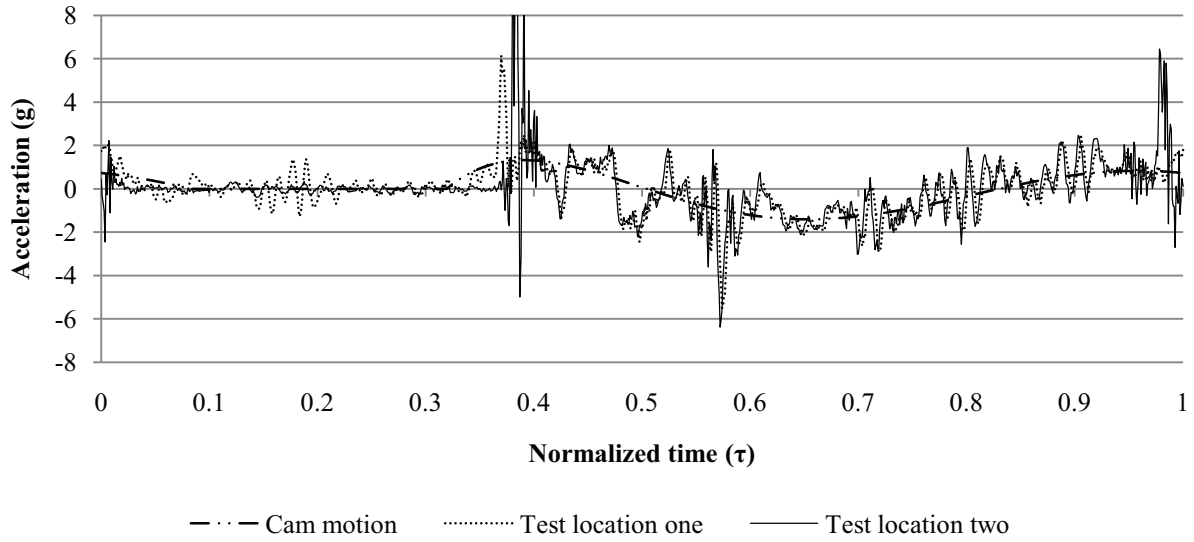


Figure 12 - Test data overlaid with theoretical accelerations

There are also two large spikes of measured accelerations at 0.39τ and 0.98τ , which are generated by (1) the coupling of the over-travel mechanism, and (2) the impact between the detector and the break pin. The larger of the two spikes corresponds to the coupling of the over-travel mechanism after the dwell.

Theoretical and Measured Data Comparison

The physical Empty Open Nest Detector has changing boundary conditions, because the over-travel mechanism couples and decouples every cycle. With that fact in mind, there would be expected difference in the computed model and measured data. Due to the complexity of the situation and the limited time allotted for this project, the changing boundary condition problem was never attempted. For the purpose of this project, the most important regions are the detection windows for the dwell and plunge motion, where the detections occur.

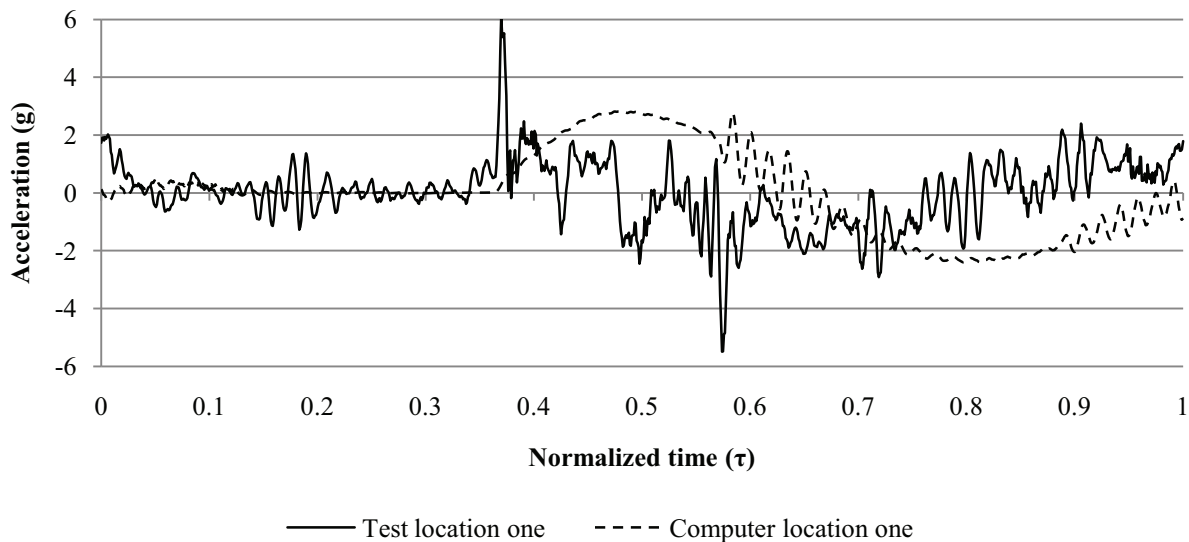


Figure 13 - Mass one acceleration comparison

Figure 13 shows a notable difference between the measured acceleration and computed acceleration for mass one, the detector body. There are some high frequency noises in both data sets throughout the motion, as expected. A slight retardation of the computed acceleration phase around 0.38τ indicates that the calculated phase shift was not as severe as originally thought. During the coupled motion of the over-travel mechanism, a significant difference is evident. The equivalent mass of the over-travel mechanism is approximately 30% of that of the detector body, and is a large contributor to the error.

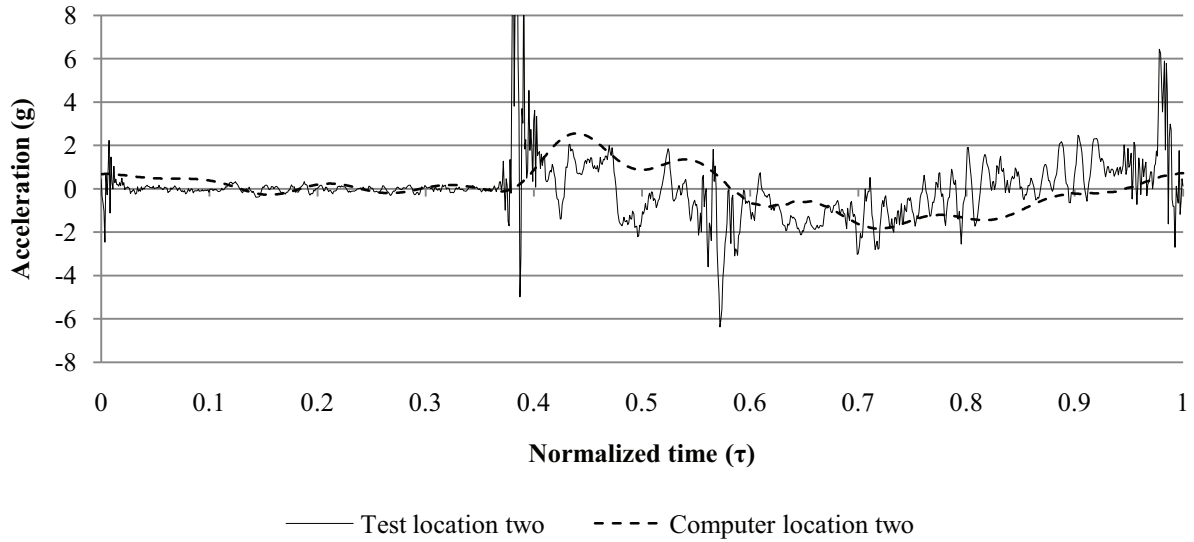


Figure 14 - Mass two acceleration comparisons

Acceleration data for the over-travel housing is shown in Figure 14, where the differences between the two data sets are much less than those recorded for the detector body. The phase shift at 0.38τ is much closer together, and shows that the phase lag predicted is correct. Over the lift motion between 0.45τ and 0.94τ , there is much more high frequency noise in the recorded data. Overall, the shapes of the computed and measured accelerations are similar.

Design Ideas

Single Lever Solutions

The levers are design to amplify a 0.003 inch motion that could be caused by debris presence or a closed nest. In these solutions, the moving link is pivoted on a frame rigidly attached to the over-travel mechanism, and actuated by the slider's nose 0.5 inch away. To reduce frictional wear, a cam roller can be employed instead of a pin to transfer the motion from the slider to the link. The link is spring loaded onto the nose to prevent the two surfaces from separating, so that the slider and roller are kept in constant contact.

Single Lever with Through Beam

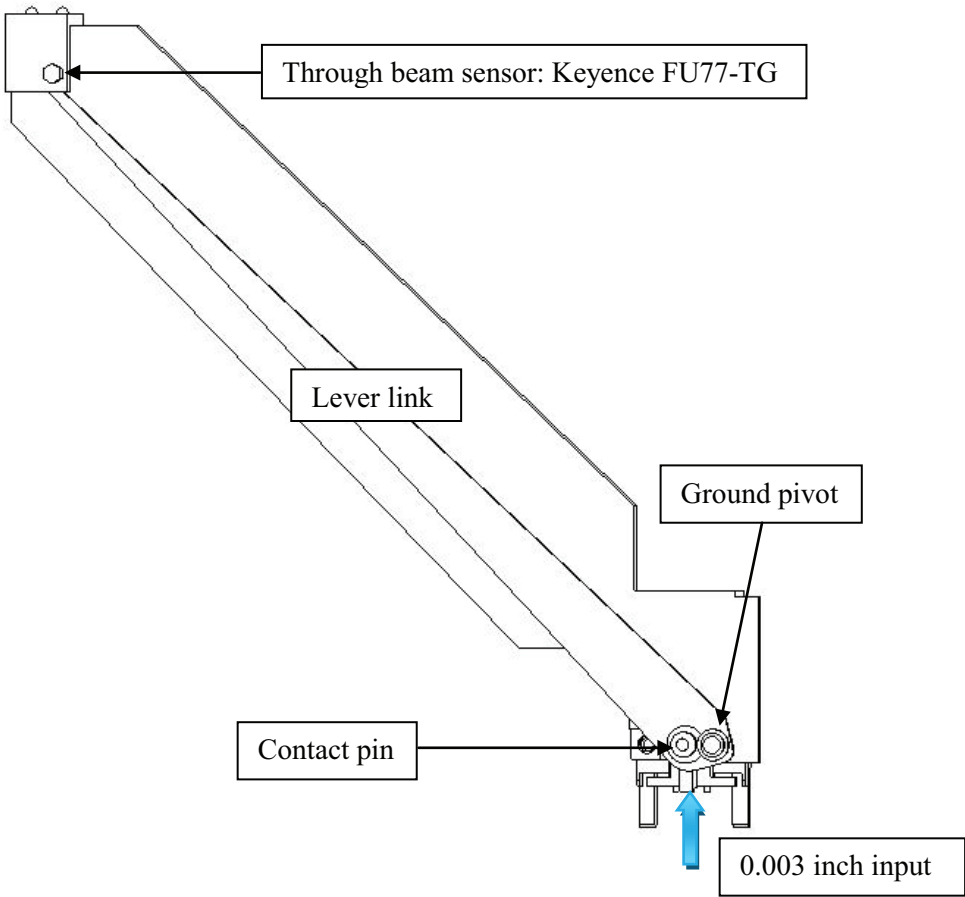


Figure 15 - 15 Inch Lever Design

This design uses a through beam sensor (Keyence FU-77TG) to detect the movement of the 15 inch lever. Since the through beam has a diameter of 0.10 inch, the link's motion must be sufficient to produce such difference between the normal and fail condition. The link length needed to provide this 0.10 inch motion is approximately 15 inches. The design for the 15 inch lever is shown in Figure 15.

The fail-safe mechanism for this design is as follows:

- When the detector is in the air (fail-safe check) – The sensor's beam is not broken
- When the detector is fully on the nest (normal condition) – The sensor's beam is broken
- When the nest is closed or debris is present (fail condition) – The sensor's beam is not broken

The length of the link causes several major problems that hindered the design's success. The amplified movement requires a 15 inch long link. Such a long link will not only cause vibration issues, but also protrude outside of the machine guard.

Single Lever with Displacement Sensor

A different single link design was produced to reduce the shortcomings of the single link through beam design. By replacing the through beam with a displacement sensor (Keyence EV-108M), a much smaller amplification was needed (Figure 16).

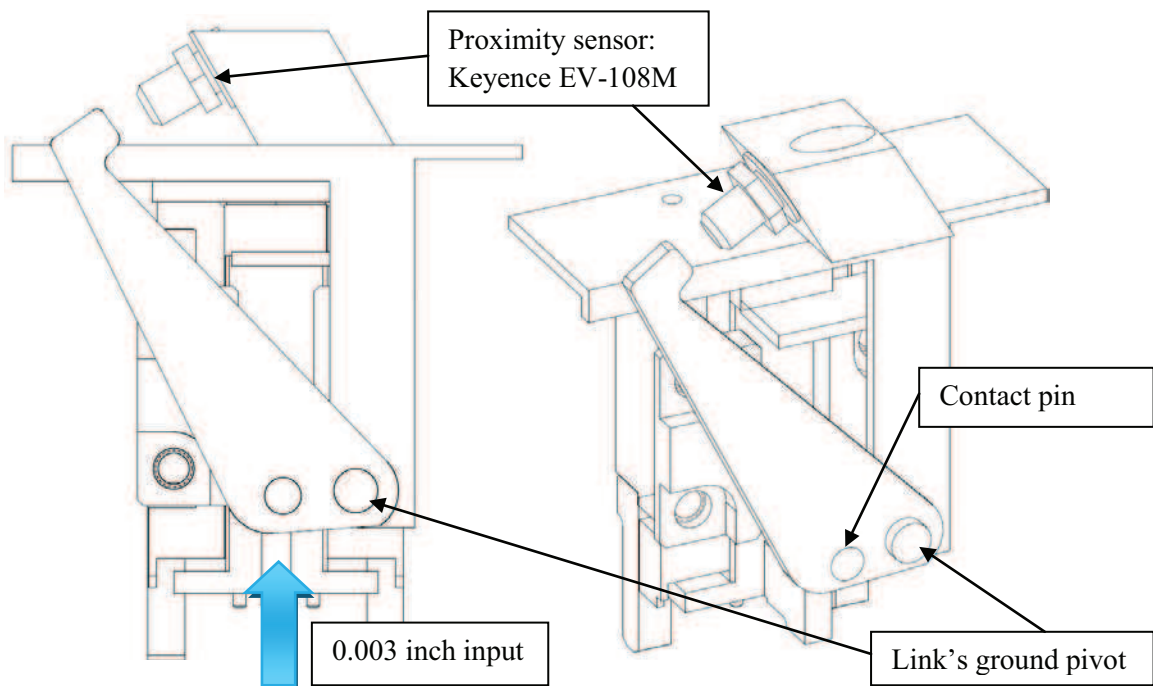


Figure 16 – Single-Lever Mechanism with Proximity Sensor

With a shorter lever, the vibration would not be as large as with to the 15 inch lever. However, this design requires the use of a much more sensitive sensor, which increases the complexity of the initial setup. The detector senses motion by a conductive method, and translates the proximity of objects into an analog electrical signal. The displacement sensor can be programmed to output different signals at three ranges.

- When the detector is in the air (fail-safe check) – The link is furthest from the sensor, and the voltage is lowest. This would be the lower “fail” range.
- When the detector is fully on the nest (normal condition) – The voltage is in its middle range. A range needs to be carefully selected so that it is not overly sensitive, but can still pick up the presence of debris.
- When the nest is closed or debris is present (fail condition) – The voltage is highest because the link is closet. This is set to be the high “fail” range.

A similar setup is currently in used on a newer machine in the production facility. As expected, the middle “fail” range is difficult to setup, and has been reported to be overly sensitive. From the company’s standpoint, the sensor is set up to be conservative so that flawed products are not delivered. Operators and mechanics have reported that thin filaments and oil residue can trigger the fail mechanism on the new machines.

Another problem with this design is the limited computing power of the machine controllers. The logic controllers on the newer machines have greater computing abilities necessary for this sensor. Furthermore, the sensor is difficult to set up since the three ranges need to be carefully set to accommodate the 0.003 inch motion.

Slider Solution

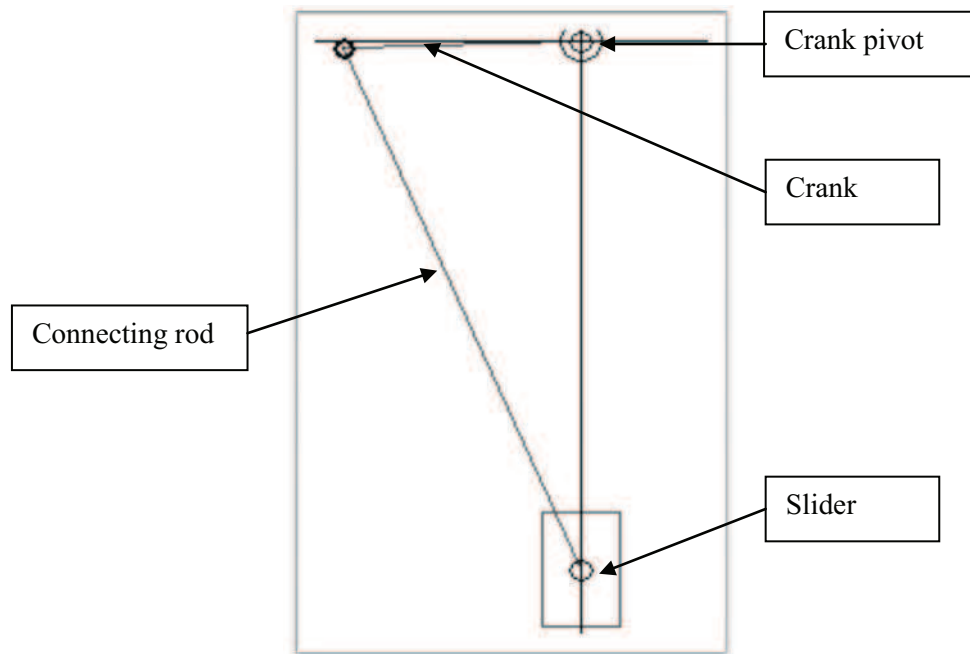


Figure 17 - Slider Design

The idea of this design is to move the slider with a 0.003 inch motion to rotate the crank. The slider shown in Figure 17 would be rigidly attached to the nose of the slider, and translate the linear motion into an angular motion. If debris is present, the crank would rotate and trip the sensor.

The size of the crank was a major constraint to this design, in order for the crank to rotate through a significant angle, the crank would have to be very small. A short crank will travel through a larger angle from the 0.003 inch input. This leads to the problem of designing a small link that is sufficiently robust for the application. In addition, the sensor would have to be able to sense the motion of a small object. For these reasons, the design was deemed unfeasible.

Four-bar Linkage Solution

A four-bar linkage design originated from a two staged single lever solution. This design uses four links (including ground) to amplify the 0.003 inch motion. The lengths between the pins are carefully selected to maximize the deflection at the fourth link.

The four-bar linkage utilizes a fail-safe mechanism and operates in a similar fashion compare to the single link through beam solution.

Four-bar Linkage Design

The four-bar linkage was chosen for further development for several considerations: vibrations, complexity, robustness, ease of setup, compactness, and costs.

Initial Four-bar Mechanism

The first four-bar design was positioned on the top of the slider and detector as shown in Figure 18. A pin attached to the crank would transfer the 0.003 inch motion into the linkage. This pin will have one end contacting the slider's top while pressed into the crank at the other end. Any motion in the slider would be converted into an angular input in the crank. The linkage would then magnify the angular input via a set of links. This magnified motion would be detected by an Optical Sensor (Fairchild Slotted Switch QVB21114). The arrangement of the links, slider, and other components are shown Figure 18.

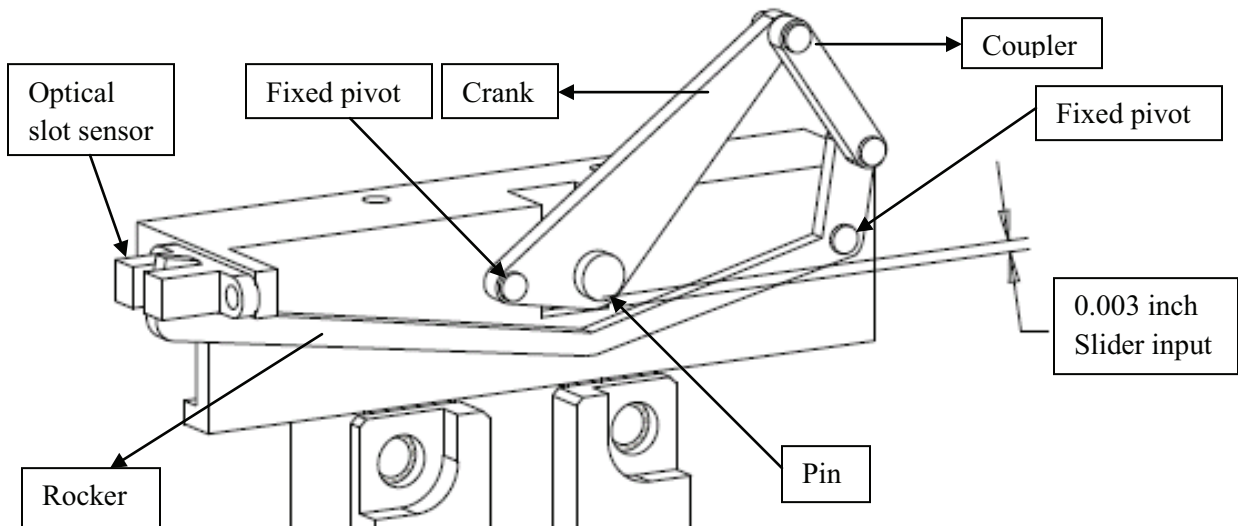


Figure 18 - Initial Four-bar Mechanism Design

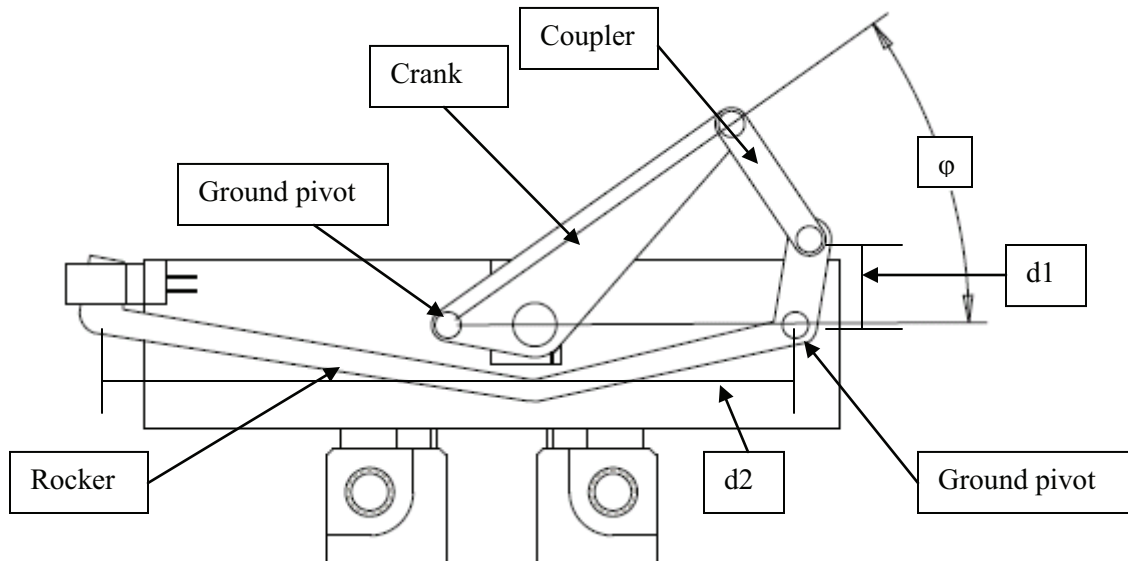


Figure 19 – Four-bar Mechanism Front View

The crank, coupler, and rocker were designed to optimize the displacement from the slider. Position analysis was performed for different sets of link lengths. The analysis began by maximizing the angular motion caused by the slider motion of 0.003 inch. Considering that a 0.25 inch pin was required for strength reasons, the shortest possible distance between the ground pivot and the contact pin was 0.50 inch. With a contact pin position 0.5 inch away from the ground pivot, a 0.003in linear travel would generate a 0.344 degree of rotation. A four-bar linkage is designed to maximize an angular input of 0.344degree, and different link lengths were iterated to this end

The crank is designed so that the starting angle of the four-bar linkage is not necessarily zero, this is achieved by offsetting the pin and the crank-to-coupler pivot by some angle ϕ as indicated in Figure 19. With this geometry, the starting angle of the four-bar linkage is ϕ as defined on the crank, and the goal is to maximize the rocker's motion between ϕ and $\phi+0.344$ degrees. The angular displacement of the rocker between crank angle ϕ and $\phi+0.344$ degree is graphed in Figure 20. Note that not all positions are defined because at some crank angles the linkage is indeterminate.

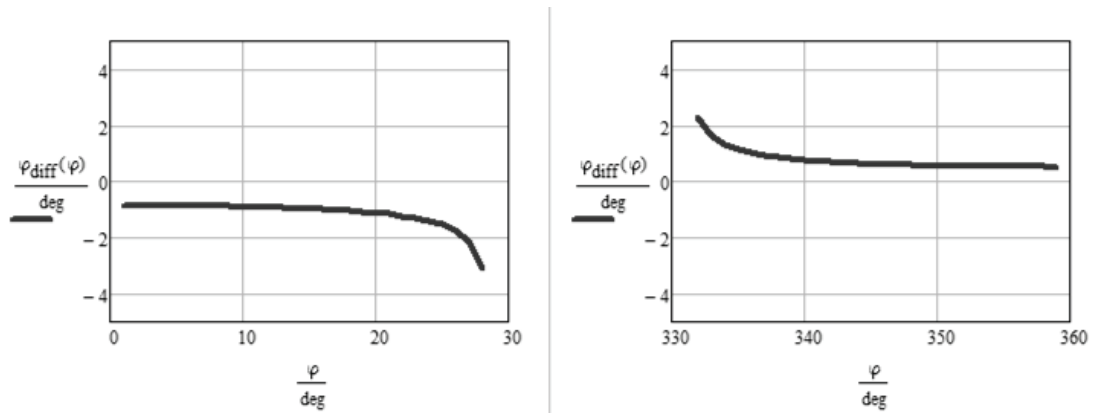


Figure 20 - Optimizing Crank Geometry

For this initial lay out, the optimized φ was found to be approximately 27 degrees. A starting angle of 27 degrees on the crank would generate an angular travel of 2.13 degrees at the rocker, a great increase from the original 0.344 travel. This angular displacement would then be transformed into a linear displacement at the end of the rocker. This linear displacement can be maximized using a lever-like geometry for the rocker with different ratios.

Depending on the ground-to-coupler (d_1 on Figure 19) to ground-to-end of link (d_2 on Figure 19) used on the rocker of this additional material, the linear displacement can vary. For this initial design, a 4 inch rocker length would generate a 0.150 inch linear displacement, which is close to a 50 times amplification from the original 0.003 inch travel from the slider.

Optimized Four-bar Mechanism

Further developments led to the design shown in Figure 21, which places the links on different planes. This design allows for much stronger pins on all the links and stronger links that will encounter less vibration issues. Furthermore, a cam roller was used to replace the contact pin. The optimal link lengths are determined to be: 2.5 inch ground, 0.50 inch coupler, 0.50 inch rocker, and 3.0 inch crank. Based on these link lengths, the crank is extended to include a pickup point to contact the slider, and the rocker is extended to trigger a sensor.

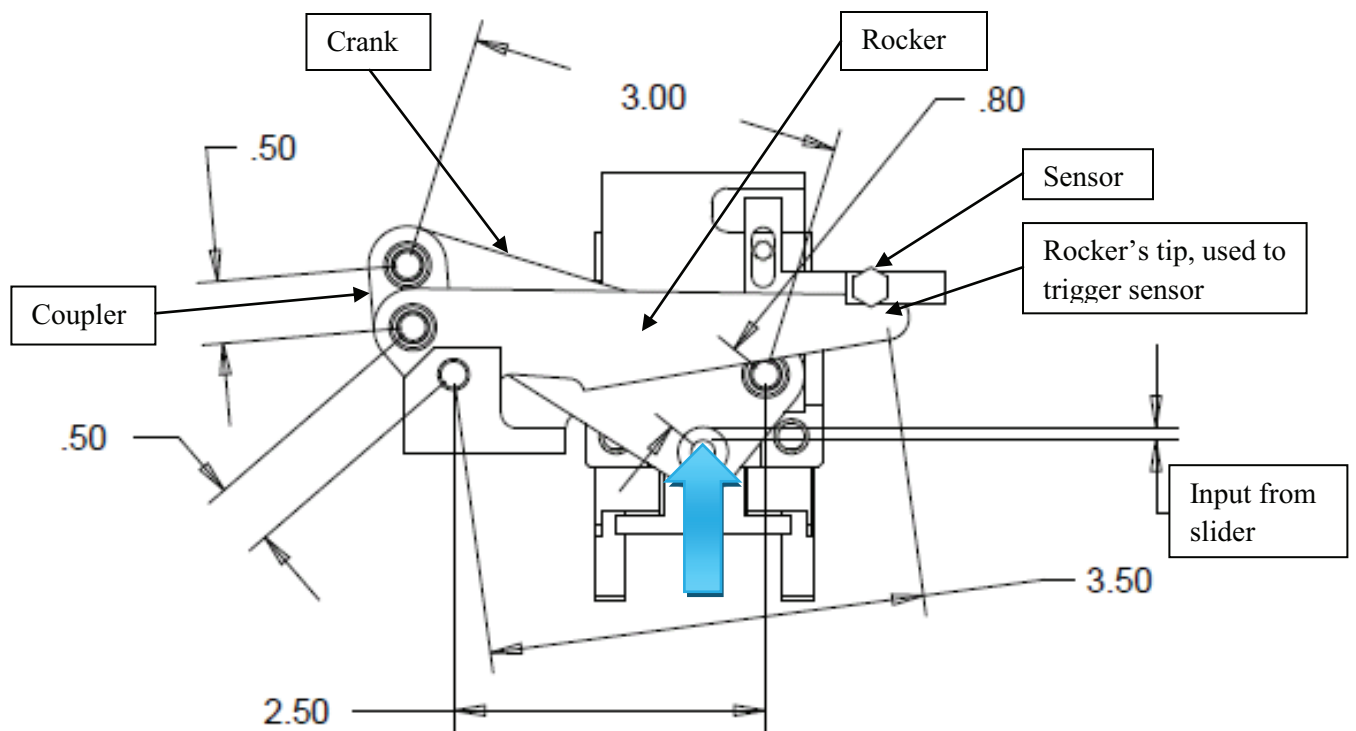


Figure 21 - Final Four-bar Mechanism Front View

Frame

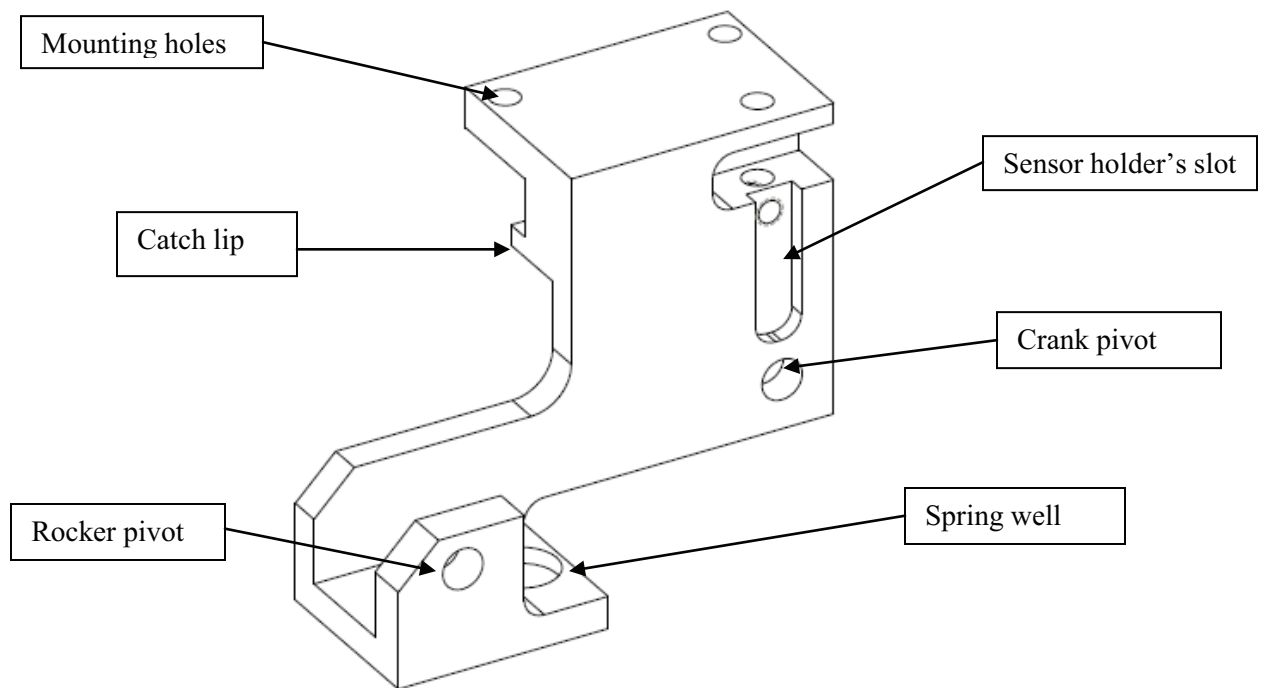


Figure 22 - Frame for four-bar solution

A frame was created to serve as a ground for the pivots on the moving links (crank, coupler, and rocker) in the assembly. The mounting frame designed in this project is shown in Figure 22, where several important features are highlighted. This frame will be mounted onto the top of the over-travel housing via the two existing holes created for the contact which the frame will replace.

Several geometrical features are necessary to accommodate other mating parts. A catch lip was needed to prevent the slider from falling down into the conveyor. A similar feature was found on the contact component that has been replaced. In addition, a slot was cut on the right of the part to mount a sensor holder. This separation of the frame and sensor holder allows for slight adjustments in the beam's height to accommodate manufacturing variations.

Two links are directly pivoted to the frame, the crank and rocker, and are attached to their respective pivots as indicated in Figure 22. These links are mounted on two planes off set in their axial direction, so that the links can be made wider and stiffer and not collide with any other links.

On the rocker pivot extension built on the left of the frame, a spring well was created so that a spring can be inserted to force close the roller against the slider. A matching notch was created in the rocker to retain the spring as well.

Sensor Holder

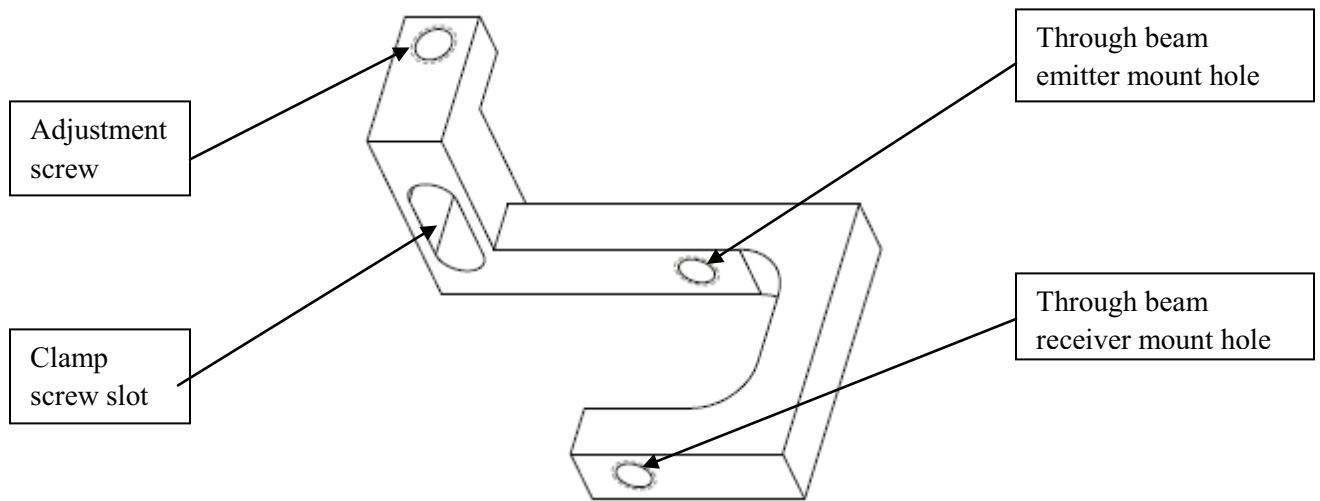


Figure 23 - Beam holder for four-bar solution

A separate beam holder was created to mount the two stations of the through beam; the geometry of the part is shown in Figure 23. Doing so will allow a mechanic to adjust the height of the “pass” condition to accommodate manufacturing error. An arc on the component was required to allow for this adjustment so that the beam holder will not interfere with the other moving links. An inverted “L” shaped piece was added to this arc to mate with the beam holder’s slot on the frame.

The Crank

The geometry of the crank was modified so that the pin resting on the slider would not be collinear to the ground pin. Using trigonometry, a lateral offset could increase the angular displacement caused by the slider. Three positions were defined for the motion of the crank as shown in Figure 24. The variables ‘a’ and ‘b’ are defined in Figure 21.

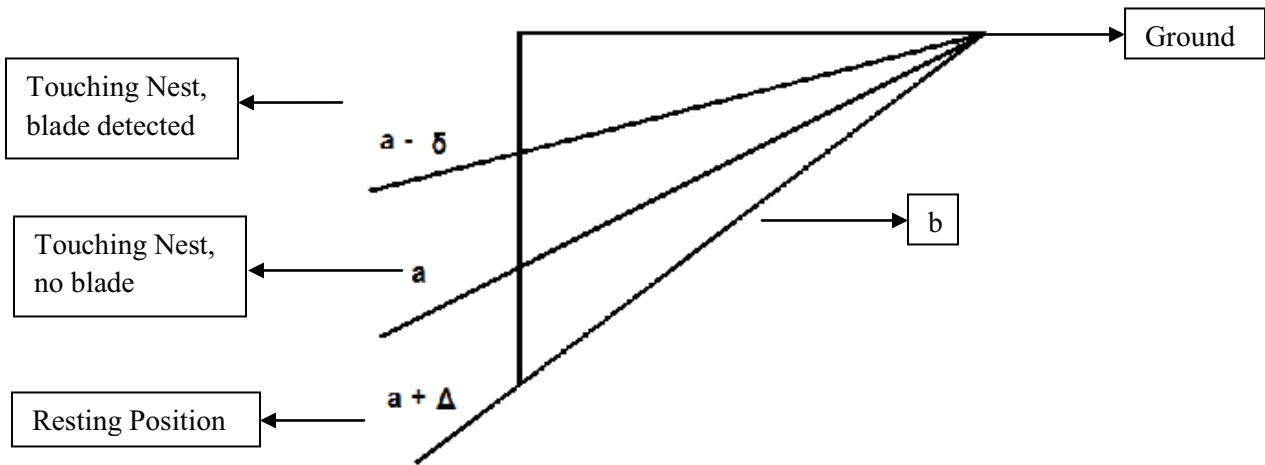


Figure 24 - Determining Crank Pin Positions

The angular travel caused by the 0.003 inch of upward travel is graphed as a function of the distance 'a' as a fraction of 'b' in Figure 25. The angular displacement increase significantly as $a \rightarrow b$. When $a = b$, the link would be vertical, and the crank would turn into a structure, at angles where 'a' and 'b' are similar, the pressure angle would be too low and inefficient at force transmission. The optimal distance 'a' was found to be 80% of 'b', which moves away from the pressure angle problem slightly while providing a significant increase in angular displacement.

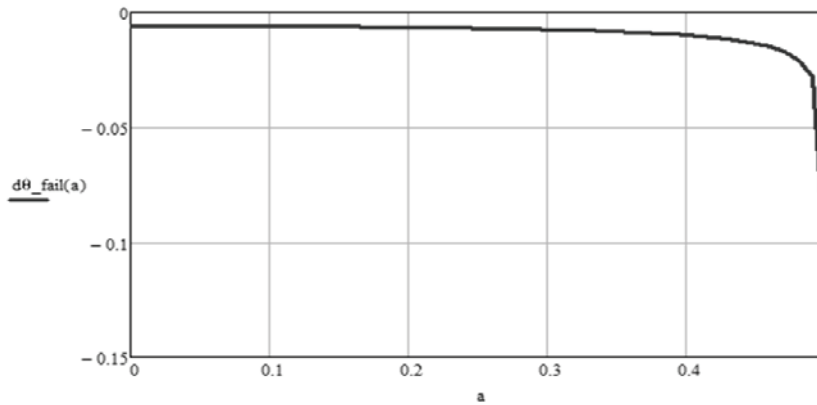


Figure 25 - Determining Crank Pin Positions

As done in the previous linkage analysis, angle ϕ from the horizontal was also solved for the crank. The optimized ϕ was found to be 15 degrees with a link length of 3 inches.

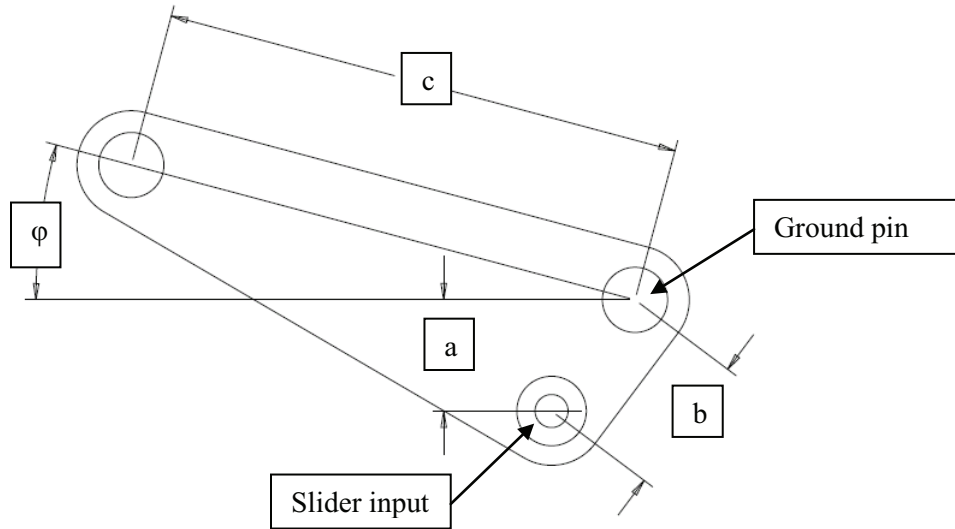


Figure 26 - Final Crank Dimensions

The geometry of the crank is defined in Figure 26. Length ‘b’, the distance between the slider input on the crank and the ground pin, was finalized to be 0.8 inch. Length ‘c’ was set to be 3 inches resulting in an angular rotation of 0.569 degree for the crank from the 0.003 inch slide input.

The Coupler

The purpose of the coupler is to connect the crank to the rocker. From numerous iterations of the linkage, matching the length of ‘d’ with that of ‘e’ creates the greatest amount of motion for the rocker. Both of these distances are set to 0.5 inch. Figure 27 shows the coupler’s geometry, a small indentation on one side was necessary to accommodate for a snap ring and washer set.

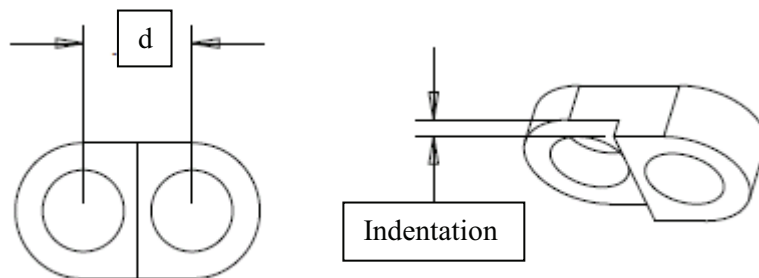


Figure 27 – Coupler Geometry and Dimension

The Rocker

Given the 0.569 degree angular rotation of the crank, length 'd' of the coupler and 'e' of the rocker were sized to create the greatest possible rotation of the rocker. The resulting geometry of the rocker is shown in Figure 28, and would generate 2.17 degrees of rocker rotation from 0.569 degree of crank input.

Length 'e' is 0.5 inch and 'f' was chosen to be 3.8 inch, 'f' was chosen to translate the 2.17 degree of rotation into a linear distance. This resulted in a 0.21 inch linear displacement at the detection area at the tip of the rocker. A spring cap was added at the lower side of the link to accommodate a spring so that the four-bar linkage can be force closed against the slider nose.

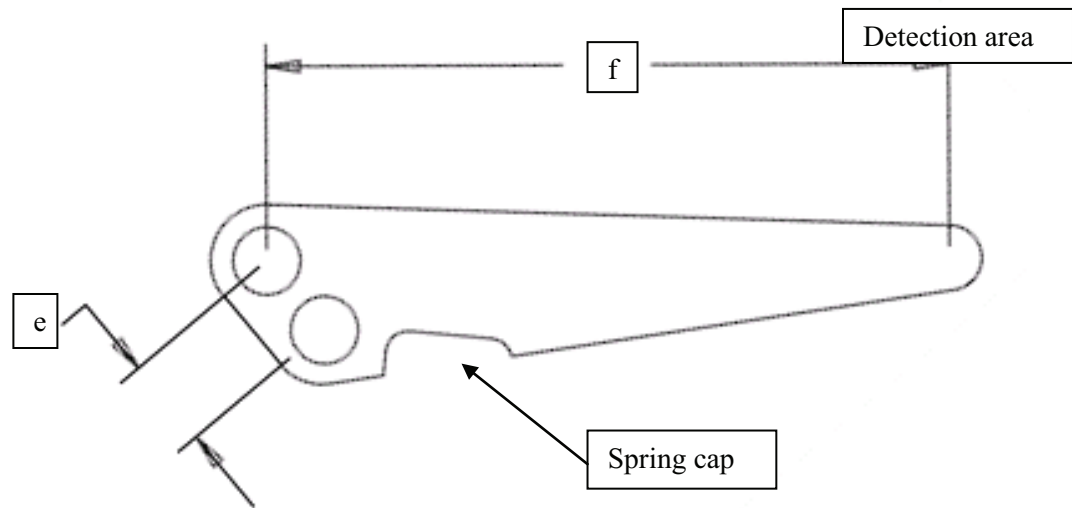


Figure 28 - Final Rocker Dimensions

Spring-Loading the Rocker

A spring was attached to the rocker to assure the four-bar system is always in contact with the detector slider. Placing the spring on the rocker instead of the crank would also help reduce backlash. In order to determine the spring's characteristics, the four-bar linkage was modeled as a one DOF (one mass) model as shown in Figure 5. The effective mass found for the system was of 1.494 kg.

Based on the geometry of the frame, a spring of a 0.75 inch free-length was chosen [2]. Maximum deflection on the spring would be of about 0.25 inches due to the 0.087 inch stroke at the rocker's spring cap. Several springs has the necessary deflection limits, #257[2] was favorable because it provides the linkage with a preload of 3.158lbf (15.647 N).

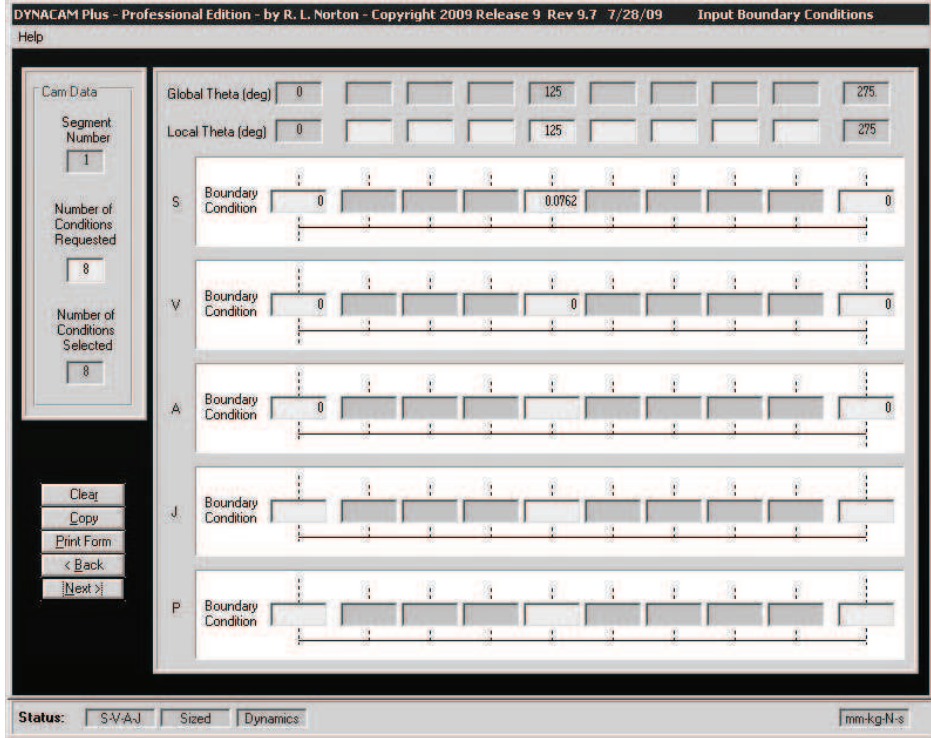


Figure 29 - Modifying the station cam to simulate detector motion

The cam that drives the Empty Open Nest Detector station was modified to simulate the slider motion with a 0.875 stroke (Figure 29). This modified cam was used to simulate the behavior of the four-bar linkage system with the calculated spring, and it was found that the spring selected will withstand the motion generated by the detector (Figure 30).

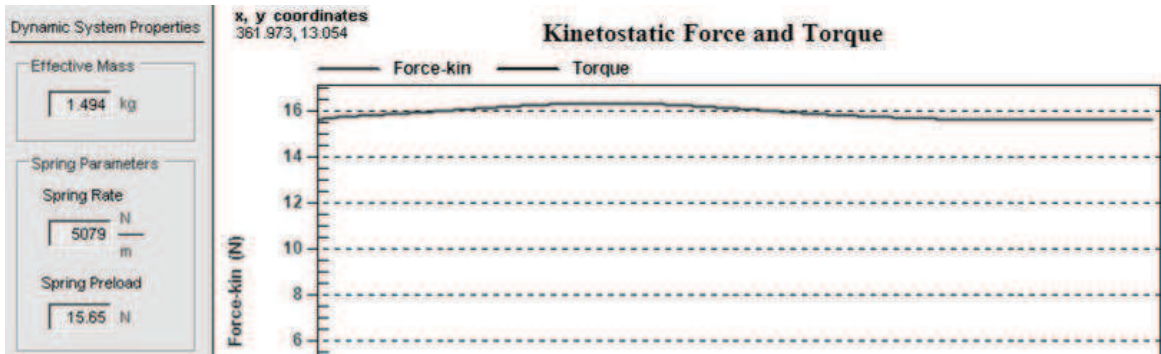


Figure 30 - Spring-loaded four-bar linkage system

Detection

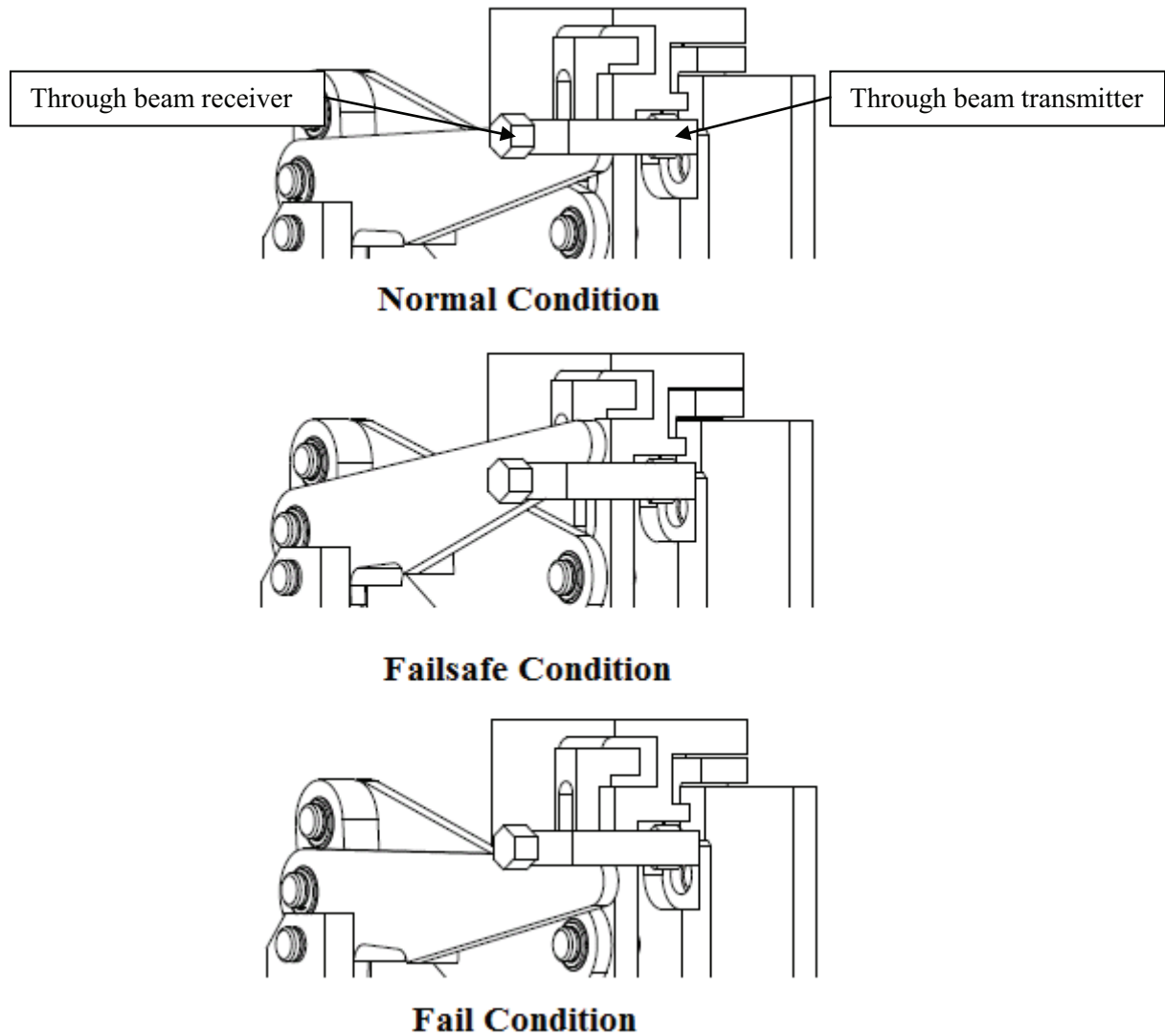


Figure 31 -Four-Bar Linkage Fail-Safe Conditions

This design utilizes a 0.10 inch diameter through beam sensor (Keyence FU-77TG) to detect the movement of the rocker. A fail-safe mechanism is demonstrated in Figure 31, where “fail” signal is generated by the passing of the beam, and “pass” is generated by a blocked beam. At the normal condition, the link’s tip would block the through beam, but at failsafe and fail conditions, the through beam would be allowed through. Blocking of the beam is accomplished by two different methods, for the failsafe condition, the link is lifted upwards and away from the sensor, whereas in the fail condition, the link moved through the beam and come to rest under the beam.

Error Analysis

Links (+0.005in)	Displacement (inches)
All 4	0.14282
1,2,3	0.14825
1,2,4	0.1457
1,3,4	0.14078
2,3,4	0.14382
1,2	0.15167
1,3	0.14593
1,4	0.14339
2,3	0.14943
2,4	0.14688
3,4	0.14168
1	0.14901
2	0.15308
3	0.14698
4	0.14445
All 4 minus	0.15026
Max	0.15308
Min	0.14078
Difference of travel	0.0123

Table 2 - Error Analysis

A major concern for this design is the tolerances between the pins, which are the link lengths. If too much backlash exists between the parts, the 0.003 inch motion from the detector would be nullified, meaning that the tolerances between the parts could potentially silence the 0.003 inch motion from the slider.

An error analysis was conducted to investigate the amount of allowable tolerance between the pin locations on the links. The worse-case tolerance was assumed to be ± 0.005 inch. The links length listed in the first column in Table 2 was increased by 0.005 inch and those not listed were decreased by 0.005 inch, with an exception on “All 4 minus,” where all 4 links were decreased by 0.005 inch.

The end results display the maximum (0.153 inches) and minimum (0.140 inches) linear distance that the rocker will move given the tolerances. Therefore, the rocker’s travel has a difference of 0.012 inch, or that a 0.005 inch tolerance on each link would generate a 0.012 inch error. With the current geometry of the rocker’s tip, this error is acceptable, and the detector will continue to function as planned.

Testing Prototype

Parts were sent to an outside vendor for machining in order to test the final design. During the assembly, we discovered that the geometry of the frame made the assembly of some links difficult, especially the rocker. These difficulties are mostly caused by the proximity of the joints, which was intended during design to produce the maximum amount of motion.

When testing on the machine station, the greatest problem encountered was spring-loading placed at the rocker. The spring placed on the rocker created a preload of 3.16lbf (15.65 N) on the link, and an effective preload of 13.19lbf on the crank-slider surface on the cam roller. A schematic is shown in Figure 33 showing the locations of the applied forces. This preload on the linkage is greater than the preload on the over-travel spring and prevent the intended operation of the detector.

The spring inside the detector, as shown in Figure 32, was found to have a preload of 2.91lbf and served to maintain the over-travel mechanism in contact with the detector body until the cam pushes it further. Since the over-travel spring preload is lower, the over-travel always slides with respect to the detector body before the slider moves in the over-travel's slot. In this case, for the detector to operate over-travel spring would have to bottom out so that the over-travel housing and the detector body is touching. Only then would the cam's motion be moving the over-travel housing down towards the nest.

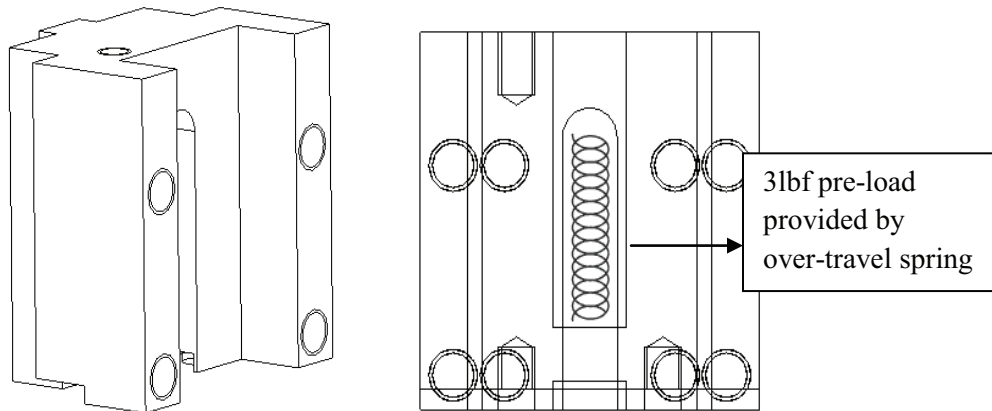


Figure 32 - Spring inside detector body

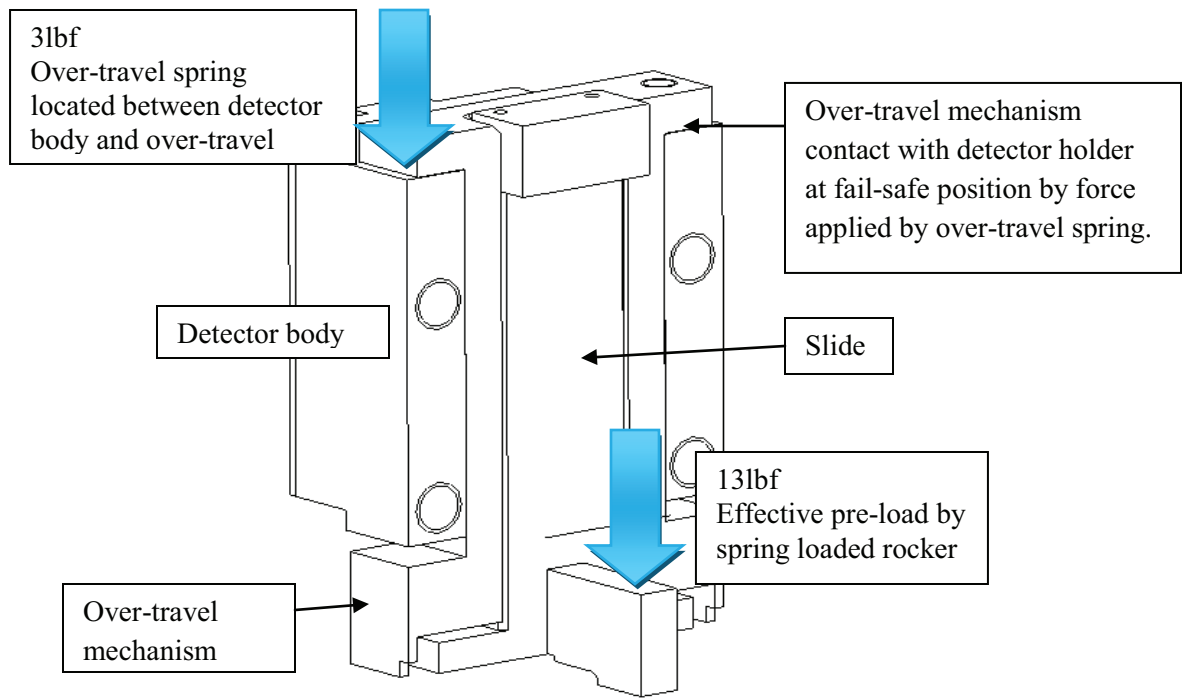


Figure 33 - Spring forces schematic on detector

The spring-loading on the linkage needed to be modified to set a preload value less than that of the detector's over-travel spring. For this purpose, the spring-loading was moved to the crank so that there would not be a multiplication factor involved. The new spring will be placed directly over the crank-slider surface with a spring constant of 2.446lb/in and a preload of 1.71bf. Modifications were made on both the crank and frame to accommodate for this spring.

Revised Prototype

In order to lessen the preload applied between the over-travel mechanism and slider, the spring was relocated to the crank instead of the rocker. As identified earlier, placing the spring directly over the crank-slider contact point would eliminate the multiplication factor that created such a strong preload in the original model. To simplify the effects of spring effects, the original springs associated with the slider is removed, since the spring loaded linkage will accomplish the same mean.

The Frame

Several other modifications were applied to the frame, as shown in Figure 34. The original spring well located near the rocker pivot was removed since the spring has been relocated. A coaxial hole was drilled

on the far wall of the rocker pivot to ease assembly and create a simple support for the rocker-ground pivot. To allow a greater distinction between the fail-safe and normal position, the catch lip was lowered so that the rocker's tip would be higher at the fail-safe position.

The spring is reallocated to the top side of the crank, this location allows for sufficient room to allow for a compression spring to act downwards on the top of the crank. This forces the cam follower to stay in contact with the slider and provide the same function as the original spring on the rocker. Figure 34 shows the modified frame with the extension on the top and a hole to accommodate a pin to prevent the spring from escaping or buckling.

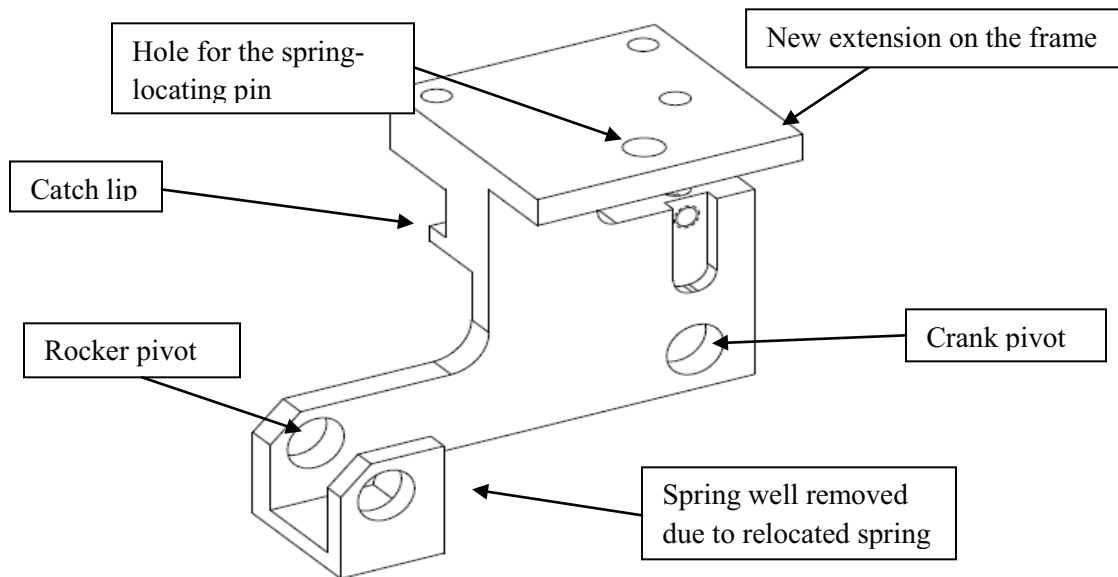


Figure 34 - Frame Design II

The Crank

The crank was be modified to provide a flat horizontal surface vertical of the cam follower for the spring to rest on. In addition, the location of this support surface determines the length of the spring. The preload from the spring has to be less than the over travel spring in order for the detector to function properly, and was made approximately half that of the over-travel spring.

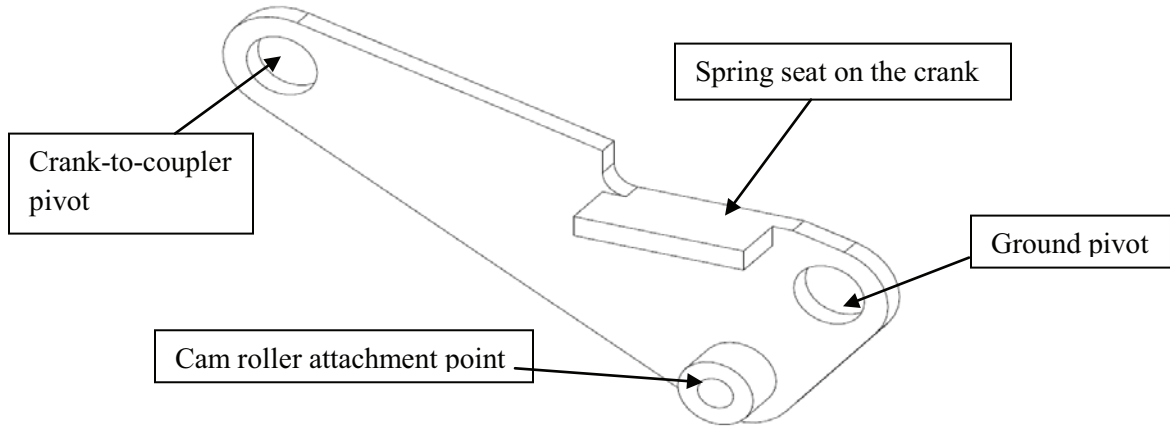


Figure 35 - Crank Design II

Spring Selection

Spring for Four-bar Pre-load Mechanism

The spring needs to be chosen with the initial length and pre-load in mind. The crank only rotates about 0.5 degree between its up-most and down-most position, so the pre-load remains largely unchanged over the course of motion. The distance between the extension on the frame and the spring seat on the crank is 1.21 inch. The outer diameter of the spring must be able to fit between the space provided by the frame and the rocker, while not interfering with the motion of the rocker.

The effective mass of the entire linkage mechanism was obtained from a lumped mass model and used in order to determine its necessary preload force. From the maximum acceleration obtained from the cam motion, the necessary force was found to be 4.6lbf. Therefore, a preload force of 5lbf was necessary from a spring. Due to geometric restriction, the spring dimensions are restricted to an outside diameter of 0.366 inch, and a compressed length of 1.24 inch. Since this 5lbf preload force on the four-bar linkage still resulted larger than the 3lbf pre-load force on the over-travel mechanism, changes on the existing over-travel spring was made.

Spring for Over-travel Mechanism

The existing over-travel mechanism has a spring constant of 8.22lb/in is compressed to a length of approximately 0.88 inch from 1.25 inch, resulting in a 2.98lb pre-load force. In order to accommodate for the dynamics forces of the linkage, a stiffer spring is needed. From our sponsor's inventory, a spring with constant 69.62lb/in, 1.1 inch free-length was chosen, providing a 15.32lb preload force.

Furthermore, two existing springs located between the slider and the over-travel mechanism, as circled in Figure 36, were removed. Their spring forces of the two slider springs complicate the interaction between the over-travel housing and the slider. The preload on the slider is replaced by the four-bar mechanism's preload, and reduces the complexity of the system..

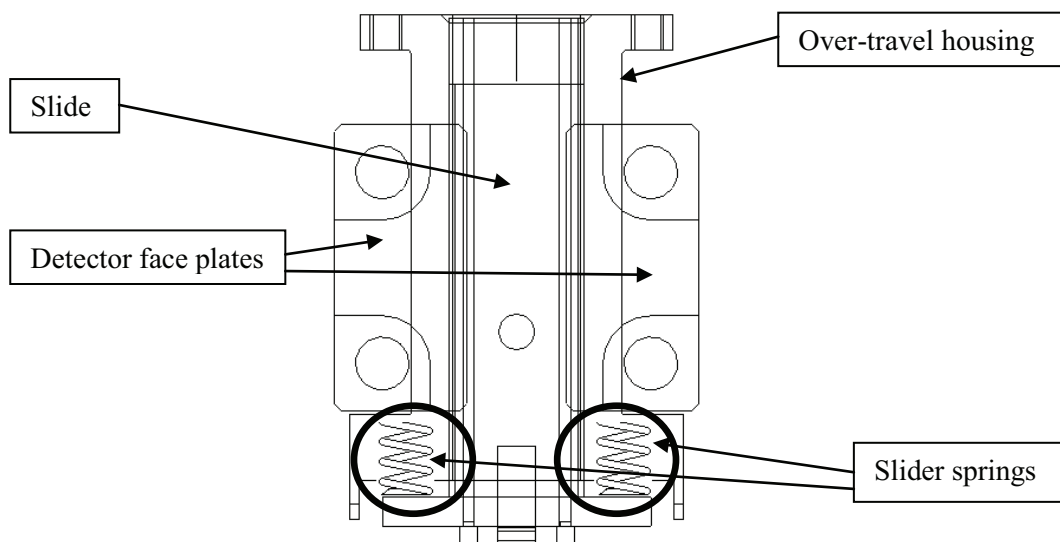


Figure 36 – Springs between Slider and Over-travel Mechanism

Testing

After the aforementioned modifications, static and full speed testing of revised prototype was conducted and operation of the mechanism was successful. Minor modifications to the frame had to be made before testing on production machines, because the dimensions of each machine vary slightly and could interfere with the new detector. All three conditions were identified by the machine: fail-safe, empty and open nest condition (pass), and non-empty nest condition (fail). A high-speed video was taken in order to observe vibrations on the rocker that is connected to the detection flag. Though vibrations were present on the prototype, the linkage motion was calm and consistent during the two detection windows. Several improvements were made on the final design to further improve the linkage's dynamic characteristics.

Final Design

The problems encountered with the prototype were all addressed in the final design. Most of these problems were meant to accommodate dimensional variation of the machines, so that each detector would not need custom fitment to this new design. Another major issue that was not addressed in the prototype was the bearing ratios of each pin joint. Small bearing ratios in the prototype caused unwanted movement and vibrations in the links. The minimum bearing width is about 1.5 times the diameter of the pivoting pin (Norton, 456). So for this case where 0.25 inch pins are used, the minimum bearing width is 0.375 inch.

The overall view of the final design is shown in Figure 37, the dimensions of the links are largely unchanged from those shown in Figure 21 since the same kinematic motion of the linkage is desired. The majority of the changes are more apparent when viewed from the side of the detector.

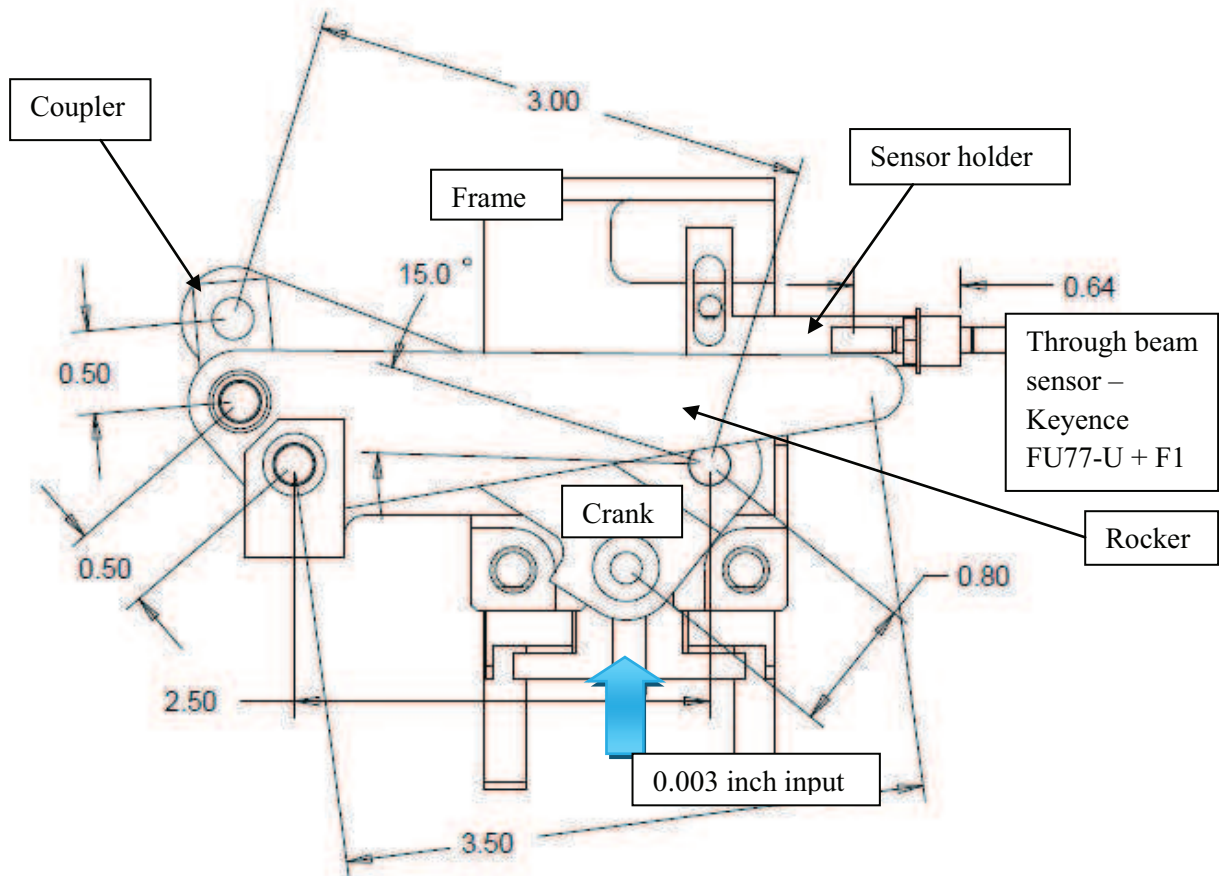


Figure 37 - Overall view of final design

From the left view of the detector (Figure 38), the modifications of the links are most apparent. Due to the proximity of the nest station, the detector is restricted from extending in the direction of index. In that case, the 1.10 inch saddle width of the frame cannot be changed, so the walls of the rocker pivots were decreased to accommodate for wider links necessary to achieve more desirable bearing ratios. Realizing that for links to rotate, only one link needs to rotate with respect to the other so that one link can be rigidly fixed to the pin. The connecting links therefore only need one side to have the ideal bearing ratio, while the other side would need to withstand the given bearing load. As a result, the rocker-to-ground pivot allows the rocker to have a simple support with bearing width of 0.75 inch with the ground pin as shown in Figure 38. With such a design, the coupler had to be made so that it can withstand the moments exerted at the pins. The coupler now has both of its pivoting pins fixed onto the main body, which allow the link to be thinner. This change allows the coupler-to-rocker pivot to have a width of 0.30 inch given the decrease in coupler width. Since the frame was unobstructed in the backward direction, the crank has room to widen its crank-to-coupler pivot to 0.38 inch. Likewise, the crank-to-ground pivot was also extended to achieve the same bearing ratio as shown in Figure 38. In the same figure the ground-to-crank pivot is also shown to be 0.37 inch, and is short of the ideal length because of interference with the detector's retaining plate.

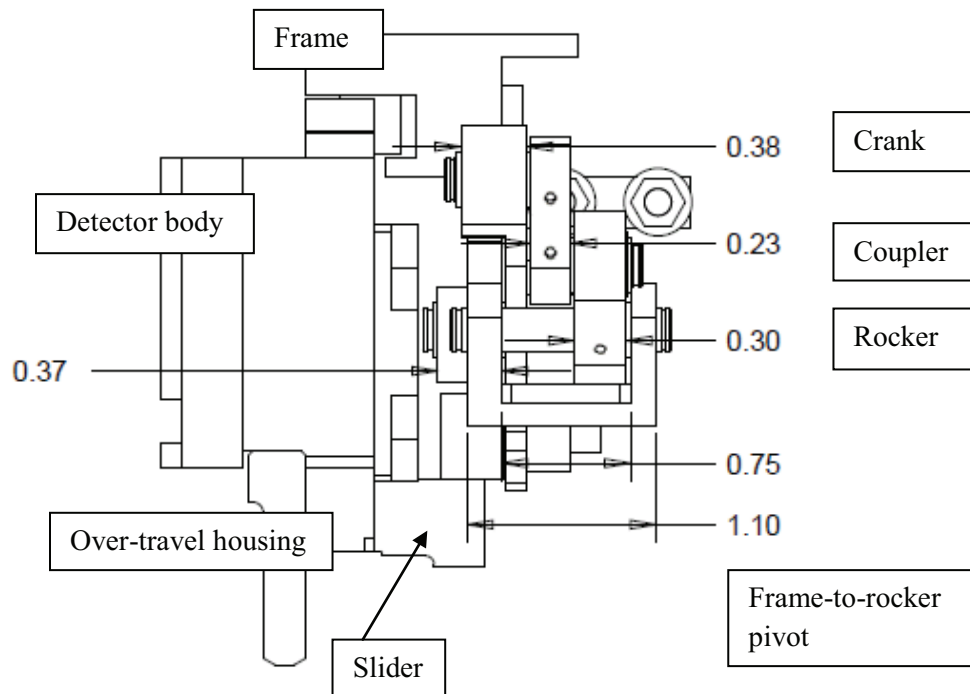


Figure 38 - Left view of final design

Besides the bearing ratios, several other modifications were made to the detector to ease assembly of the detector into the station and set-up of the device. In order to reduce the interference of the frame and the next station, the extension for the spring support is reduced to the closet possible distance (1.59 inch) to the frame's front plate as shown in Figure 39. The catch lip for the slider was lowered from 0.36 inch to 0.37 inch, as shown in Figure 39, and this would move the fail-safe position of the rocker's tip further from its normal condition location. By moving the rocker's tip further from the beam at fail-safe, the chances of false signals are decreased.

The interference and installation problems mostly originate from interference with the sensor-holder and the hex nut on the sensor (Keyence FU77-TG). For the final design, the sensor is changes to a Keyence FU77-U with a F1 lens. Details of this detector and sensor holder will be discussed later, but this sensor allow for a reduction in width of the detector assembly. The final width measures 1.83 inch from the face of the over-travel housing, and is a 0.21 inch reduction over the original design.

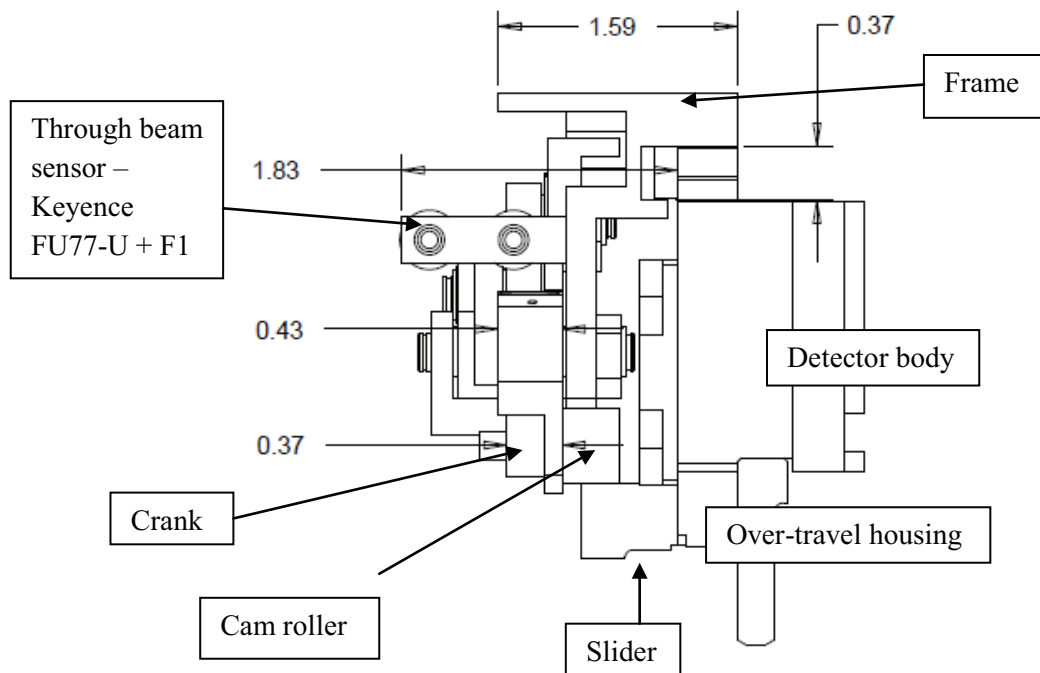


Figure 39 - Right view of final design

The additional bosses created on the moving links increased the equivalent mass of the system, and increase the necessary preload provided from the spring. Equivalent mass has been increased from 1.49kg to 3.51kg, and the necessary preload is recalculated with DYNACAM. The calculations are shown in Appendix E – Linkage Pre-load, and a total of 33.383N or 7.5lbf is required.

Crank

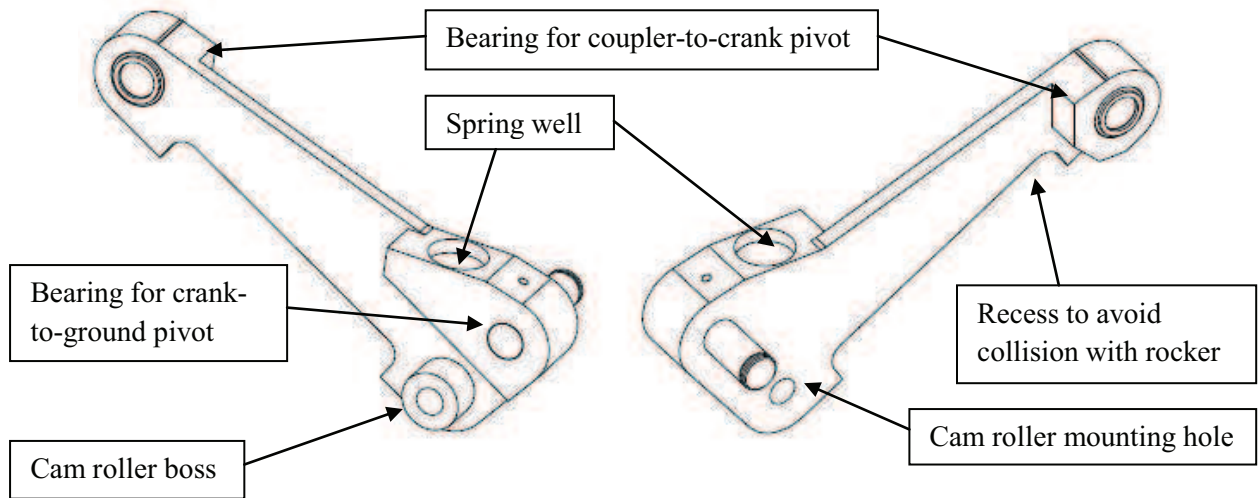


Figure 40 - Crank for final design

Several important features have been added to the crank to provide the necessary bearing ratios, accommodate springs and pivot pins, as well as avoiding collision with neighboring links. Bosses have been created on both sides of the crank to satisfy the bearing ratio, as shown Figure 40. Beneath the crank-to-coupler pivot, a recess was created to prevent the crank from hitting into the rocker's pin. The boss near the crank-to-ground pivot serves as a spring well to secure the spring and a bearing for the pivot pin. The geometry of the boss shown in Figure 40 was meant to ease manufacturing because the spring well and pivot bearing were in close proximity of each other, and is more easily manufactured as one feature. A separate boss is created to accommodate for the cam roller's shank, the height is which was determined by the length of the cam roller.

Coupler & Pin Fitment

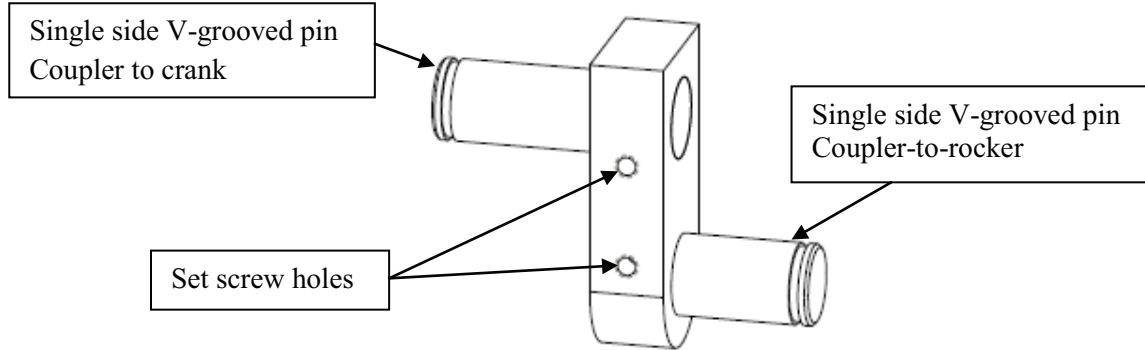


Figure 41 - Coupler for final design

The coupler was redesigned to support two rigidly fixed pins and remove the need to accommodate for bearing ratios. The pins will be fixed by a close tolerance fit, V-groove, and screw mounting method. The pins will be made with V-groove at one end, so that a screw can be threaded through the coupler's side and into the groove. Figure 41 shows the locations of these set screws on the coupler. This method would lock the pins axially and rotationally by the friction generated between the groove surface and the screw's head. To simplify the part for manufacturing, the top and side of the coupler was design to be a straight edge, but bottom of the coupler remains rounded to avoid interference with the rocker.

Rocker

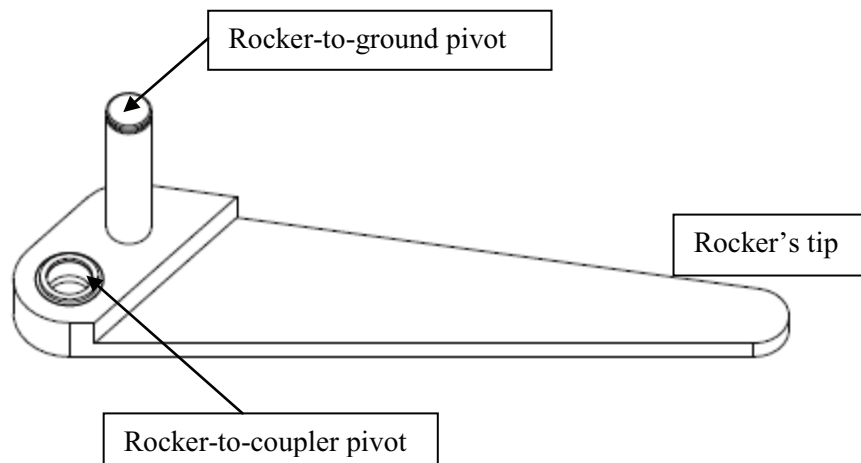


Figure 42 - Rocker for final design

The rocker will now contain the pin that fills the frame's simple support, and also receive the pivot pin from the rocker with sufficient bearing length. The final product is shown in Figure 42, showing the

added bearing. The rocker-to-ground pivot pin would be mounted to the link and fixed, doing so will remove the need for a large boss which would increase the inertia of the linkage. The rocker-to-coupler pivot boss is shorter than the ground pivot boss because the width of that bearing is constrained by the overall dimension of the frame. The length of the rocker's tip remains unchanged.

Sensor Holder

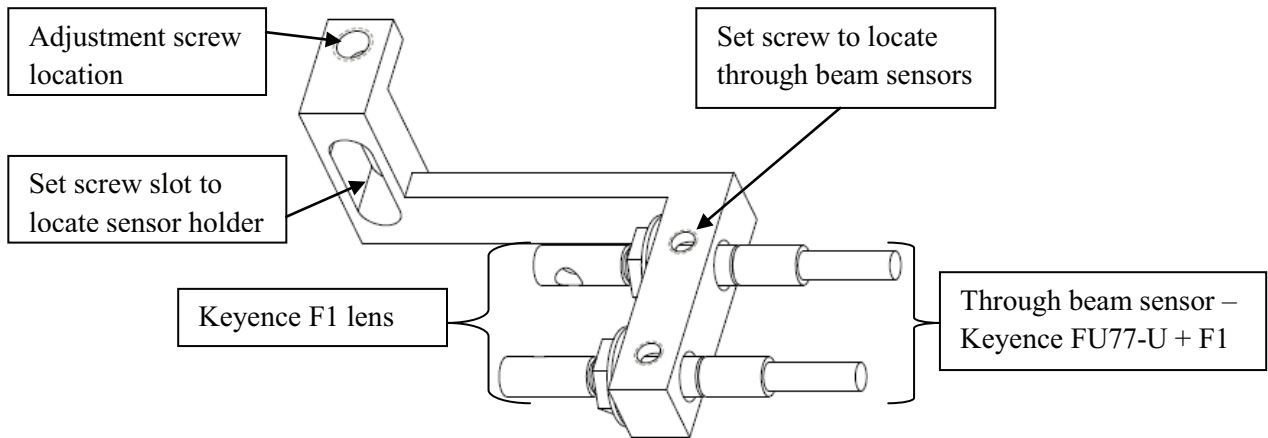


Figure 43 - Sensor holder for final design

The beam holder was redesigned to be more compact with the use of a new sensor. As mentioned previously, the sensor chosen for the final design was the Keyence FU77-U in order to reduce the total width of the overall assembly. This required a few changes to the sensor holder design, as shown in Figure 43. The previous arc component on the holder was modified to a simple arm where the sensors are attached to. To prevent rotation, the previous threaded holes were changed to clearance holes where the sensors will be located with a set of nuts and washers. Set screws were also added to the top of the clearance holes to limit rotation of the sensors in the clearance holes.

Frame

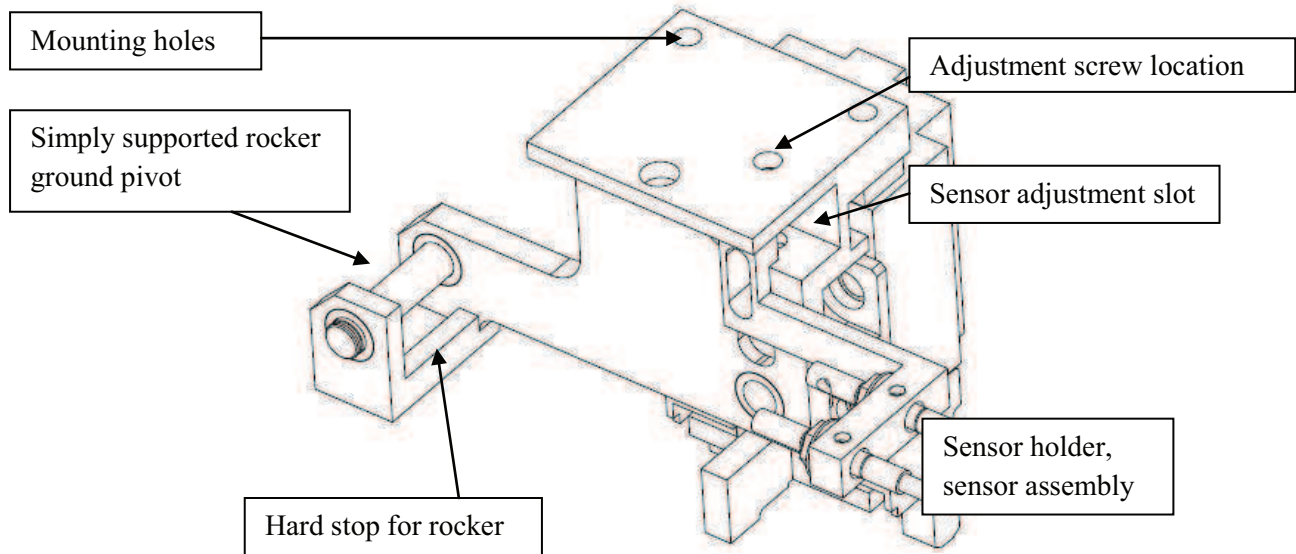


Figure 44 - Frame for final design

Modifications on the final design of the frame were made to reduce movement on the rocker's tip and prevent the linkage from toggling. The prototype design of rocker did not provide a sufficient bearing ratio to restrict movement in the axial direction, and allowed the rocker to vibrate in that direction, and potentially impact the sensor. To restrict the movement of the rocker link, the rocker pin is now supported at two locations on the frame as shown in Figure 44. This simple support will replace the previous cantilever design and increase the rocker link's bearing ratio. A hard stop was also added to the frame in order to stop the rocker motion before the linkage reaches toggle position. The height of the frame was increased to provide a location to the preload spring for the crank. With that height increase, the sensor adjustment slot was modified to allow greater adjustment of the sensor holder.

Conclusion & Recommendation

Material Considerations

The prototype was made in aluminum for ease of manufacturing at the time, but after careful analysis, aluminum is found to be the most feasible material for this device. Steel will increase the mass of the device by a factor of three, and will increase the dynamic load by an equal amount. This increase will need a stiffer spring in both the crank preload and the over-travel mechanism. An increased preload will increase the impact on the nest, and could cause premature wear on the break-pin surface.

Modification to Slider's Height

The existing detector has an insulator between the slider and contact piece which acts as a shim and an insulator. A shim was used in the existing design to adjust for the 0.003 inch gap and allow the slider to move above the top surface of the over-travel housing. Since the electrical circuit is removed in the new design, the insulator is acting solely as a shim. If the height of the slider were decreased by at least the thickness of the insulator, a shim would be unnecessary, and the frame can be placed directly on top of the over-travel housing.

Modification to Slider's Nose

The slider's nose can be modified such that a hole can be made, such that a pin can be inserted through the crank and the nose of the slider. This would switch from the force-closed contact to a form-closed contact, and would decrease the required strength of the spring on the crank. This in turn would mean that a softer spring can be used in the over-travel mechanism and decrease the impact force of the detector.

Modification to Casting

A major problem is that the casting of the next station varies greatly on all of the machines. An indentation at the back of the casting is required for the operation of the new detector. Small differences in the indentation's dimensions could interfere with the detector frame and prevent installation and operation of the detector. If this indentation in the next station's casting was increased, the detector would be able to travel through its motions without fear of crashing into the next station, and the detector would not have to be custom-fitted to each machine.

Bibliography

1. Norton, R.L. (2009). “Modeling Cam Follower System”. *Cam Design and Manufacturing Handbook*. 2nd Ed. Industrial Press: New York. pp 265 – 332.
2. Norton, R.L. (2008). “Spring Data”. *Design of Machinery*. 4th Ed. McGraw Hill: New York. pp 781 – 784.
3. Norton, R.L. (2008). “Analytical Linkage Synthesis”. *Design of Machinery*. 4th Ed. McGraw Hill: New York. pp 222 – 278.

Appendix

Appendix A - Empty Open Nest Detector Station Mass Model

Equivalent Mass and Spring Calculations

Mass of components:

$$m_{\text{lowerlever}} := 4.7343 \text{ lb} = 2.147 \text{ kg}$$

$$m_{\text{roller}} := 2.7342 \times 10^{-1} \text{ lb} = 0.124 \text{ kg}$$

$$m_{\text{rodend}} := 1.9149 \times 10^{-2} \text{ lb} = 8.686 \times 10^{-3} \text{ kg}$$

$$m_{\text{conrod}} := 0.8114 \text{ lb} = 0.368 \text{ kg}$$

$$m_{\text{upperlever}} := 2.2154 \text{ lb} = 1.005 \text{ kg}$$

$$m_{\text{bearing}} := 8.2286 \times 10^{-2} \text{ lb} = 0.037 \text{ kg}$$

$$m_{\text{carrier}} := 9.9175 \times 10^{-1} \text{ lb} = 0.45 \text{ kg}$$

$$m_{\text{detbody}} := 6.1538 \times 10^{-1} \text{ lb} = 0.279 \text{ kg}$$

$$m_{\text{othousing}} := 1.8697 \times 10^{-1} \text{ lb} = 0.085 \text{ kg}$$

$$m_{\text{slider}} := 1.3957 \times 10^{-1} \text{ lb} = 0.063 \text{ kg}$$

$$m_{\text{cover}} := 4.9003 \times 10^{-2} \text{ lb} = 0.022 \text{ kg}$$

$$m_{\text{contact}} := 9.4538 \times 10^{-2} \text{ lb} = 0.043 \text{ kg}$$

$$m_{\text{plate}} := 2.0948 \times 10^{-2} \text{ lb} = 9.502 \times 10^{-3} \text{ kg}$$

Moment of inertia:

$$I_{\text{lowerlever}} := 1.1373 \times 10^2 \text{ lb} \cdot \text{in}^2 = 0.033 \text{ m}^2 \cdot \text{kg}$$

$$I_{\text{upperlever}} := 3.008 \times 10^1 \text{ lb} \cdot \text{in}^2 = 8.803 \times 10^{-3} \text{ m}^2 \cdot \text{kg}$$

Spring rates:

$$k_{\text{upperlever_left}} := \frac{100 \text{ lbf}}{5.664 \times 10^{-3} \text{ in}} = 3.092 \times 10^6 \frac{\text{N}}{\text{m}}$$

$$k_{\text{upperlever_right}} := \frac{100 \text{ lbf}}{5.266 \times 10^{-3} \text{ in}} = 3.326 \times 10^6 \frac{\text{N}}{\text{m}}$$

$$k_{\text{lowerlever}} := \frac{100 \text{ lbf}}{1.614 \cdot 10^{-2} \text{ in}} = 1.085 \times 10^6 \frac{\text{N}}{\text{m}}$$

$$A_{\text{hex}} := \frac{3 \cdot \sqrt{3}}{2} \cdot \left(\frac{0.56 \text{ in}}{\sqrt{3}} \right)^2 = 0.272 \text{ in}^2$$

$$k_{\text{con}} := \frac{(10.4 \times 10^6 \text{ psi}) \cdot A_{\text{hex}}}{29.75 \text{ in}} = 9.494 \times 10^4 \frac{\text{lbf}}{\text{in}} \quad k_{\text{con}} = 1.663 \times 10^7 \frac{\text{N}}{\text{m}}$$

$$k_{\text{w1a161}} := 1.438 \times 10^9 \frac{\text{N}}{\text{m}}$$

$$k_{\text{w1a481}} := 1.435 \times 10^3 \frac{\text{N}}{\text{m}}$$

Pivot radius:

upperlever_left := 6.218 in	a := upperlever_left = 0.158 m
upperlever_right := 6.250 in	b := upperlever_right = 0.159 m
lowerlever_left := 5.00 in	e := lowerlever_left = 0.127 m
lowerlever_right := 16.481 in	f := lowerlever_right = 0.419 m

Equivalent masses:

$$m_2 := m_{\text{housing}} + m_{\text{slider}} + m_{\text{contact}} + 2 \cdot m_{\text{cover}} + m_{\text{plate}} = 0.245 \text{ kg}$$

$$m_1 := m_{\text{carrier}} + m_{\text{bearing}} + m_{\text{detbody}} = 0.766 \text{ kg}$$

$$m_2^{\text{eff}} := m_2 \cdot \left(\frac{a}{b} \right)^2 \cdot \left(\frac{f}{e} \right)^2 = 2.634 \text{ kg}$$

$$m_1^{\text{eff}} := m_1 \cdot \left(\frac{a}{b} \right)^2 \cdot \left(\frac{f}{e} \right)^2 = 8.241 \text{ kg}$$

$$m_{\text{upperlever}}^{\text{eff}} := \frac{I_{\text{upperlever}}}{b^2} = 0.349 \text{ kg}$$

$$m_{\text{lowerlever}}^{\text{eff}} := \frac{I_{\text{lowerlever}}}{e^2} = 2.063 \text{ kg}$$

$$m_{0\text{eff}} := (m_{\text{eff_upperlever}} + 2m_{\text{rodend}} + m_{\text{conrod}}) \left(\frac{f}{e}\right)^2 + m_{\text{eff_lowerlever}} = 10.046 \text{ kg}$$

Equivalent springs:

$$k_a := \left[\frac{1}{k_{\text{upperlever_left}} \left(\frac{a}{b}\right)^2} + \frac{1}{k_{\text{upperlever_right}}} \right]^{-1} \quad k_a = 1.594 \times 10^6 \frac{\text{N}}{\text{m}}$$

$$k_b := \left(\frac{1}{k_a} + \frac{1}{k_{\text{con}}} \right)^{-1} \quad k_b = 1.454 \times 10^6 \frac{\text{N}}{\text{m}}$$

$$k_c := \left(\frac{1}{k_b} + \frac{1}{k_{\text{lowerlever}}} \right)^{-1} \quad k_c = 6.214 \times 10^5 \frac{\text{N}}{\text{m}}$$

$$k_{1\text{eff}} := k_c \left(\frac{f}{e}\right)^2 = 6.752 \times 10^6 \frac{\text{N}}{\text{m}}$$

$$k_{2\text{eff}} := k_{w1a481} \left(\frac{a}{b}\right)^2 \left(\frac{f}{e}\right)^2 = 1.543 \times 10^4 \frac{\text{N}}{\text{m}}$$

MatLab File : twodof.m

```
clear; clc;
% This program calculates the response to a two-DOF
% system subject to seismic excitation
% Input model parameters

% m0 = mass 0, kg
% m1 = mass 1, kg
% m2 = mass 2, kg
% k0 = spring constant 0, N/m
% k1 = spring constant 1, N/m
% k2 = spring constant 2, N/m
% z0 = damping ratio 0, dimensionless
% z1 = damping ratio 1, dimensionless
% z2 = damping ratio 2, dimensionless
% Fi = cam follower preload at s=0, N
% speed = machine speed in cycles/minute

m0 = 44.839;
m1 = 8.241;
m2 = 2.634;
k0 = 4000;
k1 = 6.752e6;
k2 = 1.543e4;
z0 = 0.1;
z1 = 0.05;
z2 = 0.05;
Fi = 200;
speed = 225;

% calculate damping coefficients
c0 = 2*z0*sqrt(k0/(m0+m1+m2));
c1 = 2*z1*sqrt(k1/m1);
c2 = 2*z2*sqrt(k2/m2);

% Construct matrix equation
m=[m1 0 ; 0 m2];
c=[c1+c2 -c2 ; -c2 c2];
k=[k1+k2 -k2 ; -k2 k2];

% Solve Eigenvalue Problem
% u = Modal matrix (not yet normalized to the mass matrix)
% d = squares of natural frequencies
[u,d]=eig(k,m);

% Normalize the U matrix
% U1 = normalized mode 1 shape
% U2 = normalized mode 2 shape
% scale1 = mode 1 scale factor
% scale2 = mode 2 scale factor

u1 = u(:,1);
scale1 = 1/sqrt(transpose(u1)*m*u1);
U1 = scale1 * u1;
u2 = u(:,2);
scale2 = 1/sqrt(transpose(u2)*m*u2);
```



```

U2 = scale2 * u2;

% Re-assemble Modal Matrix from normalized modal vectors
U = [U1 U2];

% Normalize damping
% C = Modal damping matrix
C = transpose (U)*c*U;

% Construct equations of motion in modal form
% Assume proportional damping by throwing out non-diagonal terms of
% normalized damping matrix
spring1 = d (1,1);
spring2 = d (2,2);

% using the above-calculated c's (questionable) and C matrix,
% damp1 = C (1,1);
% damp2 = C (2,2);

% assigning damping ratios directly to the modal form,
damp1 = 2*z1*sqrt (spring1);
damp2 = 2*z2*sqrt (spring2);

% save parameters of modal equations to disk file for use in subroutine
save parameters U k1 c1 spring1 spring2 damp1 damp2;

% load the input motion functions into global memory
global s;
global sprime;
global sprimeprime;
load s -ascii;
load sprime -ascii;
load sprimeprime -ascii;

% Solve the ODEs
% number = number of data points for input and output data
% tspan = column vector of discrete times to solve equation for
cycles = 4;
number = length (s);
global tspan;
tspan = linspace (0, cycles*60/speed, number);
tspan = tspan';

% y0_1 = initial conditions on displacement and velocity for mode 1
% y0_2 = initial conditions on displacement and velocity for mode 2
% set initial conditions equal to follower displacement and velocity
nu_0 = inv (U)*[s (1) ; s (1)];
nuprime_0 = inv (U)*[sprime (1) ; sprime (1)];
y0_1 = [nu_0(1);nuprime_0(1)];
y0_2 = [nu_0(2);nuprime_0(2)];
[t,y1] = ode45 ('twodofmode1',tspan,y0_1);
[t,y2] = ode45 ('twodofmode2',tspan,y0_2);

% Create vectors of modal positions from the solution matrices
nu1 = y1 (:,1);
nu2 = y2 (:,1);

```

```

% Create vectors of modal velocities from the solution matrices
nu1prime = y1(:,2);
nu2prime = y2(:,2);

% Construct output position from mode shapes
x1 = U(1,1)*nu1 + U(1,2)*nu2;
x2 = U(2,1)*nu1 + U(2,2)*nu2;
% Construct output position from mode shapes
x1prime = U(1,1)*nu1prime + U(1,2)*nu2prime;
x2prime = U(2,1)*nu1prime + U(2,2)*nu2prime;

% Construct output accelerations from kinematic functions
x1dblprime = (1/m1)*(k2*(x2-x1) + c2*(x2prime-x1prime) ...
    - k1*(x1-s) - c1*(x1prime-sprime));
x2dblprime = (1/m2)*(-k2*(x2-x1) - c2*(x2prime-x1prime));

% Plot x1 and x2 results
figure(1)
plot(t,x1,t,x2);
title('Displacement of mass 1 and mass 2')

% figure (2)
plot(t,s-x1);
title('Displacement difference of mass 1')

% figure (3)
plot(t,s-x2);
title('Displacement difference of mass 2')

% Plot v1 and v2 results
figure(4)
plot(t,x1prime,t,x2prime)
title('Velocities of mass 1 and mass 2')

% Plot v1 and v2 results
figure(4)
plot(t,x1dblprime,t,x2dblprime)
title('Accelerations of mass 1 and mass 2')

```

MatLab File : twodofmode1

```
function yprime = twodofmode1 (t,y);
global tspan s sprime;

% load modal equation parameters from file 'parameters'
load parameters U k1 c1 spring1 spring2 damp1 damp2;

% return input motion values given t
position = interp1 (tspan,s,t,'linear');
velocity = interp1 (tspan,sprime,t,'linear');

% normalize input motion values
N1 = U (1,1)*(k1*position+c1*velocity);

% return yprime vector for mode 1
yprime = [y (2)
          N1 - damp1*y (2) - spring1*y (1)];
```

MatLab File : twodofmode2

```
function yprime = twodofmode1 (t,y);
global tspan s sprime;

% load modal equation parameters from file 'parameters'
load parameters U k1 c1 spring1 spring2 damp1 damp2;

% return input motion values given t
position = interp1 (tspan,s,t,'linear');
velocity = interp1 (tspan,sprime,t,'linear');

% normalize input motion values
N2 = U (1,2)*(k1*position+c1*velocity);

% return yprime vector for mode 2
yprime = [y (2)
          N2 - damp2*y (2) - spring2*y (1)];
```

Appendix B – MathCAD, Linkage Position Analysis

$$\delta := 0.003$$

$$\Delta := 2 \cdot \delta$$

$$b := 0.5$$

$$a := 0, 0.01 \dots b$$

$$c := 0, 0.2 \dots 4.0$$

$$\theta_0(a) := \text{asin}\left(\frac{a + \Delta}{b}\right)$$

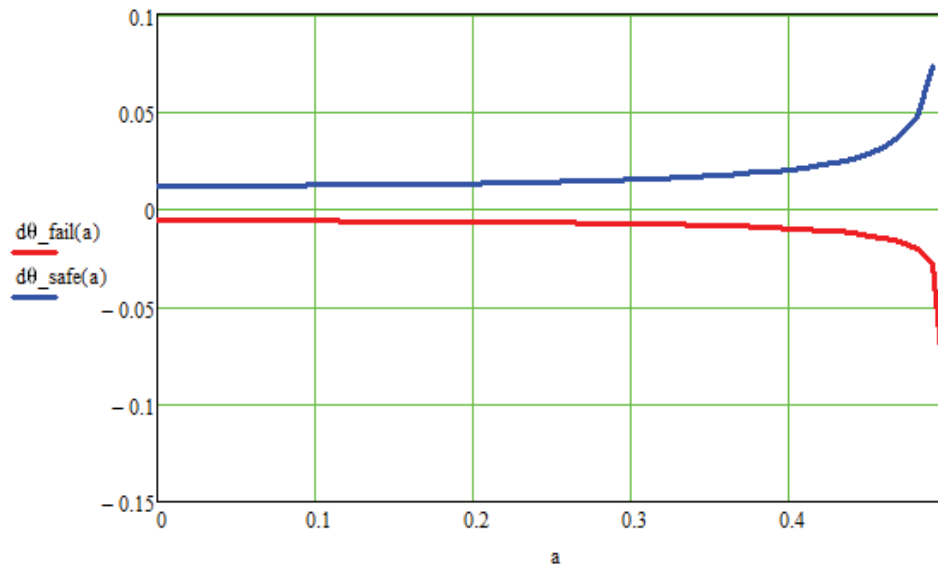
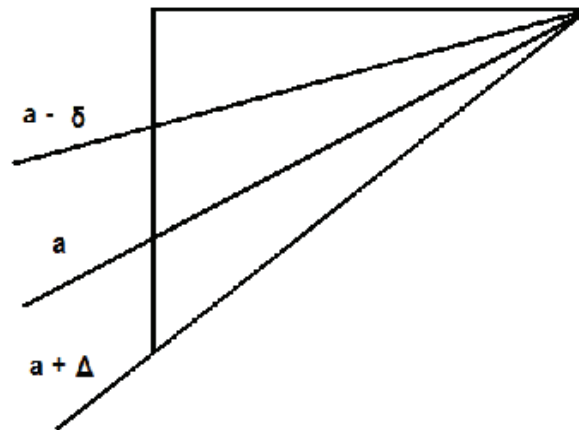
$$\theta_1(a) := \text{asin}\left(\frac{a}{b}\right)$$

$$\theta_2(a) := \text{asin}\left(\frac{a - \delta}{b}\right)$$

$$d\theta_{\text{fail}}(a) := \theta_2(a) - \theta_1(a)$$

$$d\theta_{\text{safe}}(a) := \theta_0(a) - \theta_1(a)$$

Single Link Solution -
Initial link position not horizontal.



$$d\theta_{\text{fail}}(0.40) = -0.569 \text{ deg}$$

Appendix C – MathCAD, Optimizing Geometry of Links [3]

Fourbar Analysis

Define debris thickness

$$\delta := 0.003$$

$$b := 0.50$$

$$a := 80\% \cdot b$$

A starting point with a triangle, and no longer horizontal

$$\beta_1(a) := \text{asin}\left(\frac{a}{b}\right)$$

$$\beta_2(a) := \text{asin}\left(\frac{a - \delta}{b}\right)$$

$$d\beta := \beta_1(a) - \beta_2(a) = 0.569 \cdot \text{deg}$$

$$\varphi := 0 \text{deg}, 1 \text{deg}.. 360 \text{deg}$$

$$L_1 := 2.5 \quad L_2 := 3.0 \quad L_3 := 0.50 \quad L_4 := 0.50$$

$$K_1 := \frac{L_1}{L_2} = 0.833 \quad K_2 := \frac{L_1}{L_4} = 5 \quad K_3 := \frac{L_2^2 - L_3^2 + L_4^2 + L_1^2}{2 \cdot L_2 \cdot L_4} = 5.083$$

$$A(\varphi_2) := \cos(\varphi_2) - K_1 - K_2 \cdot \cos(\varphi_2) + K_3$$

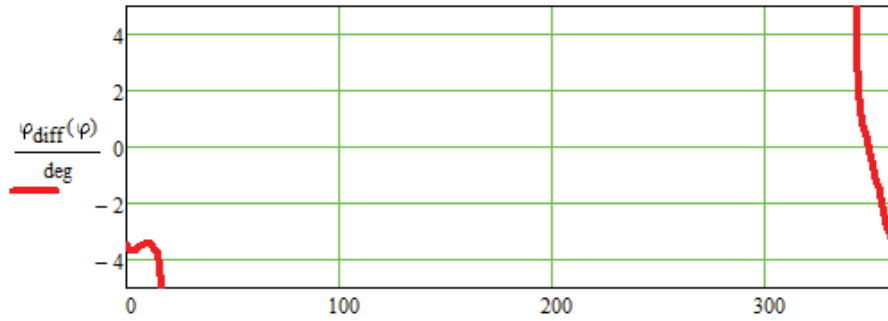
$$B(\varphi_2) := -2 \cdot \sin(\varphi_2)$$

$$C(\varphi_2) := K_1 - (K_2 + 1) \cdot \cos(\varphi_2) + K_3$$

$$\varphi_{4_1}(\varphi_2) := 2 \cdot \text{atan}\left(\frac{-B(\varphi_2) + \sqrt{B(\varphi_2)^2 - 4 \cdot A(\varphi_2) \cdot C(\varphi_2)}}{2 \cdot A(\varphi_2)}\right) +$$

$$\varphi_{4_2}(\varphi_2) := 2 \cdot \text{atan}\left(\frac{-B(\varphi_2) - \sqrt{B(\varphi_2)^2 - 4 \cdot A(\varphi_2) \cdot C(\varphi_2)}}{2 \cdot A(\varphi_2)}\right)$$

$$\varphi_{\text{diff}}(\varphi_2) := \varphi_{4_1}(\varphi_2) - \varphi_{4_2}(\varphi_2 + d\beta)$$



$$\theta = 15 \text{ deg}$$

$$\varphi_{\text{diff}}(\theta) = -4.01 \cdot \text{deg}$$

$$\varphi_{4_2}(\theta) = 33.615 \cdot \text{deg}$$

$$3.5 \cdot \sin(\varphi_{\text{diff}}(\theta)) = -0.245$$

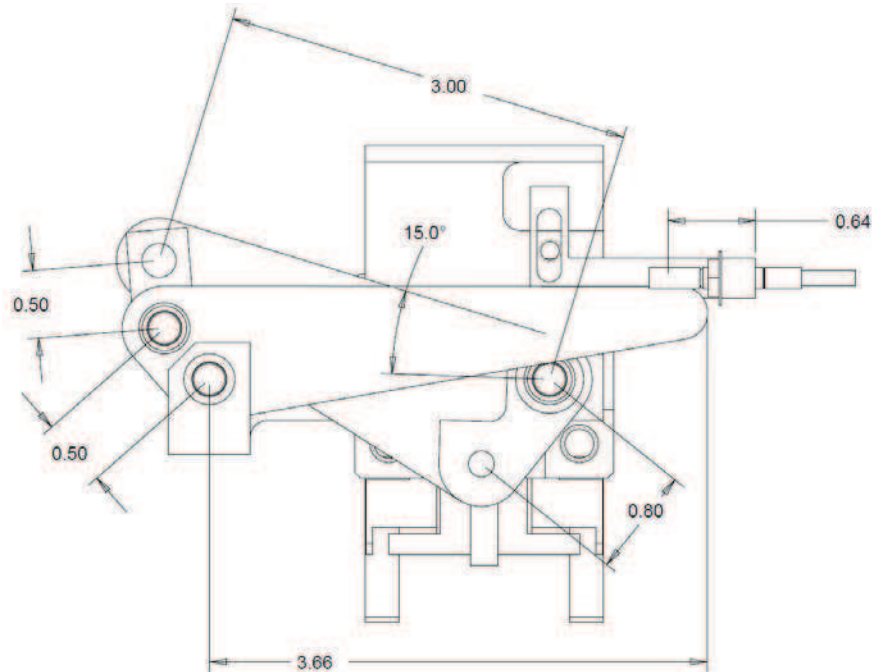
$$\frac{\varphi}{\text{deg}}$$

$$\text{asin}\left(\frac{0.25}{3.5}\right) = 4.096 \cdot \text{deg}$$

$$\varphi_{4_2}(\theta + d(\beta)) = 37.625 \cdot \text{deg}$$

+

Appendix D – Four-bar Linkage Mass Model



$$M_{\text{crank}} := 8.5171 \cdot 10^{-2} \text{ lb} = 0.039 \text{ kg}$$

$$I_{\text{crank}} := 2.0809 \cdot 10^{-1} \text{ lb} \cdot \text{in}^2 = 6.09 \times 10^{-5} \text{ m}^2 \cdot \text{kg}$$

$$M_{\text{rocker}} := 5.9450 \cdot 10^{-2} \text{ lb} = 0.027 \text{ kg}$$

$$I_{\text{rocker}} := 1.0679 \cdot 10^{-1} \text{ lb} \cdot \text{in}^2 = 3.125 \times 10^{-5} \text{ m}^2 \cdot \text{kg}$$

$$M_{\text{coupler}} := 2.6213 \cdot 10^{-2} \text{ lb} = 0.012 \text{ kg}$$

$$I_{\text{coupler}} := 3.6514 \times 10^{-3} \text{ lb} \cdot \text{in}^2 = 1.069 \times 10^{-6} \text{ m}^2 \cdot \text{kg}$$

$$M_{\text{roller}} := 2.0581 \cdot 10^{-2} \text{ lb} = 9.335 \times 10^{-3} \text{ kg}$$

Link lengths of crank and rocker:

$$a := 3 \text{ in} = 0.076 \text{ m}$$

$$e := 3.5 \text{ in} = 0.089 \text{ m}$$

$$b := 0.80 \text{ in} = 0.02 \text{ m}$$

$$f := 0.5 \text{ in} = 0.013 \text{ m}$$

Effective mass of crank and rocker:

$$M_{\text{eff_crank}} := \frac{I_{\text{crank}}}{b^2} + M_{\text{roller}} = 0.157 \text{ kg}$$

$$M_{\text{eff_rocker}} := \frac{I_{\text{rocker}}}{f^2} = 0.194 \text{ kg}$$

Solve effective mass for stations A, B, C:

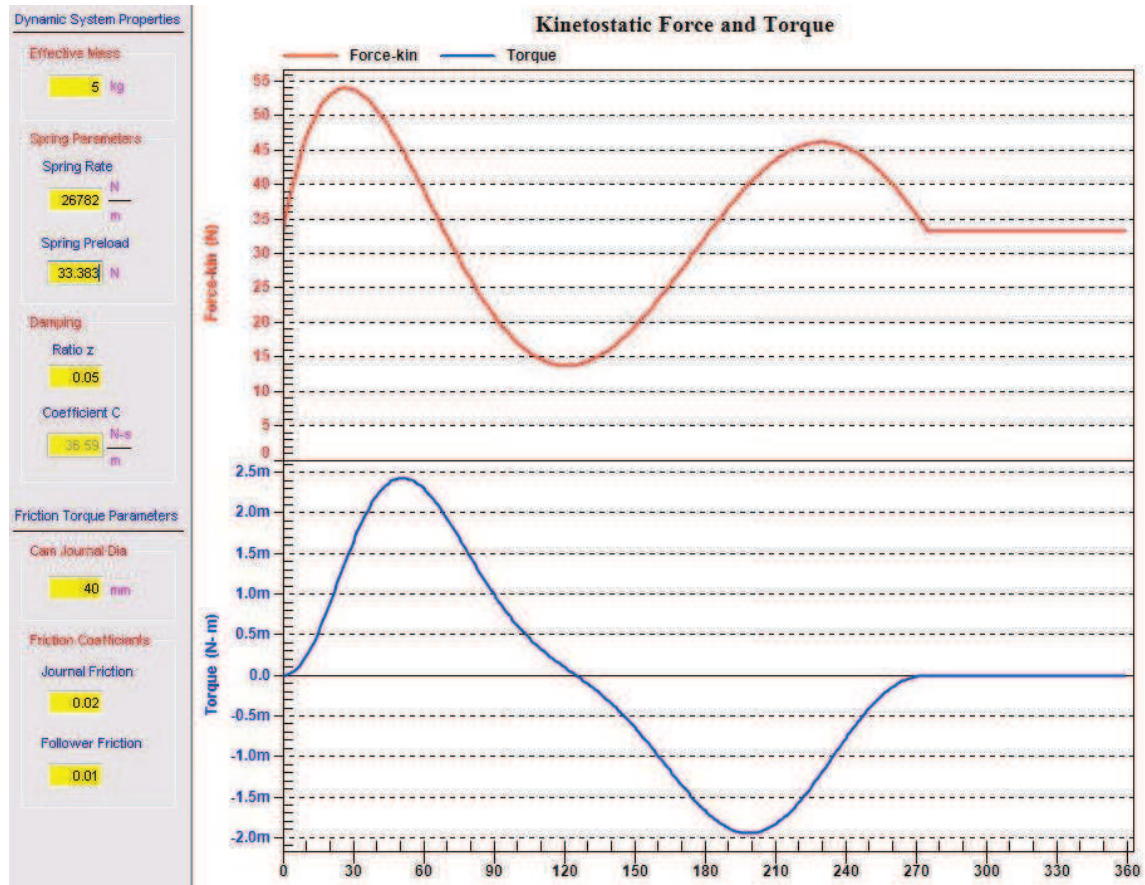
$$M_{\text{Aeff}} := M_{\text{eff_rocker}} = 0.194 \text{ kg}$$

$$M_{\text{Beff}} := M_{\text{Aeff}} + M_{\text{coupler}} + M_{\text{eff_crank}} = 0.362 \text{ kg}$$

$$M_{\text{Ceff}} := \left(\frac{a}{b}\right)^2 \cdot M_{\text{Beff}} = 5.097 \text{ kg}$$

$$M_{\text{Ceff}} = 11.237 \text{ lb}$$

Appendix E – Linkage Pre-load



Maximum inertial forces applied to rocker

$$\text{maxacc_deg} := 1793.456 \frac{\text{deg}}{\text{s}^2}$$

$$\text{minacc_deg} := -1917.945 \frac{\text{deg}}{\text{s}^2}$$

$$\text{maxacc_lin} := \text{maxacc_deg} \cdot \left(\frac{0.875 \text{ in}}{3.058 \text{ deg}} \right) = 13.035 \frac{\text{m}}{\text{s}^2}$$

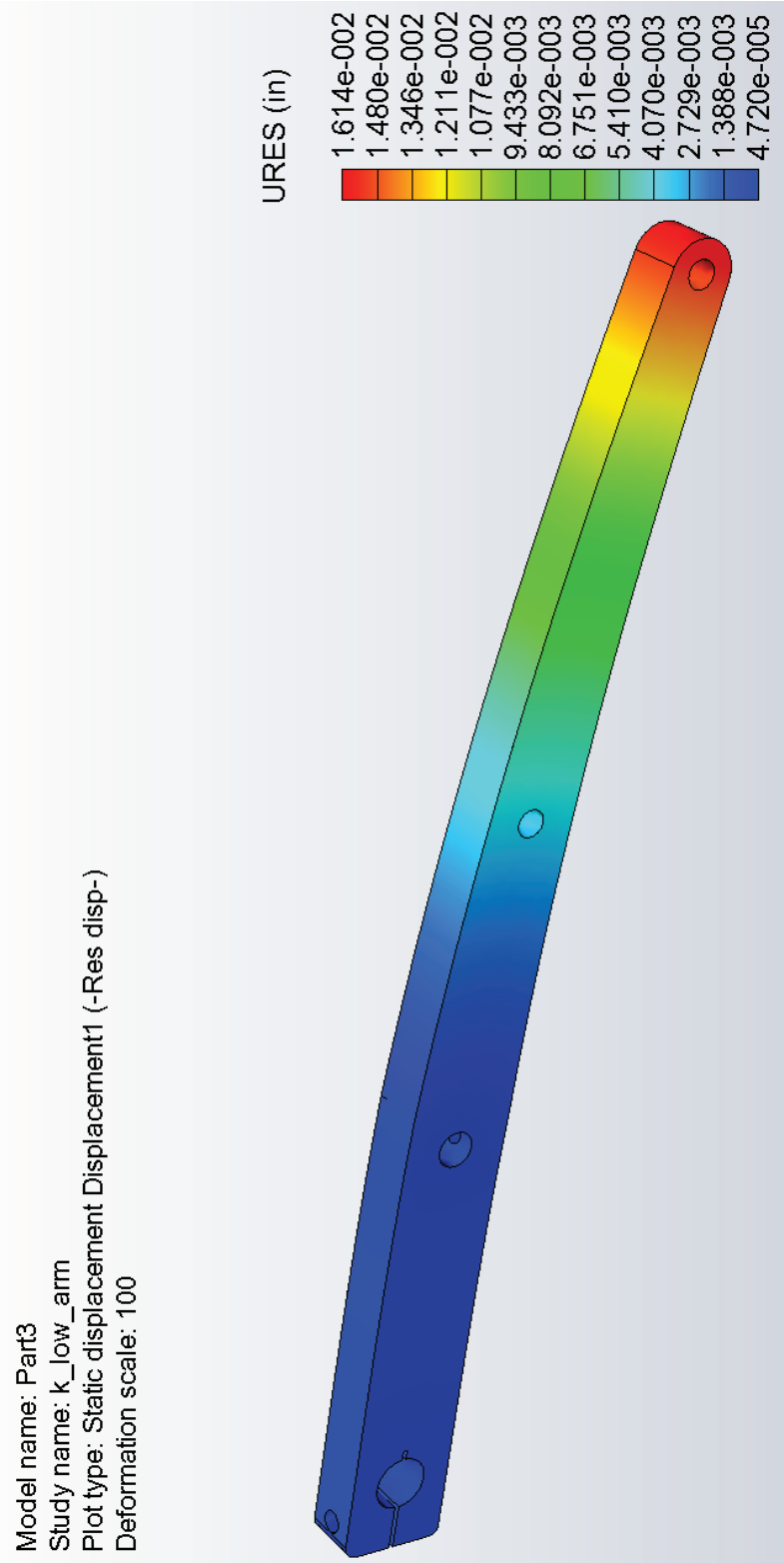
$$\text{minacc_lin} := \text{minacc_deg} \cdot \left(\frac{0.875 \text{ in}}{3.058 \text{ deg}} \right) = -13.939 \frac{\text{m}}{\text{s}^2}$$

$$M_{C\text{eff}} \cdot \text{minacc_lin} = -15.973 \text{ lbf}$$

$$M_{C\text{eff}} \cdot \text{maxacc_lin} = 14.936 \text{ lbf}$$

Appendix F – FEA Results

Lower Lever Arm

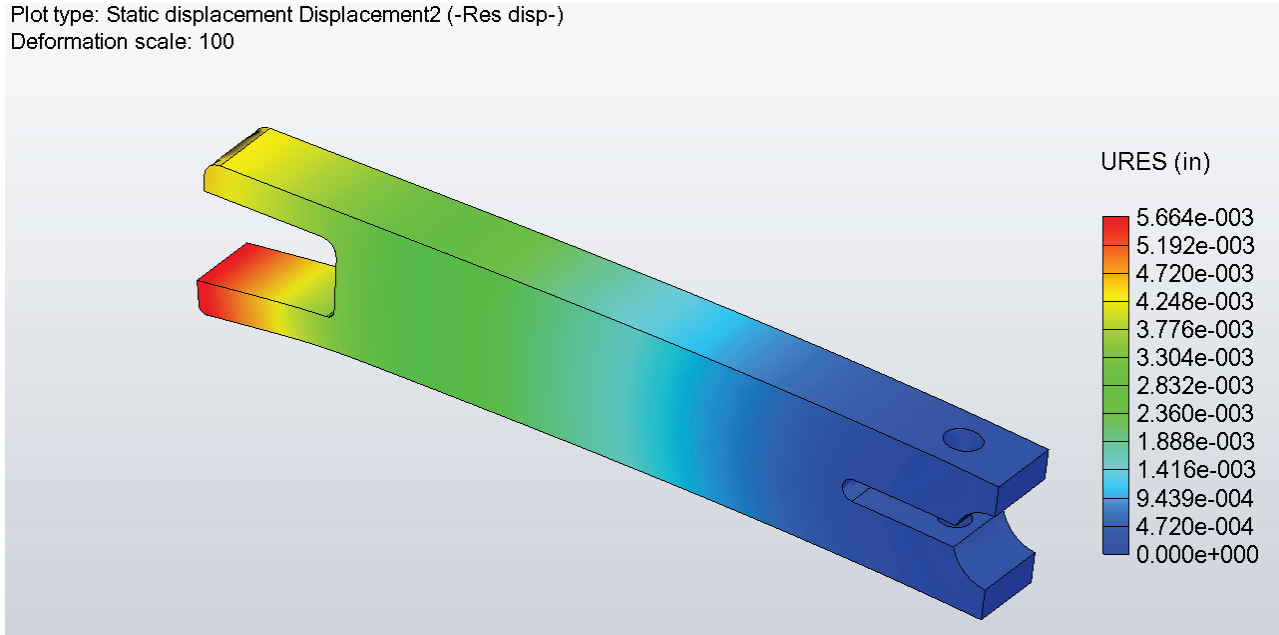


Upper Lever Arm

The upper lever arms were broken into two parts, each independently considered as a cantilever beam.

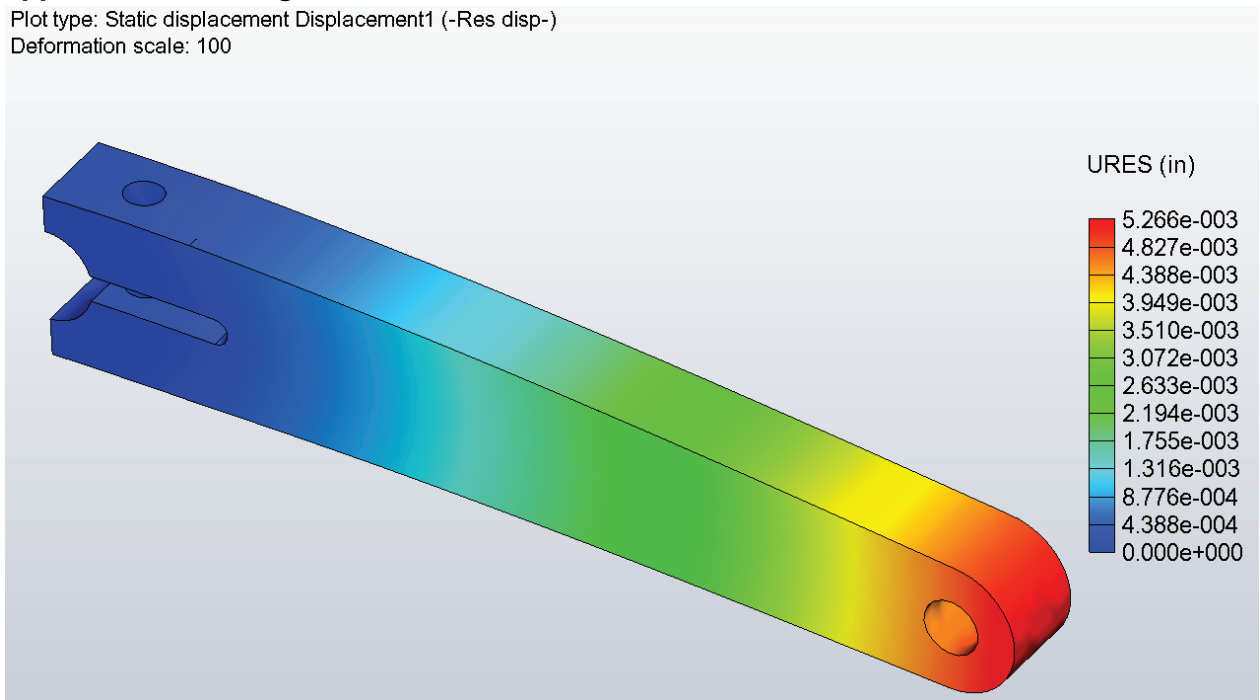
Upper Lever Arm Left

Plot type: Static displacement Displacement2 (-Res disp-)
Deformation scale: 100



Upper Lever Arm Right

Plot type: Static displacement Displacement1 (-Res disp-)
Deformation scale: 100



Appendix G – Stress Applied on Pins

From the CAD model, the moment of inertia of each link is obtained, and along with the center of gravity locations. This information is used to create a dynamic model of the linkage to solve for the force applied on each of the pins. Using the program Four-bar, the forces exerted on the pins are shown in Figure 45.

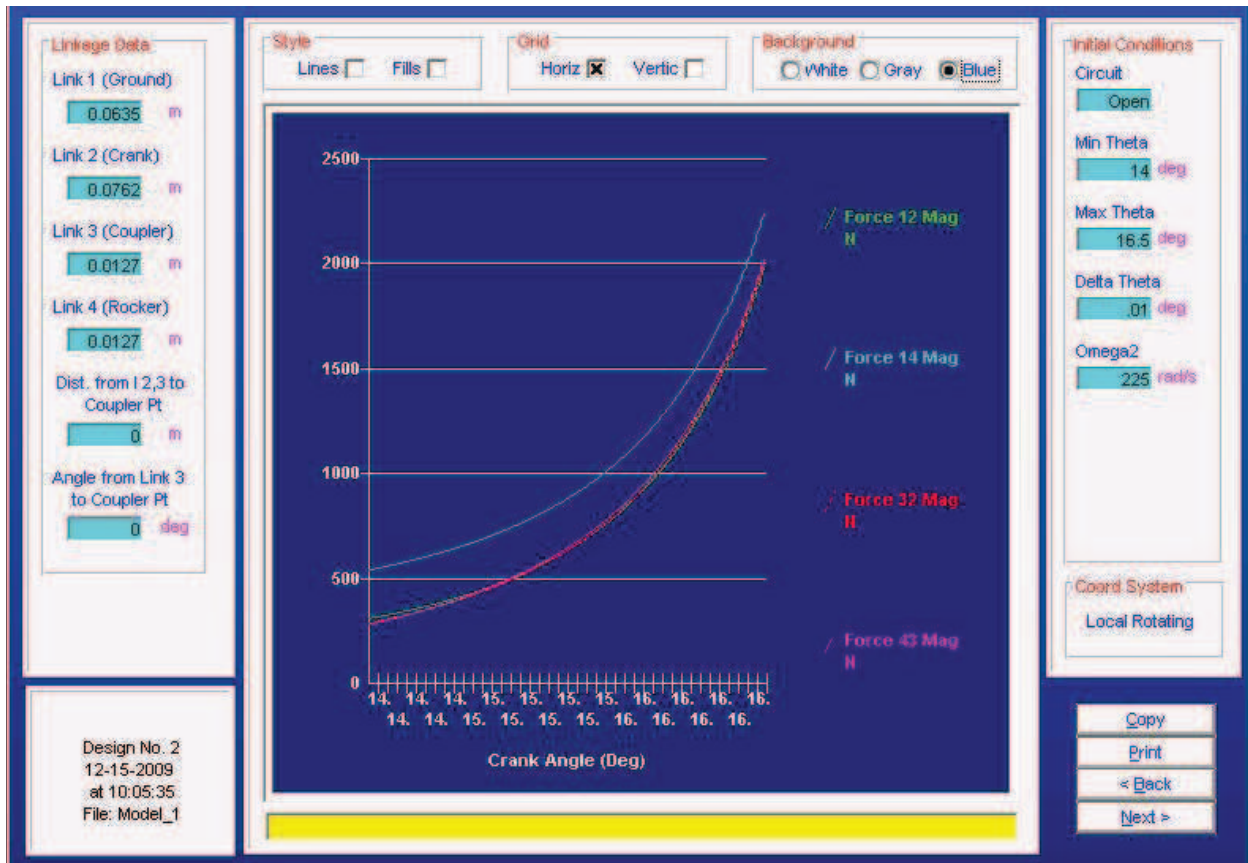


Figure 45 - Pin forces as calculated by Four-bar

The rest of the pins are same in diameter and the loads applied are similar, so only one of the forces needs to be considered. The only simply supported pin in the linkage is the rocker-to-ground link (pin 14), so that pin will be considered separately. The maximum force is considered. Figure 45 shows that the maximum force in pin 12, 32, and 43 fluctuates between 480N and 1000N between 15.00 degree and 15.99 degree, the only range that the linkage operates in. Pin 14 has a higher load that fluctuates between 650N and 1100N.

The materials of the pins are AISI A2 Air-hardening tool steel (mscmetalworking.com), and has a fatigue limit of 5.4×10^8 Pa (CES EduPack 200). Environment of the device is friendly to this material, as the temperature does not become significant, neither are corrosive chemicals present.

Rocker-to-ground (Pin 1-4)

Geometry of the simply supported rocker pin

$$d_{\text{pin}} := 0.25\text{in} = 6.35 \times 10^{-3} \text{m}$$

$$L_{\text{pin}} := 0.75\text{in} = 0.019\text{m}$$



Distributed load on the beam

$$w := \frac{10\text{GN}}{L_{\text{pin}}}$$

Define range and step function

$$S(x, q) := \text{if}(x \geq q, 1, 0)$$

$$x := 0\text{m}, 0.001 L_{\text{pin}}, L_{\text{pin}}$$

Loading function

$$q(x) := R_1 S(x, 0) \cdot (x - 0)^{-1} - w S(x, 0) \cdot (x - 0)^0 + R_2 S(x, L_{\text{center}}) \cdot (x - L_{\text{center}})^{-1}$$

Shear function

$$V(x) := R_1 S(x, 0) \cdot (x - 0)^0 - w S(x, 0) \cdot (x - 0)^1 + R_2 S(x, L_{\text{center}}) \cdot (x - L_{\text{center}})^0$$

Moment function

$$M(x) := R_1 S(x, 0) \cdot (x - 0)^1 - \frac{w}{2} S(x, 0) \cdot (x - 0)^2 + R_2 S(x, L_{\text{center}}) \cdot (x - L_{\text{center}})^1$$

The constants \$C_1\$ and \$C_2\$ are left out because the reactions are included, so they would have been resolved to zero by the boundary condition at \$x=0\$. The reactions \$R_1\$ and \$R_2\$ will be solved by the boundary condition at \$x=L \rightarrow V=0, M=0\$

$$V(L) = 0 = R_1(L - 0)^0 - w(L - 0)^1 + R_2(L - L_{\text{center}})^0$$

$$0 = R_1 - wL_{\text{center}} + R_2$$

$$M(L) = 0 = R_1(L - 0)^1 - \frac{w}{2}(L - 0)^2 + R_2(L - L_{\text{center}})^1$$

$$0 = R_1 L - \left(\frac{w}{2}\right) \cdot L^2$$

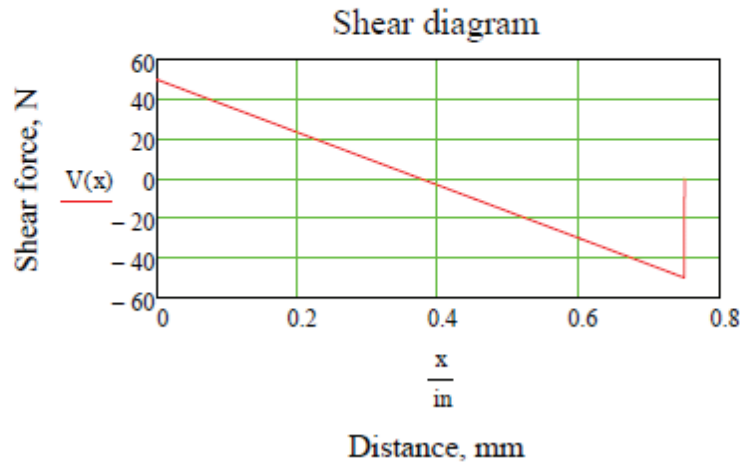
$$R_1 := \frac{w \cdot L_{\text{pin}}}{2} \quad R_1 = 50\text{N}$$

$$R_2 := w \cdot L_{\text{pin}} - R_1 \quad R_2 = 50\text{N}$$

The functions are now defined

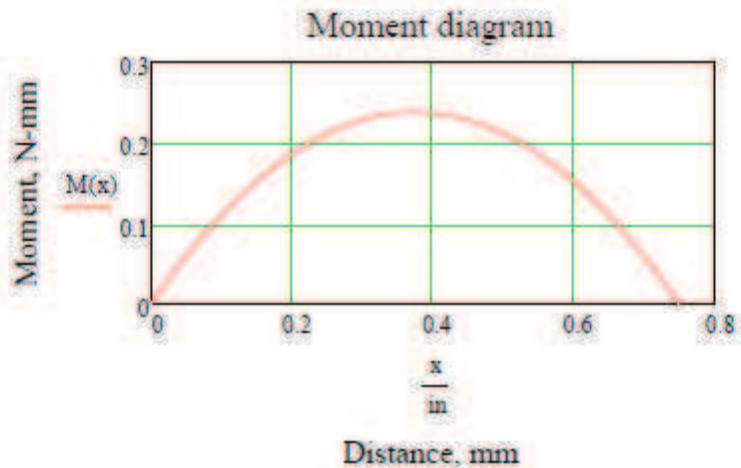
Shear function

$$V(x) := R_1 \cdot S(x, 0) \cdot (x - 0)^0 - w \cdot S(x, 0) \cdot (x - 0)^1 + R_2 \cdot S(x, L_{pin}) \cdot (x - L_{pin})^0$$



Moment function

$$M(x) := R_1 \cdot S(x, 0) \cdot (x - 0)^1 - \frac{w}{2} \cdot S(x, 0) \cdot (x - 0)^2 + R_2 \cdot S(x, L_{pin}) \cdot (x - L_{pin})^1$$



The maximum moment occur at the middle of the beam. The maximum moment will be calculated and then the corresponding bending stress.

$$loc := 0.50 \text{ in}$$

Given

$$V(loc) = 0 \quad loc := \text{Find}(loc)$$

$$loc = 9.525 \times 10^{-3} \text{ m}$$

$$M_{max} := M(loc)$$

$$I := \frac{(\pi \cdot d_{\text{pin}}^4)}{64}$$

$$\sigma_{\text{max}} := \frac{M_{\text{max}} \cdot \frac{d_{\text{pin}}}{2}}{I}$$

$$\sigma_{\text{max}} = 9.473 \times 10^6 \text{ Pa}$$

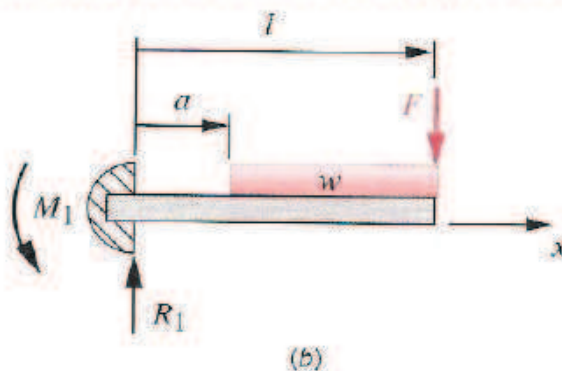
$$\sigma_{\text{shear}} = \frac{V(0\text{mm})}{\pi \left(\frac{d_{\text{pin}}}{2}\right)^2}$$

$$\sigma_{\text{shear}} = 1.579 \times 10^6 \text{ Pa}$$

Given that the fatigue limit is $5.40 \times 10^8 \text{ Pa}$, the simply supported pin 14 has a safety factor of 57, considering that the bending stress is the maximum stress experienced by the pin.

Coupler-to-Crank, Coupler-to-Rocker, Ground-to-Crank (pin 12, 23, 34)

Pin 23, 34, and 14 is a cantilever beam as supported in the below figure.



$$L := 0.38 \text{ in} = 9.652 \times 10^{-3} \text{ m}$$

$$a := 0.025 \text{ in} = 6.35 \times 10^{-4} \text{ m}$$

$$d_{\text{pin}} := 0.25 \text{ in} = 6.35 \times 10^{-3} \text{ m}$$

$$I := \frac{(\pi \cdot d_{\text{pin}}^4)}{64} = 7.981 \times 10^{-11} \text{ m}^4$$

$$w := \frac{1000 \text{ N}}{0.35 \text{ in}} = 1.125 \times 10^5 \frac{\text{N}}{\text{m}}$$

Define range and step function for functions

$$S(x, j) := \text{if}(x \geq j, 1, 0)$$

$$x := 0 \text{ m}, 0.001 \cdot L \dots L$$

$$q(x) := R_1 \cdot S(x, 0) \cdot (x - 0)^{-1} - M_1 \cdot S(x, 0) \cdot (x - 0)^{-2} - w \cdot S(x, a) \cdot (x - a)^0$$

$$V(x) := R_1 \cdot S(x, 0) \cdot (x - 0)^0 - M_1 \cdot S(x, 0) \cdot (x - 0)^{-1} - w \cdot S(x, a) \cdot (x - a)^1$$

$$M(x) := R_1 \cdot S(x, 0) \cdot (x - 0)^1 - M_1 \cdot S(x, 0) \cdot (x - 0)^0 - \frac{w}{2} \cdot S(x, a) \cdot (x - a)^2$$

The integration constants C1 and C2 were not necessary because the reactions forces are included. Use $x=L+ \rightarrow V=0, M=0$ to solve for reactions.

$$V(L) = 0 = R_1 \cdot (L - 0)^0 - M_1 \cdot (L - 0)^{-1} - w \cdot (L - a)^1$$

$$0 = R_1 - w(L - a)$$

$$R_1 = w(L - a)$$

$$M(L) = 0 = R_1 \cdot (L - 0)^1 - M_1 \cdot L^0 - \frac{w}{2} \cdot (L - a)^2$$

$$0 = R_1 \cdot L - M_1 - \frac{w}{2} \cdot (L - a)^2$$

$$M_1 = R_1 \cdot L - \frac{w}{2} \cdot (L - a)^2$$

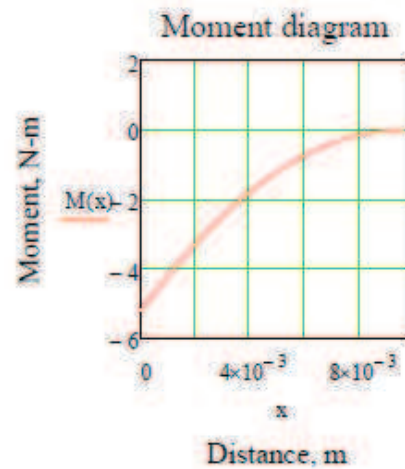
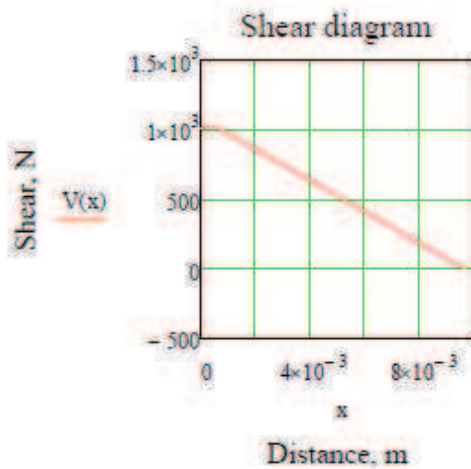
$$R_1 = 1.014 \times 10^3 \text{ N}$$

$$M_1 = 5.217 \text{ m}\cdot\text{N}$$

This set of functions are now defined

$$V(x) := R_1 \cdot S(x, 0) \cdot (x - 0)^0 - w \cdot S(x, a) \cdot (x - a)^1$$

$$M(x) := R_1 \cdot S(x, 0) \cdot (x - 0)^1 - M_1 \cdot S(x, 0) \cdot (x - 0)^0 - \frac{w}{2} \cdot S(x, a) \cdot (x - a)^2$$



Reactions forces, as solved above

$$R_1 = 1.014 \times 10^3 \text{ N}$$

$$M_1 = 5.217 \text{ m}\cdot\text{N}$$

maximum shear occur at $x=L$

$$V(a) = 1.014 \times 10^3 \text{ N}$$

maximum moment occur at $x=0$

$$M_{\max} := M(0) = -5.217 \text{ m}\cdot\text{N}$$

maximum bending stress

$$\sigma_{\text{bending}} := M_{\max} \frac{d_{\text{pin}}^{0.50}}{I}$$

$$\sigma_{\text{bending}} = -2.075 \times 10^8 \text{ Pa}$$

Given that the fatigue limit is $5.40 \times 10^8 \text{ Pa}$, the simply supported pin14 has a safety factor of 2.6, considering that the bending stress is the maximum stress experienced by the pin.

Appendix H – Setup Procedure

Material needed:

- 1) Empty open nest detector
- 2) Keyence amplifier, with power supply
- 3) Nest
- 4) 0.003inch shim approx. 1/8 inch wide
- 5) Allen key for adjustment screw

Keyence amplifier:

- 1) Power Keyence amplifier with 12-24VDC power supply
- 2) Insert emitter and receiver into amplifier
- 3) Set amplifier to “L-on”, or lights → on mode
- 4) Set amplifier strength to “Ultra”
- 5) Point emitter to receiver, make sure LED light is ON

Procedure:

Normal Condition –

- 1) Push empty open nest detector against the nest firmly, make sure that both the slider and over-travel housing is in contact with the breakpin surface.
- 2) Adjust sensor holder adjustment screw so that the beam is **BLOCKED** by the **UPPER EDGE** of the link.
- 3) Keyence amplifier should have no output signal, and LED light on the detector should be OFF.

Fail Condition –

- 4) Place 0.003inch shim on the nest, but avoid blocking the rectangular indentations on the breakpin.
- 5) Push detector firmly against the surface of the breakpin, as done in the Normal Condition setup.
- 6) Keyence amplifier should have output signal, and LED light should be ON.

The detector must be able to acknowledge both conditions without changing the adjustment screw between the two conditions. IF NOT please remove the shim between the linkage frame and the over-travel housing. Please replace with shim that is 0.020 ± 0.001 inch in thickness.

Other requirements:

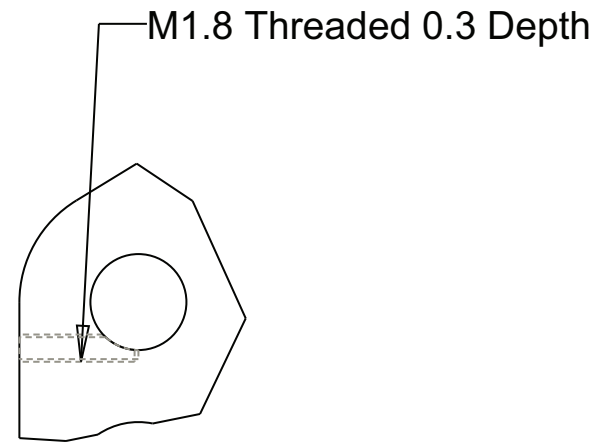
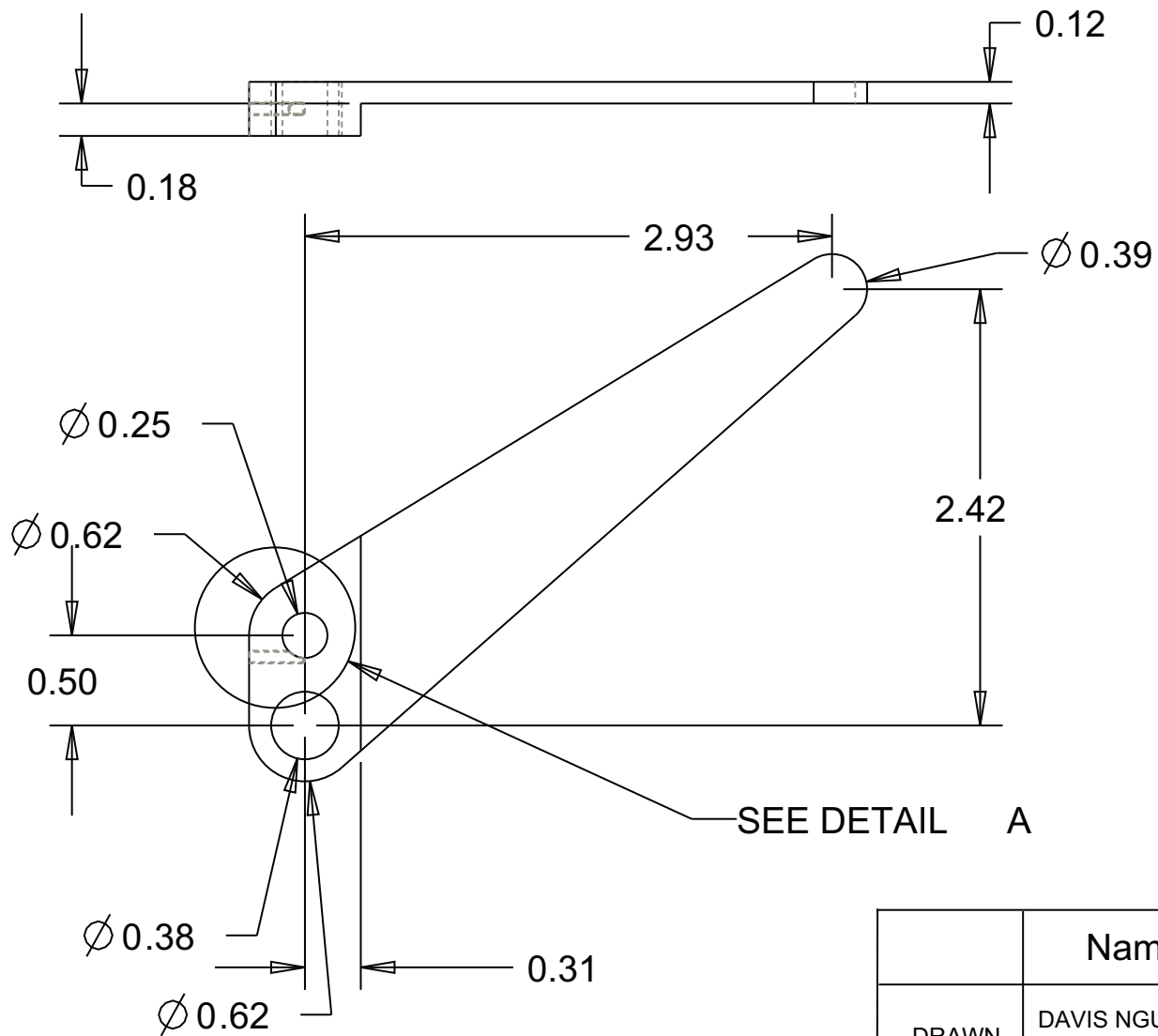
- 1) Move forward most link to its downward most position. Linkage should spring back to fail-safe state. IF NOT, replace spring with a stiffer unit and make sure that the linkage joints can rotate freely.

Appendix J – Drawings of Final Parts

NOTE:

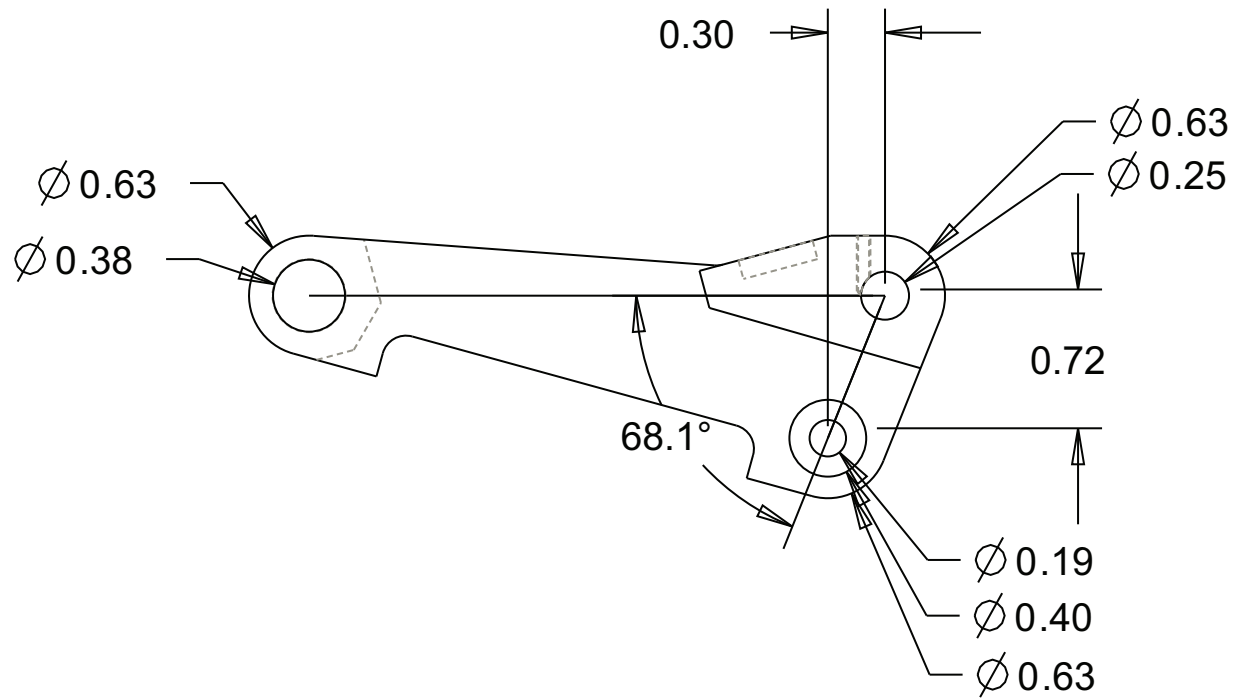
Each feature on these parts is determined to have their individual importance as described in Final Design section of the report. The most important geometry on these links are the locations of the pivot pins, as they determine the kinematics of the linkage, and ultimately the motion of the rocker flag.

Small screw holes are placed on several of the parts so that pins can be fixed to some of the links. The dimensions of these set screw holes are not concrete, and can be changed to the convenience of implementation.

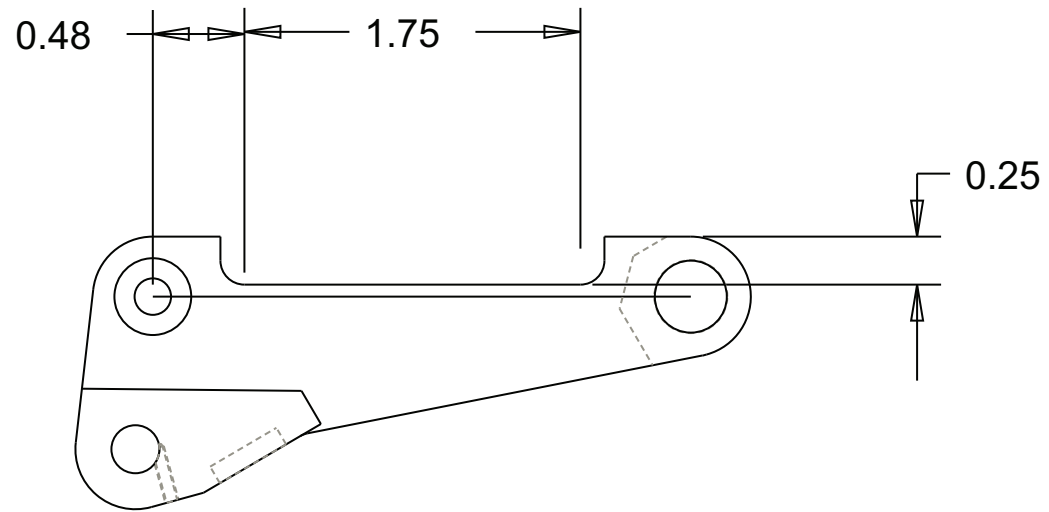


DETAIL A
SCALE 2.000

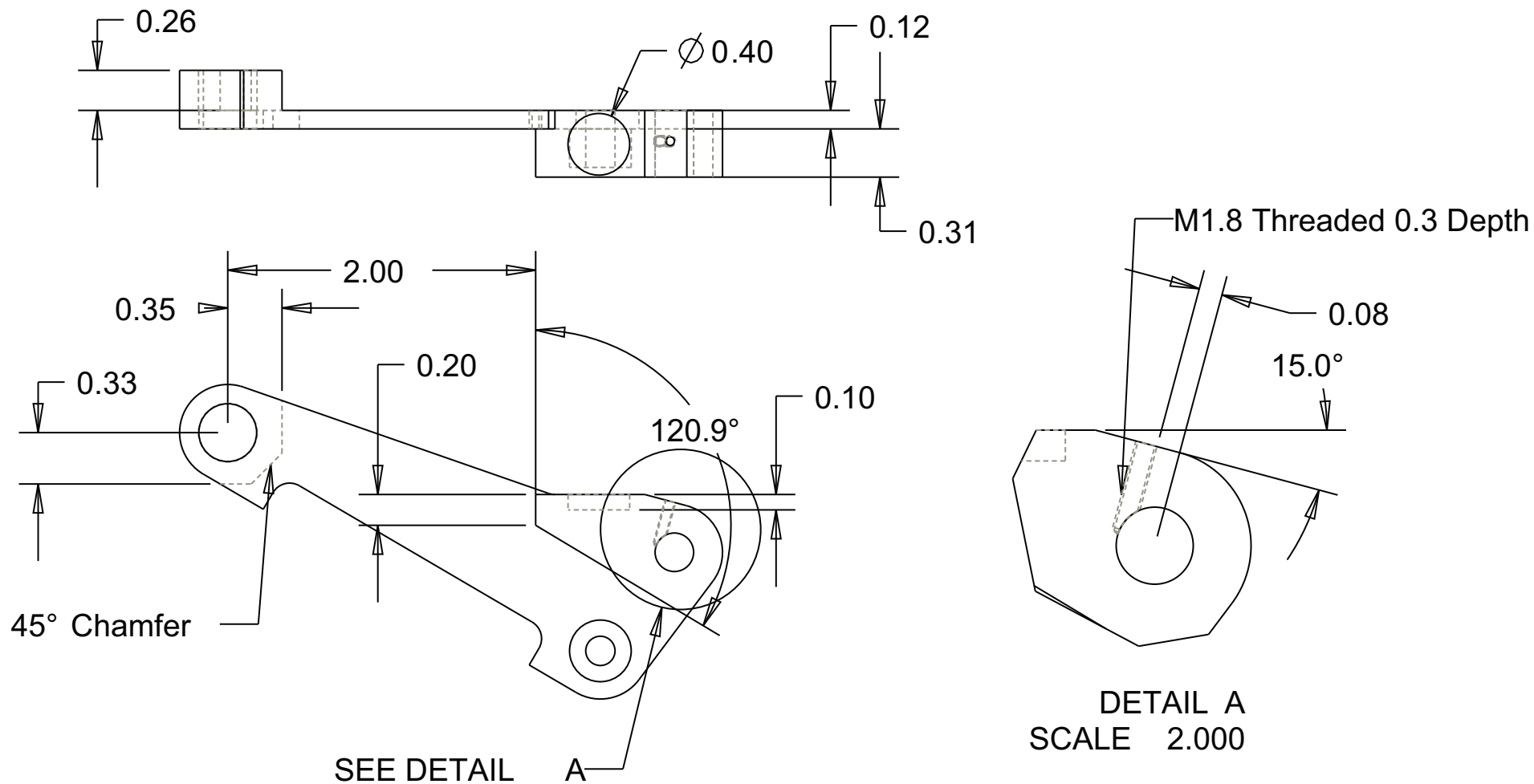
	Name	Date	WORCESTER POLYTECHNIC INSTITUTE		
DRAWN	DAVIS NGUYEN CAROL OKUMURA YUK-KWAN YUEN	12/16/2009	TITLE: ROCKER		
CHECKED ENG APPR.					
MFG APPR. Q.A			SIZE: A	DWG. NO. 01	REV:
UNLESS OTHERWISE NOTED: .X = ± 0.1 .XX = ± 0.01 .XXX = ± 0.001 ALL FRACTIONS = ± 1/64			SCALE 1:1	MQP	SHEET 1 OF 1



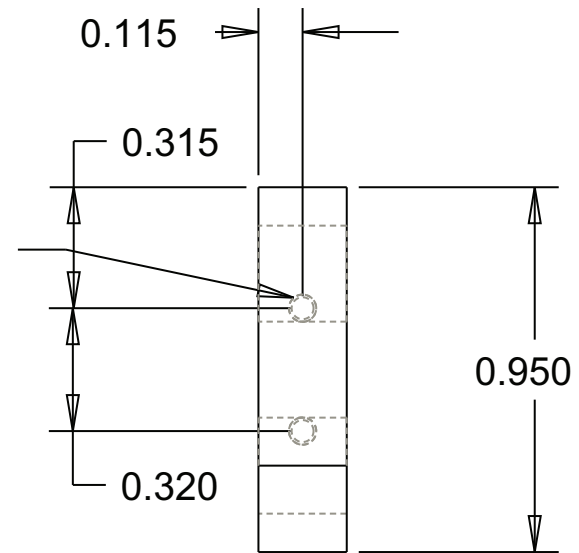
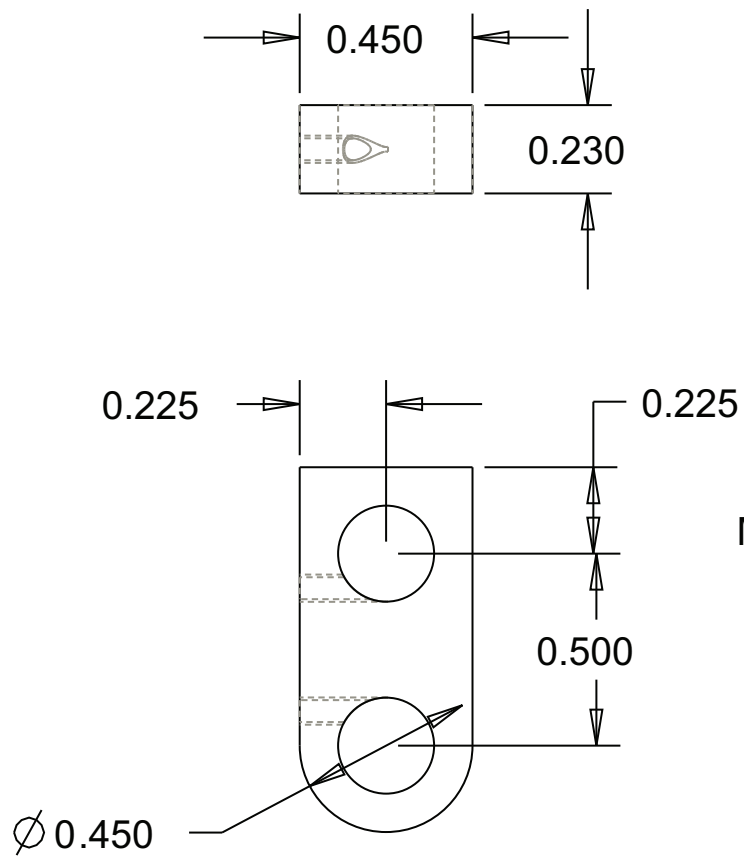
	Name	Date	WORCESTER POLYTECHNIC INSTITUTE		
DRAWN	DAVIS NGUYEN CAROL OKUMURA YUK-KWAN YUEN	12/16/2009	TITLE: CRANK		
CHECKED ENG APPR.					
MFG APPR. Q.A			SIZE: A	DWG. NO. 02	REV:
UNLESS OTHERWISE NOTED: .X = \pm 0.1 .XX = \pm 0.01 .XXX = \pm 0.001 ALL FRACTIONS = \pm 1/64			SCALE 1:1	MQP	SHEET 1 OF 3



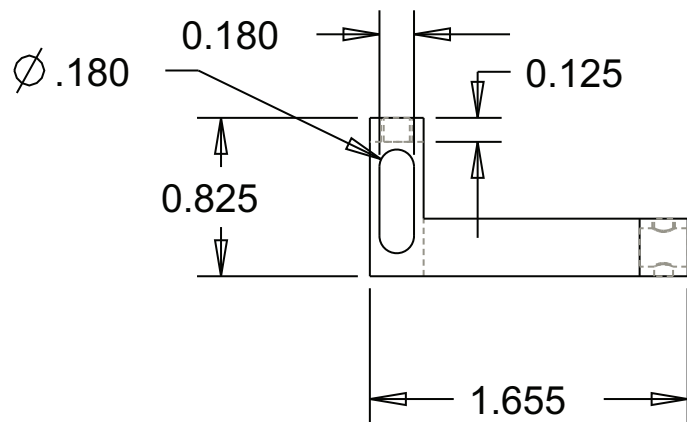
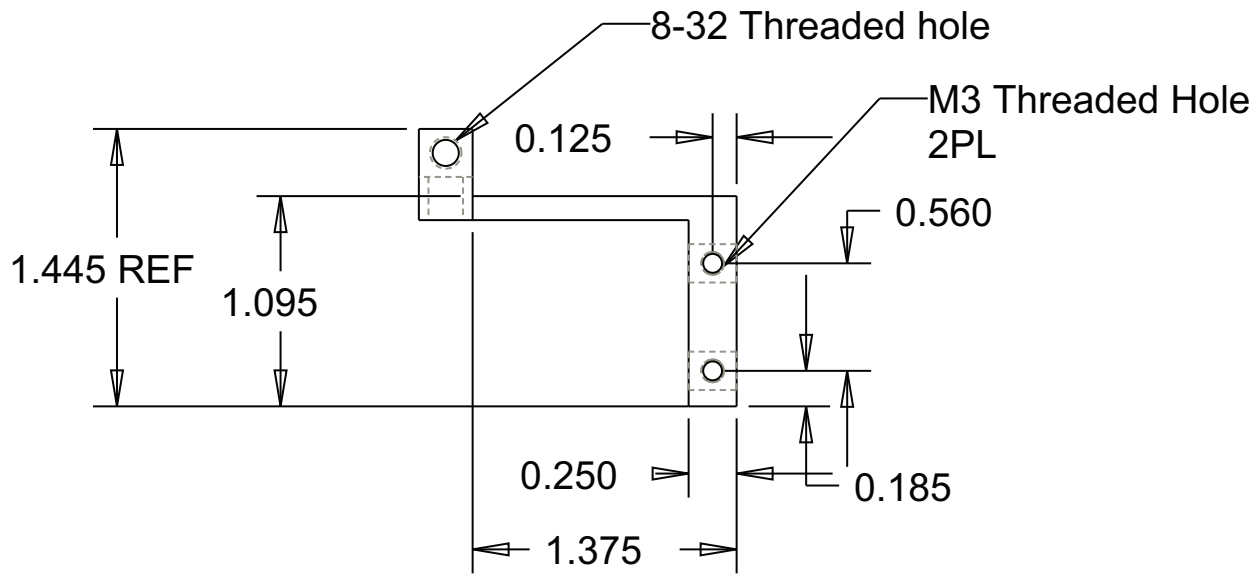
	Name	Date	WORCESTER POLYTECHNIC INSTITUTE		
DRAWN	DAVIS NGUYEN CAROL OKUMURA YUK-KWAN YUEN	12/16/2009	TITLE: CRANK		
CHECKED ENG APPR.					
MFG APPR. Q.A			SIZE: A	DWG. NO. 03	REV:
UNLESS OTHERWISE NOTED: .X = ± 0.1 .XX = ± 0.01 .XXX = ± 0.001 ALL FRACTIONS = ± 1/64			SCALE 1:1	MQP	SHEET 2 OF 3



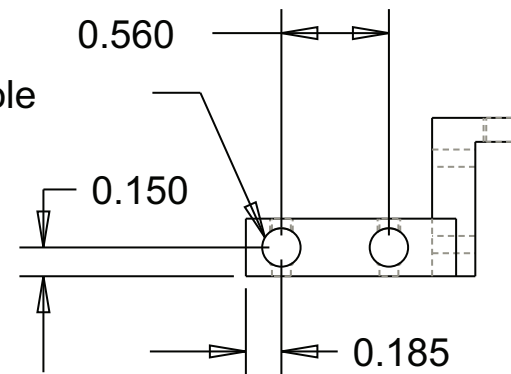
	Name	Date	WORCESTER POLYTECHNIC INSTITUTE		
DRAWN	DAVIS NGUYEN CAROL OKUMURA YUK-KWAN YUEN	12/16/2009	TITLE: CRANK		
CHECKED ENG APPR.					
MFG APPR. Q.A			SIZE: A	DWG. NO. 04	REV:
UNLESS OTHERWISE NOTED: .X = ± 0.1 .XX = ± 0.01 .XXX = ± 0.001 ALL FRACTIONS = ± 1/64			SCALE 1:1	MQP	SHEET 3 OF 3



		Name	Date	WORCESTER POLYTECHNIC INSTITUTE		
DRAWN	DAVIS NGUYEN CAROL OKUMURA YUK-KWAN YUEN		12/16/2009	TITLE: COUPLER		
CHECKED ENG APPR.						
MFG APPR. Q.A				SIZE: A	DWG. NO. 05	REV:
UNLESS OTHERWISE NOTED: .X = ± 0.1 .XX = ± 0.01 .XXX = ± 0.001 ALL FRACTIONS = ± 1/64				SCALE 1:1	MQP	SHEET 1 OF 1

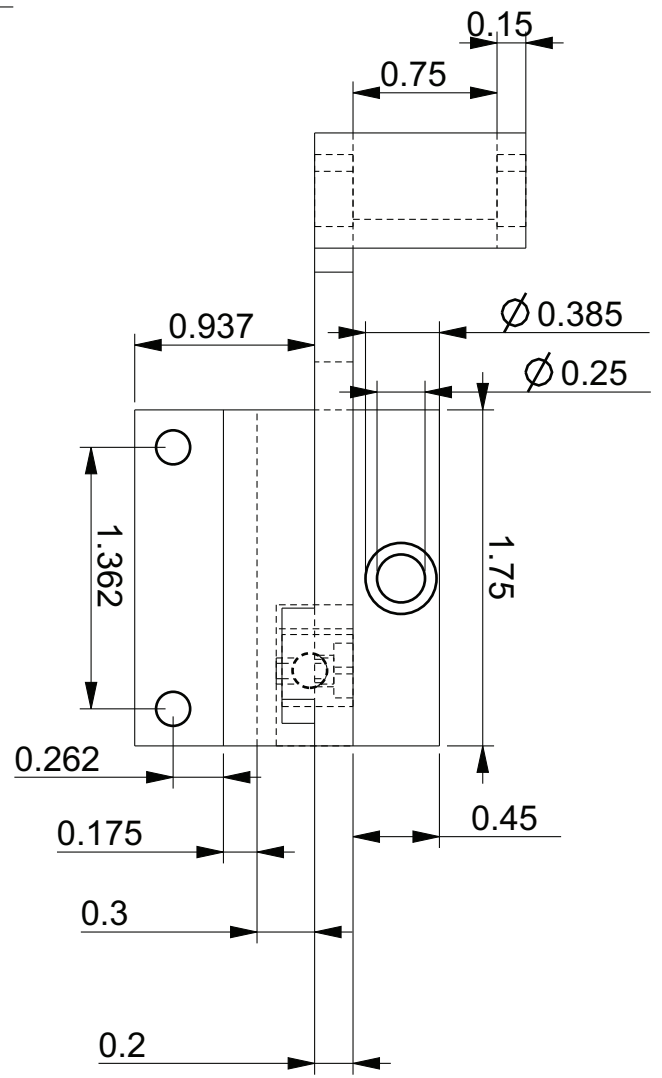
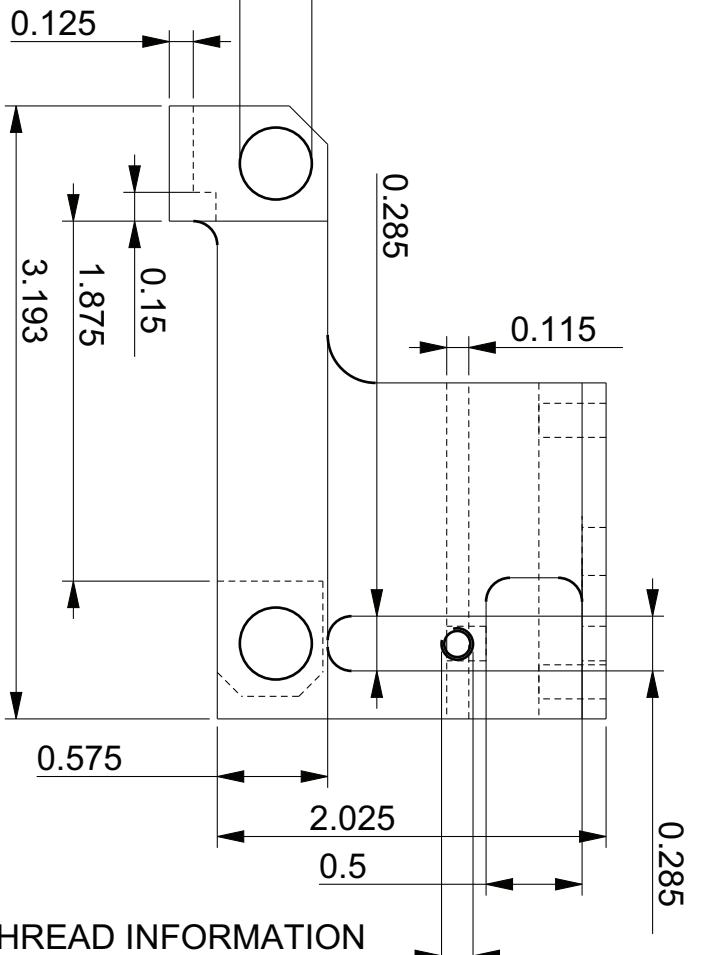


0.2in Clearance Hole
2PL



		Name	Date	WORCESTER POLYTECHNIC INSTITUTE		
DRAWN	DAVIS NGUYEN CAROL OKUMURA YUK-KWAN YUEN	12/16/2009	TITLE: Sensor Holder			
CHECKED ENG APPR.			SIZE: DWG. NO. REV:			
MFG APPR. Q.A			A		06	
UNLESS OTHERWISE NOTED: .X = ± 0.1 .XX = ± 0.01 .XXX = ± 0.001 ALL FRACTIONS = ± 1/64			SCALE 1:1		MQP	SHEET 1 OF 1

Ø 0.375 (2 PLACES)



0.164@THREAD INFORMATION

